Bosonic Randomized Benchmarking with Passive Transformations

Mirko Arienzo,[1,*] Dmitry Grinko,[2,3] Martin Kliesch,[1] and Markus Heinrich[4,5]

[1] *Hamburg University of Technology, Institute for Quantum-Inspired and Quantum Optimization, Blohmstraße 15, Hamburg, Germany*

[2] *Institute for Logic, Language and Computation, University of Amsterdam, Amsterdam, Netherlands*

[3] *QuSoft, Amsterdam, Netherlands*

[4] *Heinrich Heine University Düsseldorf, Faculty of Mathematics and Natural Sciences, Düsseldorf, Germany*

[5] *Institute for Theoretical Physics, University of Cologne, Cologne, Germany*

(Received 27 September 2024; revised 14 January 2025; accepted 12 February 2025; published 7 April 2025)

Randomized benchmarking (RB) is the most commonly employed protocol for the characterization of unitary operations in quantum circuits due to its reasonable experimental requirements and robustness against state preparation and measurement (SPAM) errors. So far, the protocol has been limited to discrete or fermionic systems, whereas extensions to bosonic systems have been unclear for a long time due to challenges arising from the underlying bosonic Hilbert space. In this work, we close the gap for bosonic systems and develop an RB protocol to benchmark passive Gaussian transformations on any particle-number subspace, which we call *passive bosonic RB*. The protocol is built on top of the recently developed filtered RB framework [J. Helsen *et al.*, PRX Quantum 3, 020357 (2022), M. Heinrich *et al.*, Randomized benchmarking with random quantum circuits, arxiv:2212.06181 [quant-ph]] and is designed to isolate the multitude of exponential decays arising for passive bosonic transformations. We give explicit formulas and a Julia implementation for the necessary postprocessing of the experimental data. We also analyze the sampling complexity of passive bosonic RB by deriving analytical expressions for the variance. They show a mild scaling with the number of modes, suggesting that passive bosonic RB is experimentally feasible for a moderate number of modes. We focus on experimental settings involving Fock states and particle-number-resolving measurements, but also discuss Gaussian settings, deriving the first results for heterodyne measurements.

DOI: 10.1103/PRXQuantum.6.020305

I. INTRODUCTION

The characterization of quantum devices, and, in particular, of the involved unitary operations, is a fundamental task in quantum information processing [1,2]. While being a well-studied field for discrete-variable systems, a similar standing for continuous-variable (CV) systems has not yet been achieved. In fact, there are only very few works apart from CV tomography and the first rigorous guarantees for the latter were proven only recently [3,4]. The required number of measurements is experimentally extremely challenging [5–11] and as a result, full quantum tomography is often not feasible for CV systems. Moreover, tomographic protocols typically suffer from state preparation and measurement (SPAM) errors, as in the discrete-variable case.

Bosonic quantum systems play a major role in the design of quantum computing platforms. Most prominently, this includes photonic quantum computing as a popular proposal for scalable quantum computers [12–17]. The biggest advantages of this model rely on the implementation of particle sources, detectors, and linear optical circuits on the same integrated chips [18–21], and access to mixed schemes for quantum error correction [22]. Bosonic systems also offer interesting nonuniversal models of computation to test quantum supremacy, such as (Gaussian) boson sampling [23–25], which have been implemented successfully in real experiments recently [26–28].

Most challenges in the characterization of bosonic systems can be attributed to the particularities of the bosonic Hilbert space [5,29]. For instance, protocols that rely on scrambling techniques via unitary designs are challenging to adapt, since Gaussian unitaries only form a unitary 1-design [30,31], and unitary 2-designs cannot exist for CV systems, unless rigged Hilbert spaces are considered [32].

*Contact author: mirko.arienzo@tuhh.de

Such issues constrain characterization protocols to very specific settings, where the implemented unitary operators (which may include non-Gaussian single-mode unitaries) are only benchmarked with respect to a restricted set of input states [33].

For discrete-variable systems, randomized benchmarking (RB) [34–43] is the most widespread family of protocols for the estimation of average gate fidelities. Its popularity is due to its robustness against SPAM errors and its rather low demands on the measurement effort [44]. The standard RB protocol is as follows: To a fixed initial state, apply a sequence of Haar-random (Clifford) unitaries, followed by a final *inversion gate* canceling the action of the entire sequence. Then, the success probability of restoring the initial state decays exponentially with the length of the sequence, and the decay rate is a proxy for the average gate fidelity of the gate set.

Recent efforts led to general guarantees for RB protocols with general finite or compact groups [45–50] instead of only unitary 2-designs. Due to the nonexistence of the latter, this generality is clearly important when considering RB of CV systems. However, there is still a fundamental problem: The RB signal generally consists of a linear combination of exponential decays in correspondence with the relevant irreducible representations (irrep) of the used group [45–47]. Estimating these decay rates is already difficult in practice if more than a few irreps are involved [47,50] and may become impossible in the CV setting.

Very recently, a bosonic randomized benchmarking protocol using random displacements has been put forward [51]. Due to the Abelian character of the (projective) Heisenberg-Weyl group and the considered noise models, the complicated behavior involving many decays is avoided in this setting, allowing for a simple analysis.

However, for more complicated—in particular non-Abelian—groups, one cannot hope for such a simple analysis. To resolve the problems coming with many irreps, filtered RB has been recently proposed [47,50], building on insights from character RB [46]. This protocol omits the inversion gate and instead performs a suitable postprocessing of the data. During the postprocessing, contributions associated to individual irreps can be isolated in a SPAM-robust way, allowing to handle compact groups with many irreps.

In this work, we introduce a RB protocol for the benchmarking of passive bosonic (Gaussian) transformations, called *passive bosonic RB*, or short *passive RB*. The passive RB protocol can be understood as a bosonic incarnation of the filtered RB framework [50], and we build on its results to give a comprehensive analysis of passive RB, including its sampling complexity, under the assumption of gate-dependent, stationary, and Markovian noise.

In contrast to the discrete-variable systems explicitly considered in Ref. [50], reasonable guarantees for a filtered RB protocol in bosonic systems are harder to obtain. This is because the action of passive transformation on the full bosonic Hilbert space is considerably more complicated than, e.g., the action of the qubit Clifford group, and thus a well-behaved protocol requires a careful identification of relevant and feasible experimental settings.

In the passive RB protocol, we navigate these complications by considering experiments where the input state is a number state and particle-number-resolving (PNR) measurements are performed, resembling boson-sampling experiments [23]. For practical reasons, we propose to use collision-free states with at most one particle per mode. We then show that the passive RB successfully benchmarks the average quality of passive transformations on a fixed number of particles, thereby separating the effect of particle-number-preserving noise from particle loss using different postprocessing of the same experimental data. In general, we prove that there are as many decay rates as we have particles in the experiments—however it is sufficient to only estimate a constant number of them in practice. By representation-theoretic means, we derive explicit and concise formulas for the functions used in the postprocessing and provide a Julia implementation. As the protocol involves non-Gaussian elements, the classical postprocessing requires the computation of matrix permanents, and it is therefore generally inefficient [23]. Specifically, we expect the postprocessing to be feasible for approximately 30 particles and modes, thus allowing the protocol to target an experimentally interesting regime. The inefficiency of the postprocessing should not be unexpected, as a similar behavior can be found in linear cross-entropy benchmarking [50,52]. There, the postprocessing involves the simulation of random circuit sampling, which is also known to be computationally hard [53–56]. We simulate the passive RB protocol for a small number of modes, demonstrating that it works as intended. Finally, we analyze the sampling complexity of our protocol by computing the relevant variances. We evaluate the obtained expressions numerically and find a very mild scaling with the number of modes m, which seems be logarithmic.

The effectively finite-dimensional setting is introduced for a good reason: Probing the full bosonic Hilbert space involves infinitely many relevant irreps and thus also decay rates, which, a priori, render a meaningful analysis impossible. Moreover, such irreps would also appear with nontrivial multiplicities, making the protocol numerically challenging from a practical point of view, as it would require fitting matrix exponential decays [47,50]. As a first variation of the passive RB setup, we thus consider scenarios in which the input state is still a number state, but the measurement involves (balanced) heterodyne detectors.

The remainder of this work is structured as follows. In Sec. II we highlight our main results: Sec. II B spells out our passive RB protocol in full detail. In Sec. II C we analyze our protocol, discuss the role of input states, and prove rigorous guarantees including bounds on its

sampling complexity. Section III is devoted to a general discussion of the passive RB protocol, open problems, and possible extensions. The technical details and proofs are deferred to the technical part, Appendix B. Finally, Appendix G contains an analysis of passive RB with balanced heterodyne measurements.

II. MAIN RESULTS

A. Notation

We consider a bosonic system of $m \in \mathbb{N}_{\geq 2}$ modes described by annihilation and creation operators a_k and $a_k^\dagger$ $(k = 1, \ldots, m)$, respectively, satisfying the canonical commutation relations (CCRs)

$$[a_k, a_l^\dagger] = \delta_{kl}, \quad [a_k, a_l] = [a_k^\dagger, a_l^\dagger] = 0, \quad k, l = 1, \ldots, m,$$

where $\delta_{k,l}$ is the Kronecker δ. These operators act on the Fock-Hilbert space $\mathcal{F}_m := \bigoplus_{n=0}^\infty \mathcal{H}_n^m$, where $\mathcal{H}_n^m$ is the subspace of n bosons distributed over m modes of dimension $\dim \mathcal{H}_n^m = \binom{n+m-1}{n}$. It is spanned by the *Fock* or *number states*

$$|\mathbf{n}\rangle \equiv |n_1, \ldots, n_m\rangle := \prod_{k=1}^m \frac{1}{\sqrt{n_k!}} a_k^{\dagger n_k} |\mathbf{0}\rangle, \tag{1}$$

where $|\mathbf{n}| := \sum_{i=1}^m n_i = n$ and $|\mathbf{0}\rangle \equiv |0, \ldots, 0\rangle$ denotes the vacuum state of m decoupled one-dimensional harmonic oscillators [57]. We shall also consider coherent states, defined as $|\alpha\rangle = e^{-|\alpha|^2/2} \sum_{n=0}^\infty \frac{\alpha^n}{\sqrt{n!}} |n\rangle$ for a single mode, with a straightforward extension to the multimode setting. The set of passive transformations is the group of unitary operators on $\mathcal{F}_m$ that leave the total number of particles invariant. These are exactly the unitaries that induce a transformation of the bosonic operators as $a_k \mapsto \sum_{l=1}^m U_{lk} a_l$ for a unitary matrix $U = (U_{lk})_{l,k=1}^m$. Hence, the group of passive transformations can be identified with the unitary group $\mathrm{U}(m)$ [58]. Practically, these can also be thought as multimode interferometers, which can be decomposed in quadratically many two-mode interferometers and phase shift transformations only [16,59–62].

The mapping $\rho : \mathrm{U}(m) \to \mathrm{U}(\mathcal{F}_m)$ of $\mathrm{U}(m)$ to the group of passive transformations on $\mathcal{F}_m$ is an example of a (unitary) *representation*. Generally, we require that a representation is compatible with group operations, i.e. $\rho(gh) = \rho(g)\rho(h)$ and $\rho(g^{-1}) = \rho(g)^{-1}$. The above representation on $\mathcal{F}_m$ is *reducible*, i.e., there are subspaces $V \subset \mathcal{F}_m$, which are invariant under ρ: $\rho(g)(V) = V$ for all g. The restriction $\rho|_V$ to such a subspace V forms a representation in its own right, a so-called *subrepresentation* of ρ. V is called irreducible if it does not contain another nontrivial invariant subspace. We then call $\rho|_V$ an *irreducible subrepresentation* (irrep) of ρ. Since any $\rho(g)$ is particle-number-preserving, one can show that the irreducible subspaces of $\mathcal{F}_m$ are exactly given by the number spaces $\mathcal{H}_n^m$ [63].

B. The passive randomized-benchmarking protocol

1. Description of the protocol

The passive RB protocol follows the general procedure of the filtered RB framework [50], adapted to the group of passive transformations acting on bosonic systems. Additionally, we use postselection to isolate particle-loss rates, see Secs. II B 3 and II B 4 for details.

The protocol consists of two phases: During the *data-collection phase*, a fixed number state $\rho = |\mathbf{n}_0\rangle\langle\mathbf{n}_0|$ is used as an input to passive transformations and particle number resolving (PNR) measurements $\{|\mathbf{n}\rangle\langle\mathbf{n}|\}_{\mathbf{n}\in\mathbb{N}^m}$ are performed on the output. The collected data then undergoes a suitable *postprocessing phase*. Motivated from boson-sampling experiments, we propose to use a *collision-free* input state $\mathbf{n}_0 = (1, 1, 1, \ldots, 1, 0, \ldots, 0)$ with $n \leq m$ particles [23], see also the discussion in Sec. II C 2 below.

The passive RB protocol can be summarized as follows.

(I) **Data collection.** For different sequence lengths $l \in \mathbb{L}$, repeat the following steps $\mathbb{T}$ times:

(i) Prepare the state $\rho = |\mathbf{n}_0\rangle\langle\mathbf{n}_0|$.
(ii) Apply passive transformations $g_1, \ldots, g_l$ drawn i.i.d. from the Haar-probability measure on $\mathrm{U}(m)$.
(iii) Measure the output state using PNR detectors and store the outcome together with the sampled unitaries.

(II) **Postprocessing.** Fix a suitable irrep λ of $\mathrm{U}(m)$ and use its later-to-be-defined *filter function* $f_\lambda(\mathbf{n}, g|\rho)$. Assuming the data $\{(\mathbf{n}^{(i)}, g_1^{(i)}, \ldots, g_l^{(i)})\}_{i=1}^{\mathbb{T}}$ has been gathered, compute the following mean estimator:

$$\hat{F}_\lambda(l) = \frac{1}{\mathbb{T}'} \sum_{i=1}^{\mathbb{T}} f_\lambda(\mathbf{n}^{(i)}, g_1^{(i)} \cdots g_l^{(i)}|\rho), \tag{2}$$

where $\mathbb{T}' \leq \mathbb{T}$ is given in Sec. II B 3 below. We refer to the data series $(l, \hat{F}_\lambda(l))_{l\in\mathbb{L}}$ as the (filtered) *RB signal*. Finally, perform an exponential fit according to the model $\hat{F}_\lambda(l) = A_\lambda r_\lambda^l$ to extract the *decay rate* r_λ. Repeat for different irreps λ as needed.

The definition of the filter function is given in Sec. II B 3. We also provide a numerical implementation of the protocol, including the filter function, on GitHub [64].

For this work, we restrict our attention to number state inputs and PNR measurements and justify this choice in more detail in Sec. II B 3. At the end of the main part,

Sec. III B, we discuss extensions of the passive RB protocol to Gaussian states or measurements. We present the first results, using balanced heterodyne measurements, in Appendix G.

We would like to emphasize that Haar-random sampling from $\mathrm{U}(m)$ can be substituted by any distribution, which converges sufficiently fast to the Haar measure [50]. For the main part of this paper, we resort to the Haar measure to simplify the presentation. We refer the reader to Appendix A 2 in the technical part for more details and comments on the use of nonuniform distributions.

Finally, the procedure described above is sometimes referred to as *single-shot estimation*, in the sense that only a single shot (or measurement) is taken per sequence. In practice, it is often advantageous to use *multishot estimation* instead, where multiple shots per sequence are recorded. Then, the estimator (2) changes in an obvious way, but converges to the same expectation value as Eq. (2). Except for the sampling complexity discussion in Sec. II C 4 all results of this work also apply to the multishot estimator.

2. Decay rates and fidelities

The decay rates can be combined into an average performance measure of passive transformations on the n-particle subspace using the formula, cf. Refs. [45, Corollay 10] and [47, Eq. (242)]

$$F = (\dim \mathcal{H}_n^m)^{-2} \sum_{\lambda} d_\lambda r_\lambda, \tag{3}$$

where the sum runs over all relevant irreps λ with dimensions d_λ, see Sec. II C. As F corresponds to a weighted average, it is typically sufficient to only consider the largest weights, which coincide with the largest irreps. This means that it may not be necessary to run the postprocessing phase (II) of the protocol for *every* irrep λ. We justify this statement and make it more precise later in Sec. II C 2.

Although commonly done, we remind the reader that caution is advised if F is interpreted as the average *entanglement fidelity* of passive transformations. The intuition behind this reasoning comes from the analysis of *gate-independent errors*, for which it is straightforward to show that F indeed coincides with the entanglement fidelity of the "noise in-between gates" [45,47]. It should be clear, however, that this noise model is highly unrealistic and the relation to gate fidelities becomes more involved if gate-dependent errors are considered. This is due to the inherent *gauge freedom* of RB, a property, which RB shares with other protocols that are agnostic against SPAM errors, such as gate-set tomography [65–68]. This gauge freedom has sparked a vivid discussion of the interpretation of RB experiments, see Refs. [41,47] for more details. In particular, whether such a physical interpretation is justified or not cannot be deduced from RB results alone. If additional information about, e.g., the physical origin of noise processes is available, the interpretation of F as fidelity may be justified—we however cannot draw such a conclusion under the assumptions made in this paper. Instead, we take the point of view of Ref. [47] in that RB decays rates, and thus F in Eq. (3), should be regarded as quantities in their own right, which provide a benchmark for the average quality of the used unitaries. Besides the mentioned interpretational issues, let us note that, for discrete-variable systems, a suitable affine transformation is typically applied to Eq. (3) to produce a proxy for the better-known *average gate fidelity*. This relies on the well-known relation $F_{\mathrm{avg}} = (dF + 1)/(d + 1)$ for discrete-variable systems in d dimensions. In the setting considered here, such a transformation would result in an expression akin to the average gate fidelity, where the average is performed over input states in the n-particle subspace.

3. Details of the protocol

Choosing a number state $|\mathbf{n}_0\rangle$ as the input to the protocol has the advantage that—*ideally*—the dynamics should happen on the finite-dimensional n-particle subspace $\mathcal{H}_n^m \subset \mathcal{F}_m$ only, where $n = |\mathbf{n}_0|$. On $\mathcal{H}_n^m$, the passive transformations $\mathrm{U}(m)$ act via the totally symmetric irrep τ_n^m. To describe noise, we transition to the density operator formalism, in which this action is described by conjugation, $\omega_n^m(g)(\rho) := \tau_n^m(g)\rho\,\tau_n^m(g)^\dagger$. If we assume—for the sake of the argument—that the noise is particle-number-preserving, we can model the noisy transformations by quantum channels $\phi_n^m(g)$ on the space of bounded operators $\mathcal{B}(\mathcal{H}_n^m)$, provided that the noise is time stationary and Markovian. Regarding the $\phi_n^m(g)$ as (small) perturbations of $\omega_n^m(g)$, the filtered RB framework [50] then predicts RB decays in one-to-one correspondence with the irreps of the *reference representation* ω_n^m. As we show in Appendix B 1, the latter decomposes into exactly $n + 1$ distinct irreps λ_k [69], and this is the number of decays to expect.

Arguably, *particle loss* is one of the major noise sources in, e.g., photonic systems, hence assuming particle-number-preserving noise is unrealistic. This can nevertheless be accounted for in our framework, as we are performing PNR measurements: By postselecting on particle-number-preserving events, we obtain effective dynamics described by completely positive, *trace nonincreasing* maps $\phi_n^m(g)$ on $\mathcal{B}(\mathcal{H}_n^m)$ and we can again rely on the results in Ref. [50]. Note that this reasoning also applies to noisy PNR measurements by modeling them as a subnormalized positive operator-valued measure (POVM). This approach is justified as long as the product of the photon-loss probability and the one of photon *gain* (e.g., through thermal noise in detectors) is very small such that the error introduced by ignoring photon gain is comparable to the shot noise. We expect this to be the case in modern photonic chips.

Finally, we introduce the *filter function*, which isolates the exponential decays for each irrep $\lambda = \lambda_k$ in the postprocessing of the collected data. Let P_λ be the projector on the carrier space of λ and let d_λ be its dimension. Then, given the measurement channel $\mathcal{M}(A) := \sum_{n\in\mathbb{N}^m} \langle \mathbf{n}|A|\mathbf{n}\rangle |\mathbf{n}\rangle\langle \mathbf{n}|$, we define the filter function as [50]

$$\begin{aligned} f_\lambda(\mathbf{n}, g|\rho) &:= s_\lambda^{-1} \langle \mathbf{n}|\omega_n^m(g) \circ P_\lambda(\rho)|\mathbf{n}\rangle, \\ s_\lambda &:= d_\lambda^{-1} \operatorname{Tr}[P_\lambda \mathcal{M}] \in \mathbb{R}_{\geq 0}. \end{aligned} \tag{4}$$

We will often simply write $f_\lambda(\mathbf{n}, g|\rho) \equiv f_\lambda(\mathbf{n}, g)$ once the input state ρ is fixed. We give a more concise formula for f_λ in Sec. II C as Theorem 1. In particular, we show that $s_\lambda > 0$ as long as the number of modes m is strictly larger than 1. As the filter function is automatically zero if $|\mathbf{n}| \neq n$ due to P_λ, we can formally describe the postselection on particle-number-preserving events by defining

$$\mathbb{T}_{\mathrm{pr}} := |\{i \in [\mathbb{T}] \,|\, |\mathbf{n}^{(i)}| = n\}|, \tag{5}$$

and using the mean estimator Eq. (2) with the choice $\mathbb{T}' = \mathbb{T}_{\mathrm{pr}}$.

4. Estimation of particle-loss rates

The same postprocessing procedure can also be used to capture the estimation of particle-loss rates as follows. Define the filter function to be the indicator function [70]

$$f(\mathbf{n}) := \begin{cases} 1 & \text{if } |\mathbf{n}| = n, \\ 0 & \text{else}, \end{cases} \tag{6}$$

and set $\mathbb{T}' = \mathbb{T}$. Thus, the associated mean estimator $\hat{F}(l)$, cf. Eq. (2), simply yields the ratio $\mathbb{T}_{\mathrm{pr}}/\mathbb{T}$. To see that this leads to the wanted result, let us model particle loss by a beam splitter with transmittivity $\sqrt{p}$ in every mode (i.e., p is the probability of *not* loosing a particle). In addition, we assume transmittivities $\sqrt{p_{\mathrm{SP}}}$ and $\sqrt{p_{\mathrm{M}}}$ associated with state preparation and measurement, respectively. Hence, the probability that a sequence of l passive transformations preserves the particle number is $p_{\mathrm{SP}}^n p_{\mathrm{M}}^n p^{nl} = \mathbb{E}[\mathbb{T}_{\mathrm{pr}}/\mathbb{T}] = \mathbb{E}[\hat{F}(l)]$. Therefore, we can extract the transmittivity $\sqrt{p}$ from the data $(l, \hat{F}(l))_{l\in\mathbb{L}}$ using an exponential fit as before.

Note that the original filtered RB protocol does not perform the postselection in Sec. II B 3 above [i.e. $\mathbb{T}' = \mathbb{T}$ in Eq. (2)]. This leads to a mixing of the decay rate of particle-preserving noise with the particle-loss rate, resulting in a combined decay $(p^n r_\lambda)^l$. By performing postselection, we can consider these decays individually.

C. Analysis and guarantees

The filtered RB framework [50] implies a number of guarantees for the passive RB protocol, which we specialize and extend in the following. We rely on the *implementation-map* noise model, which we justified using the postselection argument in Sec. II B. In this model, the noise is modeled by replacing the representation ω_n^m with an implementation map ϕ_n^m on $\mathrm{U}(m)$, which takes values in the set of completely positive, trace nonincreasing superoperators on $\mathcal{H}_n^m$. This model allows for highly gate-dependent noise, which, however, needs to be stationary and Markovian.

In the following, we use the short-hand notations $\omega \equiv \omega_n^m$, $\tau \equiv \tau_n^m$, and $\phi \equiv \phi_n^m$ whenever the parameters n and m are clear from the context.

1. The RB signal

We now briefly sketch the arguments why the RB signal $\hat{F}_\lambda(l)$, cf. Eq. (2), is well approximated by an exponential decay [50]. In the implementation-map model, a straightforward calculation shows that the expected RB signal $F_\lambda(l) := \mathbb{E}[\hat{F}_\lambda(l)]$ is the contraction of a linear operator $\tilde{T}_\lambda^l$, and can thus be expanded into a linear combination of its (complex) eigenvalues, $F_\lambda(l) = \sum_j A_{\lambda,j} z_{\lambda,j}^l$. To understand the eigenvalues $z_{\lambda,i}$ of $\tilde{T}_\lambda$, we first consider the noiseless case: Then, $\tilde{T}_\lambda$ reduces to $T_\lambda(\mathcal{X}) = P_\lambda \int_{\mathrm{U}(m)} \omega(g)^\dagger \mathcal{X} \omega(g)\, dg$, also known as a *channel twirl* in the quantum information literature, composed with the irrep projector P_λ. As we show in the technical part, Appendix B 1, T_λ has a single nonzero eigenvalue given by 1. Inserting this into the expansion of $F_\lambda(l)$, we immediately see that it is constant in l, and in fact given by [50]

$$F_\lambda(l) = \operatorname{Tr}[\rho P_\lambda(\rho)]. \tag{7}$$

In the presence of noise, we instead find the expression $\tilde{T}_\lambda(\mathcal{X}) = P_\lambda \int_{\mathrm{U}(m)} \omega(g)^\dagger \mathcal{X} \phi(g)\, dg$. Given that the noise is sufficiently weak, in the sense that $\tilde{T}_\lambda - T_\lambda$ is small, matrix perturbation theory implies that $\tilde{T}_\lambda$ has a single dominant real eigenvalue $r_\lambda := z_{\lambda,0}$, which is separated from the remaining spectrum by a large gap and thus quickly dominates the signal.

Proposition 1 ([50, Theorem 8], informal). Suppose that the noise is sufficiently weak. Then, we have

$$F_\lambda(l) \approx A_\lambda r_\lambda^l, \tag{8}$$

up to an additive error $\alpha \geq 0$, which is suppressed exponentially in l, and $A_\lambda \in \mathbb{R}$, $0 < r_\lambda \leq 1$. Moreover, r_λ does *not* depend on the initial state and measurement, thus SPAM errors only affect A_λ.

In the filtered RB framework [50], noise is measured by the operator norm $\delta_\lambda := \|\tilde{T}_\lambda - T_\lambda\|_\infty$ and "weak noise" is such that $\delta_\lambda \leq 1/5$. Then, Ref. [50] gives more precise conditions on the error suppression in the expected signal.

In particular, it is sufficient to choose the sequence length as

$$l \geq \frac{\log \frac{d_\lambda}{s_\lambda} + 2\log\frac{1}{\alpha} + 4}{2\log\frac{1}{2\delta_\lambda}}, \tag{9}$$

where d_λ is the dimension of the irrep and s_λ is as in Eq. (4). In the technical part of this work, Appendix B, Proposition 2 and Theorem 3, we prove the following explicit formulae for $\lambda = \lambda_k$:

$$d_{\lambda_k} = \frac{2k+m-1}{m-1}\binom{k+m-2}{k}^2, \tag{10}$$

$$s_{\lambda_k} = \frac{m-1}{2k+m-1}\binom{k+m-2}{k}^{-1}. \tag{11}$$

In particular, we have (for $m > 1$)

$$\frac{d_{\lambda_k}}{s_{\lambda_k}} = \left(\frac{2k+m-1}{m-1}\right)^2\binom{k+m-2}{k}^3. \tag{12}$$

Hence, it is sufficient to take sequences of length $O(k\log((k+m-2)/k))$, which is $O(m\log m)$ in the *non-collision regime* $n \leq m$ (as $k \leq n$). However, we expect that these bounds are not tight. In fact, Eq. (9) is not tight in the first place [50], nevertheless improving the bound is hard in the gate-dependent noise setting. Based on the experience with discrete variable RB, we expect that already very short sequences are sufficient and conjecture that the dependence on $d_{\lambda_k}/s_{\lambda_k}$ in Eq. (9) can in fact be dropped, meaning that constant-length sequences are sufficient.

The signal form is concretely shown in Fig. 1, where we show the results of a simulation of the protocol with $|\mathbf{n}_0\rangle = |\mathbf{1}\rangle_4 \equiv |1111\rangle$, assuming lossy gates for different values of the transmittivity. By performing exponential fits, we retrieve values of the transmittivity $\sqrt{p}$ using $\mathbb{T} = 10\,000$ samples, matching the used transmittivities up to an error of 10^{-3}. We also simulated an experiment where the transmittivity is chosen at random for each transformation, resulting in decay rates that match the average over the allowed random decay rates. We provide additional details on numerical experiments in Appendix H.

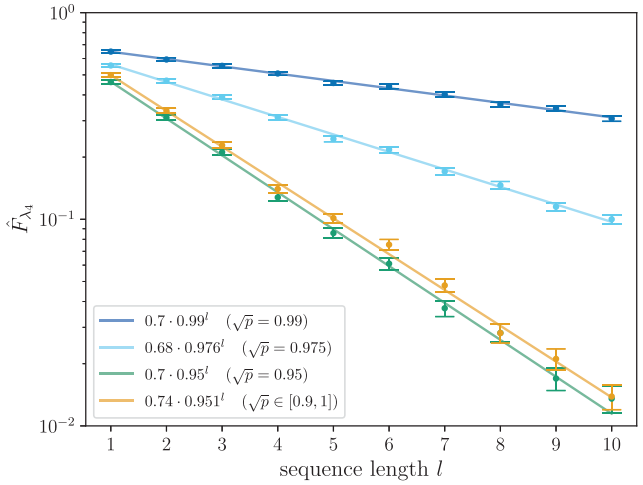

FIG. 1. Passive RB signal, Eq. (2), using $n = m = 4$ and input state $|\mathbf{1}_4\rangle \equiv |1111\rangle$ in the presence of particle-loss noise, using $\mathbb{T} = 10\,000$ samples. The last (yellow) data set corresponds to simulated gate-dependent noise where the transmittivities $\sqrt{p}$ are drawn uniformly at random from $[0.9, 1]$ for every transformation in the sequence. More details can be found in Appendix H.

2. Choice of input state

For standard RB on discrete-variable systems, the input state is typically chosen to be the all-zeros state $|0^n\rangle$, and, in fact, the choice of input state plays a minor role in this case. The underlying reason is that we typically have a single nontrivial irrep (i.e., the adjoint irrep) with respect to which all states are equivalent.

In the finite-dimensional bosonic setting, we show in Lemma 1 in Appendix B 1 that ω_n^m decomposes into $n+1$ irreps and thus there is a certain freedom in choosing the input state $\rho = |\mathbf{n}_0\rangle\langle\mathbf{n}_0|$. In principle, the passive RB protocol is agnostic of the input state. However, its choice influences the overall magnitude of the RB signal since the latter scales with the overlap of the state with the irrep of interest [50]. As the variance of F_λ exhibits the same scaling behavior, the mean estimator $\hat{F}_\lambda(l)$ also converges more rapidly for smaller overlaps and hence the overall scale set by the overlap does not influence the sampling complexity of the protocol, see also Sec. II C 4. Nevertheless, it may happen that the input state has vanishing overlap with an irrep, in which case the RB signal is identically zero and no information about decay rates can be extracted. Moreover, very small overlaps, and thus signals, may lead the numerical issues in the postprocessing.

Our proposal of using a collision-free state $\mathbf{n}_0 = \mathbf{1}_n = (1,1,1,\ldots,1,0,\ldots,0)$ is motivated by practical considerations as generating higher Fock states can be a challenging task [71–73]. In Figs. 2(a) and 2(b), we show its overlaps with the relevant irreps for $n = m$ and for $n \leq m$ with m fixed, respectively. We see that the largest overlap is always attained with the largest irrep $k = n$ and typically decreases with k, leading to small overlaps for $k \ll n$ if m is not too small. Generally, one can show that

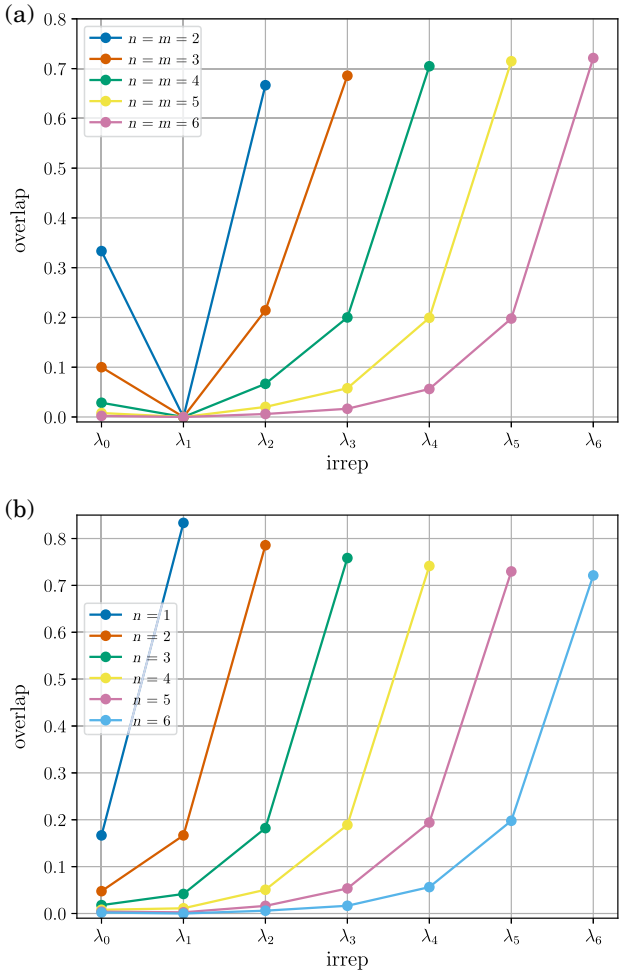

FIG. 2. Overlaps of the collision-free n-particle state $\mathbf{1}_n = (1,\dots,1,0,\dots,0)$ with the irreps $\lambda_k, k = 0,\dots,m$. Lines are shown to enhance readability of data points and their relationships. (a) For $n = m$, we observe no overlap with the adjoint irrep λ_1. For each m, the overlap is maximized by the largest irrep. (b) Overlaps for $n \le m = 6$. As before, the maximum overlap is obtained for the largest irrep λ_n. Note that the overlap with λ_1 is trivial only for $n = m$.

the collision-free state for $n = m$ particles always has zero overlap with the λ_1 (adjoint) irrep. This behavior can be avoided by optimizing $\mathbf{n}_0$, however likely leading to an input state that is hard to prepare in experiments.

As a matter of fact, the problem of vanishing and very small overlaps of the collision-free state is not severe: Recall that the overall benchmarking quantity F, cf. Eq. (3), is given as a weighted average of the decay rates r_{λ_k}, where the weights are given by the irrep dimension d_{λ_k}. Since irreps with small k also have small dimension, their contribution to the weighted average may be neglected. More precisely, if we only take into account the u largest irreps, their combined weight can be readily computed as

$$(\dim \mathcal{H}_n^m)^{-2} \sum_{i=0}^{u-1} d_{\lambda_{n-i}} = 1 - \left[\prod_{i=1}^{u} \frac{n-i+1}{n+m-i}\right]^2. \quad (13)$$

In particular, if n is fixed and $m \to \infty$, this converges to 1 for any u, and if $n = m \to \infty$, the weight converges to $1 - 4^{-u}$. As the convergence is fast in both cases, taking only a constant number of irreps (the largest ones) into account gives an exponentially good approximation to F, already for a moderate number of modes. For instance, for $n = 5$ particles in $m = 10$ modes, taking the three largest irreps covers 99.9% of the total weight. This also implies that it is sufficient to perform the postprocessing phase (II) in the passive RB protocol, Sec. II B, only a constant number of times.

3. Evaluation of the filter function

At the heart of the the passive RB protocol, Sec. II B, lies the evaluation of the filter function (4) in the postprocessing phase. We briefly sketch the central steps of its computation leading to Theorem 1 in the following and refer to the technical part, Appendices A 1 and A 4, for more details and proofs. First, note that $\omega \simeq \tau \otimes \bar{\tau}$ can be explicitly decomposed into irreps using a suitable generalization of the Clebsch-Gordan decomposition for the sum of two angular momenta in quantum mechanics [74,75]. This yields the following expansion of Fock states:

$$|\mathbf{n}\rangle\langle\mathbf{n}| \simeq |\mathbf{n},\mathbf{n}\rangle = \sum_{\lambda} \sum_{M_\lambda} \tilde{C}^{M_\lambda}_{\mathbf{n},\tilde{\mathbf{n}}} |M_\lambda\rangle, \quad (14)$$

where λ runs over the irreps of ω and the $|M_\lambda\rangle$ form a suitable basis of λ. The $\tilde{C}^{M_\lambda}_{\mathbf{n},\tilde{\mathbf{n}}}$ correspond to (generalized) SU(m) Clebsch-Gordan coefficients, up to a phase. Then, the projection onto a specific irrep λ acts by selecting only the corresponding terms in Eq. (14). Re-expressing the $|M_\lambda\rangle$ in terms of Fock states and inserting the expansion into Eq. (4) produces so-called *permanents*, which are defined for an arbitrary $r \times r$ matrix A as

$$\mathrm{Per}(A) := \sum_{\pi \in S_r} \prod_{i=1}^{r} A_{i\pi(i)}, \quad (15)$$

where S_r denotes the symmetric group over r symbols. Let us define $A_{\mathbf{n},\mathbf{m}}$ to be the matrix obtained from A by taking m_j copies of the jth column of U and then taking n_i copies of the ith row of the resulting matrix. Then, the appearance of permanents is due to the well-known fact that $\sqrt{\mathbf{n}!}\sqrt{\mathbf{m}!}\,\langle \mathbf{n}|\tau(g)|\mathbf{m}\rangle = \mathrm{Per}(g_{\mathbf{n},\mathbf{m}})$ [76], where we used the multi-index notation $\mathbf{n}! := n_1!\dots n_m!$.

Finally, we have the following concise formula that can be used for numerical computation:

Theorem 1 (PNR filter function—informal). The filter function (4) is given as

$$f_{\lambda_k}(\mathbf{n}, g) = \frac{1}{s_{\lambda_k}} \sum_M \tilde{C}^M_{\mathbf{n}_0,\bar{\mathbf{n}}_0} \sum_{\mathbf{n}_1 \in \mathcal{H}_n^m} \tilde{C}^M_{\mathbf{n}_1,\bar{\mathbf{n}}_1} \frac{|\mathrm{Per}(g_{\mathbf{n},\mathbf{n}_1})|^2}{\mathbf{n}!\mathbf{n}_1!}. \quad (16)$$

Here, M labels a so-called *Gelfand-Tsetlin* basis of the irrep λ_k and the coefficients $\tilde{C}$ coincide with Clebsch-Gordan coefficients for SU(m) up to a phase.

We give more details on the Gelfand-Tsetlin basis, the computation of Clebsch-Gordan coefficients, and the occurring phases in the technical part, Appendix A 1, and formally prove Theorem 1 in Appendix B 2. We also give an alternative formula for f_{λ_k} in Corollary 1 using matrix coefficients of the irrep λ_k. These also correspond to permanents, however, of a different dimension [77].

Generally speaking, the computation of filter functions of the form (4) requires simulation of the entire experiment. As the proposed protocol involves non-Gaussian elements, the computation of filter functions is expected to be generally inefficient. This is manifest in the occurrence of permanents in our filter functions. The computational complexity of evaluating permanents is central to the complexity-theoretic arguments for boson sampling. It is known that even approximating permanents is computationally hard [23,56]. Nevertheless, these quantities can be computed efficiently in some scenarios [78–83].

This finding should not come as a surprise, as we find a similar behavior in the discrete setting—namely linear cross-entropy benchmarking [50,52]. There, the postprocessing requires the simulation of random circuit sampling, which is known to be computationally hard, analogous to boson sampling [53–56].

In practice, Clebsch-Gordan coefficients can be computed in polynomial time in the dimension of λ [75]. This can be significantly sped up by taking advantage of the symmetries of the weight diagrams under the action of the Weyl group of SU(m) [84]. Specifically, we expect this to be feasible for $m \approx 20$–30 modes. In such a regime, the computation of the permanents appearing in Eq. (16) is also still possible, as we consider $n \leq m$ particles and, by Ryser's formula, it can be computed in time $O(n \cdot 2^n)$ [85,86].

4. Sampling complexity

In the following, we discuss the sample complexity of passive RB, i.e., the number of samples needed to guarantee that the estimator $\hat{F}_\lambda(l)$ is ϵ-close to its expected value $F_\lambda(l)$ with high probability. Recall from Eq. (2) that $\hat{F}_\lambda(l)$ is a mean estimator for the filter function f_λ. Since the latter is only poorly bounded, we compute the variance $\mathrm{Var}[\hat{F}_\lambda(l)] = \mathrm{Var}[f_\lambda]/L$ (here the variance is still taken over length-l sequences). Then, we can use Chebyshev's inequality to ensure $|\hat{F}_\lambda(l) - F_\lambda(l)| < \epsilon$ with probability $1 - \delta$ given $L \geq \epsilon^{-2}\delta^{-1}\mathrm{Var}[f_\lambda]$ samples.

In general, analyzing the variance $\mathrm{Var}[f_\lambda]$—more precisely the second moment $\mathbb{E}[f_\lambda^2]$—can be quite cumbersome, as the underlying probability distribution is given by Born probabilities involving the noisy input state, the noisy transformations, and the noisy measurements. In the filtered RB framework [50] it is however shown that—under reasonable assumptions on the noise [87]—this problem can be reduced to analyzing the second moment $\mathbb{E}[f_\lambda^2]_{\mathrm{ideal}}$ in the ideal, noiseless case. In other words, the presence of noise cannot decrease the efficiency of filtered RB. Using this assumption, we have the following result bounding the variance of passive RB:

Theorem 2 (Variance bound—informal). The variance of the passive RB protocol is bounded as

$$\mathrm{Var}[f_{\lambda_k}] \leq \mathbb{E}[f_{\lambda_k}^2]_{\mathrm{ideal}} = s_{\lambda_k}^{-2} \sum_{\mathbf{n} \in \mathcal{H}_n^m} \tilde{g}_k(\mathbf{n}, \mathbf{n}_0), \quad (17)$$

where $\tilde{g}_k(\mathbf{n}, \mathbf{n}_0)$ is a function of Clebsch-Gordan coefficients of the representations ω and $\lambda_k^{\otimes 2}$.

A formal version of Theorem 2 is given as Theorem 5 in the technical part and also proven there. It relies on expressing the second moment $\mathbb{E}[f_{\lambda_k}^2]_{\mathrm{ideal}}$ as a suitable integral of the representations $\lambda_k^{\otimes 2}$ and ω_n^m over SU(m) [43,50]. Schur's lemma then implies that the nontrivial contributions to this integral are given by the irreps of $\lambda_k^{\otimes 2}$, which are also contained in ω. We determine these irreps, which allows us to finally write $\mathbb{E}[f_{\lambda_k}^2]_{\mathrm{ideal}}$ in terms of suitable Clebsch-Gordan coefficients.

Arguably, Eq. (17) is not very explicit and it is thus not clear how $\mathbb{E}[f_{\lambda_k}^2]$ scales with k, n, and m. Finding a meaningful bound for the expression in Eq. (17) turns out to be difficult and we are left with the trivial bound

$$\mathbb{E}[f_{\lambda_k}^2] \leq s_{\lambda_k}^{-2} = \left(1 + \frac{2k}{m-1}\right) \binom{k+m-2}{k}^2, \quad (18)$$

which suggests an exponential scaling like 2^{4m} in the worst case $k = n = m$. This bound is however very loose: A numerical evaluation of the second moment (see below) reveals that the upper bound (18) already overestimates the second moment for $m = 2$ by a factor of 10 and by a factor of 10^4 for $m = 5$.

The shear number of Clebsch-Gordan coefficients that need to be evaluated for the formula (17), however, limits a numerical study to very low values of k, n, and m using standard algorithms [75,88]. To increase the available data a bit, we furthermore estimate the variance empirically using $\mathbb{T} = 10\,000$ samples from the noiseless outcome distributions. From Fig. 3(b), we can observe that this number

of samples is already enough to give reasonable estimates of $\mathbb{E}[f_{\lambda_k}^2]_{\text{ideal}}$. In Fig. 3(a), we show the empirical second moments for $m \leq 5$ using a collision-free input state $\mathbf{1}_n$ with $n \leq m$ particles (cf. Appendix H for further details on the sampling procedure). Similar to the behavior for the ideal first moments (overlaps) in Fig. 2, the second moment for a fixed m is maximized at the largest irrep $k = n$. In addition, we analyzed the scaling of the empirical second moments for $m = n = k$ with m. Although we have too few data points to make a conclusive statement, we find that the scaling is best compatible with a logarithmic scaling in m (or a polynomial of very small degree of order $m^{1/20}$). This would be a double-exponential improvement over the trivial bound, Eq. (18).

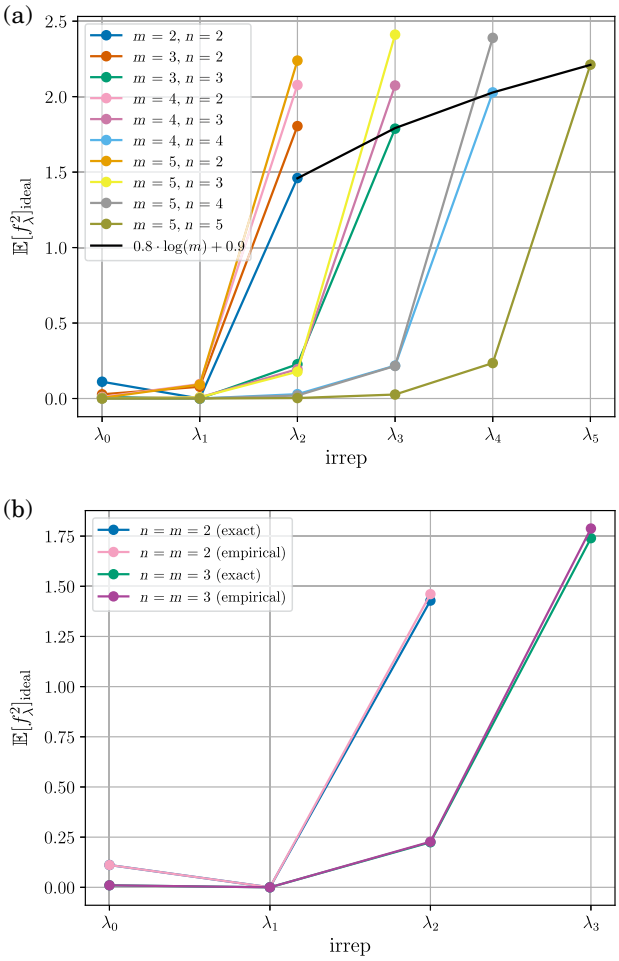

FIG. 3. Second moments of the filter function f_{λ_k} for a different number of modes m, particles n, and irreps λ_k. Lines are shown to enhance readability of data points and their relationships. (a) Empirical second moment with $\mathbb{T} = 10\,000$ samples for different values of $n \leq m$ and $m \leq 6$. The largest second moment (for fixed m) is always attained at the largest irrep $k = n$. The scaling of the second moment for $m = n = k$ with m seems to be logarithmic, however, there is insufficient data to make a definite conclusion. (b) Empirical second moment with $\mathbb{T} = 10\,000$ samples compared to the exact second moment (17) for $n = m \leq 3$. We observe that this number of samples is already sufficient to give reasonable approximations of the second moment.

III. DISCUSSION

A. Summary and open questions

Passive RB is the first RB protocol for the certification of passive bosonic transformations. Naively adopting discrete-variable RB to this setting would result in a complicated and challenging-to-analyze signal and thus additional care in the protocol detail is necessary. Using techniques from filtered RB [50], in combination with careful choices of initial state and measurement, we find an experimental setting in which a meaningful benchmark is indeed possible.

Using a collision-free n-particle state $|1, \ldots, 1, 0, \ldots, 0\rangle$ as the input and PNR measurements, we effectively produce a finite-dimensional setting in which the RB signal consists of only $(n + 1)$ decays, which can be isolated in postprocessing using *filtering*. In fact, we show that it is sufficient to only estimate a constant number of these decays to produce a meaningful benchmark for passive transformations on n particles. Moreover, the same procedure can be used to estimate particle-loss rates.

In addition, we study the sampling complexity of passive RB by computing the necessary variances. The resulting expressions, involving many Clebsch-Gordan coefficients, are difficult to analyze directly. We evaluate this expression numerically and additionally estimate the variance empirically for a small number of modes. The obtained data suggests that the variance scales only very mildly with the number of modes m (in the noncollision regime $n \leq m$), being best matched by a logarithmic function. A definite conclusion can only be drawn from a larger data set. However, this observation allows us to be cautiously optimistic that meaningful passive RB experiments are possible with a low to moderate number of samples.

So far, a bottleneck of the protocol is the evaluation of the filter function (16) during postprocessing, which essentially involves the simulation of the experiment. This can be reduced to the computation of permanents which are known to be computationally hard. A similar problem is faced in linear cross-entropy benchmarking, which requires the—equally hard—simulation of random circuit sampling. Nevertheless, the latter can still be done for a moderate and experimentally interesting number of qubits. We expect this is also possible for passive RB by speeding up the computation of Clebsch-Gordan coefficients using symmetries [84], and reducing the permanents to the relevant irreps (cf. Corollary 1). In principle, there are also explicit formulas available that could lead to a speedup [89–91]. We provide a Julia implementation of the postprocessing [64] and will study runtime improvements in future work.

The analysis of the behavior of passive RB in the presence of *particle distinguishability* is still an open problem, which we believe can be tackled by suitable extensions of the filtered RB framework. We leave this problem for future work.

We note that—in principle—character RB is also able to isolate the individual decay rates associated to irreps [46]. The main difference to filtered RB is that (i) an additional random $g \in \mathrm{SU}(m)$ is inserted before measuring, and (ii) the experimental data is postprocessed using the *character* $\chi_\lambda(g)$ of the irrep of interest evaluated at g and the dimension of λ. The randomization over g then effectively implements the projector P_λ [as in the filter function (4)]. Although the computation of the character is efficient (in n and m), the sampling complexity is much worse than for passive RB. This is because sampling out the projector P_λ converges very slowly: Using the results of this work, it is not hard to show that the variance of character RB is $\Omega(2^{2n})$ for irreps with $k \geq n/2$. Thus, both the total computational and experimental effort is exponential, while for passive RB, it is likely only the former. Another advantage of passive RB is that our scheme can also be used with nonuniform sampling, cf. Appendix A 2 b, while this is not clear for character RB.

B. Extensions of the protocol

Arguably, the most straightforward—and experimentally simplest—protocol would also involve a Gaussian input state and measurement. As already noted in the introduction, this would, however, correspond to a classical linear optics experiment and one should not expect to capture errors, which would occur in a quantum setting. Hence, it is more instructive to consider a variation of the passive RB protocol, in which either the input state or the measurement is made Gaussian.

However, one needs to be careful when leaving the effectively finite-dimensional setting, which we explored in this work. Indeed, an "inherently infinite-dimensional" RB protocol is ill behaved for the following reason: Any passive transformation $U \in \mathrm{U}(m)$ is represented as a unitary operator $\tau^m(U)$ on the full Fock space $\mathcal{F}_m := \bigoplus_{n=0}^{\infty} \mathcal{H}_n^m$. Since $\mathrm{U}(m)$ is compact, τ^m is completely reducible, and decomposes into infinitely many finite-dimensional irreps acting on the boson number subspaces [63]. Then, the conjugation representation $\omega \equiv \tau^m(\cdot)\tau^{m\dagger}$ decomposes into infinitely many irreps, too. This means we may find infinitely many decay rates (each associated to one irrep) and it is unclear how to truncate those with a regularization argument, as the irreps lack a clear physical interpretation. On top of that, the decomposition of ω is not multiplicity-free [92], which may complicate the postprocessing and affect its numerical stability [47].

As a first step, we consider a passive RB protocol with a number input state and a balanced heterodyne measurement at the end of each mode. We give some partial results for this setting in Appendix G. In contrast to the PNR setting, it is however not clear how to handle particle loss in such a protocol. We thus leave a more thorough study of passive RB protocols with Gaussian input states or Gaussian measurements for future work.

Lastly, we comment on the extension to other groups. Broadly speaking, *active* Gaussian transformations play a fundamental role in CV systems, for instance, in Gottesmann-Knill-Preskill (GKP) encoding of qubits in bosonic states [93], or in the preparation of input states for Gaussian boson-sampling experiments [24,25,94]. However, randomized benchmarking of general Gaussian transformations faces many challenging issues, most strikingly the fact that this group—the symplectic group $\mathrm{Sp}(2m,\mathbb{R})$ on m modes—is *noncompact*. As a consequence, a probability Haar measure cannot exist, and thus it is not even clear how to "randomize" in this context. Hence, the filtered RB framework focuses on compact groups [50]. Some of the ideas in Ref. [50] nevertheless carry over to the noncompact case if one considers suitable random walks on $\mathrm{Sp}(2m,\mathbb{R})$. By the central limit theorem for reductive Lie groups [95,96], such random walks converge to a Gaussian distribution on $\mathrm{Sp}(2m,\mathbb{R})$. However, this does not clarify—to the best of our knowledge—the behavior and convergence of the moment (or twirling) operator. Since $\mathrm{Sp}(2m,\mathbb{R})$ has Kazhdan's property (T) [97], the characterization of the relevant representation theory—capturing the action of active transformations onto density operators—plays a central role. This involves the well-known metaplectic (or oscillator) representation of $\mathrm{Sp}(2m,\mathbb{R})$ and can—in principle—be approached using Howe duality [98,99]. Due to infinite-dimensional irreps [100] and open convergence questions, it is however far from obvious whether a meaningful RB protocol can be developed for active transformations. We leave the resolution of these questions for future work.

C. Parallel work

In parallel to this work, Wilkens *et al.* [101] independently developed a randomized benchmarking protocol for nonuniversal, bosonic (or fermionic) analog simulators, called *randomized analog benchmarking*, which is also based on filtered RB [50]. Instead of sampling Haar randomly, they use randomized sequences generated by a family of tunable Hamiltonians. In their "noninteracting" case, their random sequences converge to the Haar measure on $\mathrm{U}(m)$ and thus the relevant representation theory (and thus postprocessing) is the same as in this work. Their work also provides a detailed numerical study of the protocol and the behavior under different noise models. Finally, the authors also discuss an "interacting" case (with on-site and in-mode interactions), which leads to a different group than $\mathrm{U}(m)$ for which all nontrivial irreps are joined

into a single one, similar as for discrete RB with unitary 2-designs.

ACKNOWLEDGMENTS

We would like to thank Ingo Roth, Jonas Haferkamp, Jonas Helsen, René Sondenheimer, Jan von Delft, Francesco Di Colandrea, and Mattia Walschaers for helpful discussions. We would like to express our gratitude to Zoltán Zimborás for bringing the new version of Piquasso [102] to our attention. Furthermore, we are grateful to the anonymous referees of the TQC and AQIS conferences for helpful comments on the manuscript.

This work has been funded by the Deutsche Forschungsgemeinschaft (DFG, German Research Foundation)—Grants No. 441423094 and No. 547595784, by the German Federal Ministry of Education and Research (BMBF) within the funding program "quantum technologies – from basic research to market" via the joint project MIQRO (Grant No. 13N15522), and by the Fujitsu Germany GmbH and the Dataport as part of the endowed professorship "Quantum Inspired and Quantum Optimization." D.G. was supported by an NWO Vidi grant (Project No. VI.Vidi.192.109). M.H. has conducted part of this research while visiting QuSoft and Centrum Wiskunde & Informatica, Amsterdam, and would like to express his gratitude for their support and hospitality. Publishing fees supported by Funding Programme Open Access Publishing of Hamburg University of Technology (TUHH).

APPENDIX A: TECHNICAL BACKGROUND

1. Representation Theory

In this appendix, we review the main technical tools used in the proofs of our main results, shown in Appendix B. First, we review irreps of SU(m) and the Clebsch-Gordan decomposition in terms of Gelfand-Tsetlin patterns, then we briefly review additional technical details concerning filtered randomized benchmarking.

a. Representations of SU(m)

As SU(m) is a compact Lie group, we can use *weight theory* to understand its representation theory, see, e.g., Refs. [103–105]. To this end, we consider the diagonal subgroup of SU(m), the elements of which can be written as

$$\mathrm{diag}(e^{i\theta_1},\dots,e^{i\theta_{m-1}},e^{-i\sum_{j=1}^{m-1}\theta_j}). \tag{A1}$$

Hence, the diagonal subgroup is isomorphic to the $(m-1)$-torus $T^{m-1}\simeq(S^1)^{\times(m-1)}$. Since T^{m-1} is Abelian, the restriction of any irreducible representation ρ of SU(m) to T^{m-1} decomposes into one-dimensional, irreducible subrepresentations, given by characters of T^{m-1}:

$$\rho|_{T^{m-1}}\simeq\bigoplus_{w\in\mathbb{Z}^{m-1}}\chi_w\otimes\mathbb{1}_{m_w}. \tag{A2}$$

Here, $\chi_w(\theta)=e^{iw^\top\theta}$, $w\in\mathbb{Z}^{m-1}$, are characters of T^{m-1} and m_w are the *(inner) multiplicities*. Then, the *weights* of ρ are given by the vectors w for which $m_w\neq 0$. The *weight space* of w is the isotypic component of w, i.e., the carrier space of $\chi_w\otimes\mathbb{1}_{m_w}$, and has dimension m_v. We can order weights lexicographically, i.e., $v>w$ if and only if $v_i>w_i$ for all i. We then say that the weight v is higher than w. Importantly, the *theorem of the highest weight* [103, Theorems 9.4 and 9.5] states that every irrep has a unique highest weight and is uniquely determined by it. Hence, we can characterize the irreps of SU(m) by studying the structure of weights.

A convenient way of doing that is given by *Young diagrams*: Let $n\geq 0$ be a non-negative integer and let $\lambda=(\lambda_1,\dots,\lambda_m)$ be a partition of n, i.e., $\lambda_1\geq\lambda_2\geq\cdots\geq\lambda_m\geq 0$ with $\sum_{i=0}^{m}\lambda_i=n$. Any such partition is identified with a Young diagram, namely a collection of boxes arranged in left-justified rows with a weakly decreasing number of boxes in each row, where the ith row contains λ_i boxes, e.g.,

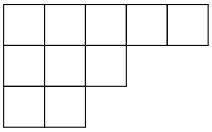

(A3)

corresponds to $\lambda=(5,3,2)$. Young diagrams uniquely determine irreps of SU(m) up to constant shifts, namely, $(\lambda_1,\dots,\lambda_m)$ and $(\lambda_1+c,\dots,\lambda_m+c)$ identify the same irrep for any integer c. Therefore, as the rank of SU(m) is $m-1$, by convention we assume $\lambda_m=0$ without loss of generality. In the following we will not distinguish between Young diagrams and the corresponding irreps, unless otherwise specified.

For a given irrep λ, the *dual (or contragredient)* representation λ^* is defined as $\lambda^*(g):=\lambda(g^{-1})^T$ for each $g\in\mathrm{SU}(m)$, acting on the vector space dual of λ's carrier space. Notably, λ^* is also irreducible, see Ref. [103, Proposition 4.22]. In a fixed orthonormal basis, we also have $\lambda^*\cong\bar{\lambda}$, where $\bar{\lambda}(g):=\overline{\lambda(g)}$ for each $g\in\mathrm{SU}(m)$ denotes the complex conjugate representation of λ (with respect to the fixed basis). For any irrep $\lambda=(\lambda_1,\dots,\lambda_m)$, this implies λ^* is identified by the *dual* Young diagram $\bar{\lambda}:=(\lambda_1-\lambda_m,\lambda_1-\lambda_{m-1},\dots,\lambda_1-\lambda_2,0)$. More practically, $\bar{\lambda}$ is constructed by completing λ to a $m\times\lambda_1$ rectangular Young diagram, and rotating the diagram formed by the

newly added boxes by 180°. For instance,

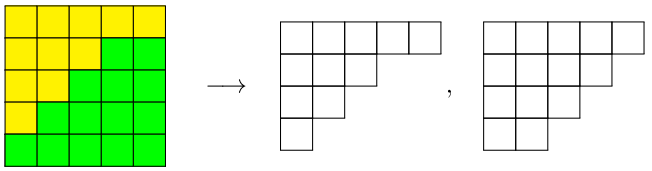

(A4)

are dual Young diagrams in SU(5).

A *semistandard Young tableaux* is a filling of a Young diagram with entries taken from any totally ordered set (here, $\mathbb{N}$) such that the entries are weakly increasing across each row and strictly increasing down each column. For instance,

1	1	2	2	3
2	2	3		
3	4			

,

1	1	1	1	1
2	2	3		
3	4			

(A5)

are semistandard Young tableaux of shape $\lambda = (5,3,2,0)$. For a fixed irrep λ of SU(m), the semistandard Young tableaux of shape λ label an orthonormal basis of λ, sometimes referred to as the *Weyl basis*. For instance, the Young tableaux

1	1
2	

,

1	1
3	

,

1	2
2	

,

1	2
3	

,

1	3
2	

,

1	3
3	

,

2	2
3	

,

2	3
3	

. (A6)

identify an orthonormal basis for the SU(3) adjoint irrep $\lambda = (2,1,0)$.

b. Gelfand-Tsetlin patterns

A more convenient way of labeling basis vectors for any irrep $\lambda = (\lambda_1, \ldots, \lambda_m)$ of SU(m) is by *Gelfand-Tsetlin (GT) patterns*. A GT pattern M of shape λ and length m is represented by a triangular table with m rows, the j th row containing j integers (counting from the bottom to the top)

$$M = \begin{pmatrix} M_{1,m} & & M_{2,m} & & \cdots & & M_{m-1,m} & & M_{m,m} \\ & M_{1,m-1} & & M_{2,m-1} & \cdots & M_{m-2,m-1} & & M_{m-1,m-1} & \\ & & \ddots & & \vdots & & \iddots & & \\ & & & M_{1,2} & & M_{2,2} & & & \\ & & & & M_{1,1} & & & & \end{pmatrix}, \tag{A7}$$

and $M_{i,m} = \lambda_i$ for every $i \in [m]$ (and, in particular, $M_{m,m} = 0$ by convention). The entries satisfy the *interlacing* or *inbetweenness* condition:

$$M_{i,j+1} \geq M_{i,j} \geq M_{i+1,j+1} \tag{A8}$$

for every $i \in [m-1]$ and $j \in [m-1]$. We remark that by convention the indices in a GT pattern are swapped, namely the first one is the column index (which is increasing from left to right, as usual), while the second one is the row index. We denote the set of GT patterns of shape λ by GT(λ).

An orthonormal basis for λ—referred as the Gelfand-Tsetlin basis—is given by state vectors $\{|M\rangle\}$, where M is a valid GT pattern with top row $\mathbf{M}_1 \equiv (M_{1,1}, \ldots, M_{1,m}) = \lambda$. Hence, the dimension of λ is equal to the number of such states, for which the following formula holds:

$$\dim \lambda = \prod_{1 \leq i \leq j \leq m} \left(1 + \frac{M_{i,m} - M_{j,m}}{j - i}\right). \tag{A9}$$

In terms of the GT basis, the highest weight vector of λ is identified by the pattern maximizing the inbetweenness conditions, namely

$$M_{\max} = \begin{pmatrix} M_{1,m} & & M_{2,m} & & \cdots & & M_{m-1,m} & & M_{m,m} \\ & M_{1,m} & & M_{2,m} & \cdots & M_{m-2,m} & & M_{m-1,m-1} & \\ & & \ddots & & \vdots & & \iddots & & \\ & & & M_{1,m} & & M_{2,m} & & & \\ & & & & M_{1,m} & & & & \end{pmatrix} \tag{A10}$$

(likewise, the lowest weight vector of λ is obtained by minimizing the inbetweenness conditions).

GT patterns are in one-to-one correspondence with semistandard Young tableaux. In fact, for a given Young tableau T of shape λ, the shape of the corresponding GT pattern M is the same shape as T and the entry $M_{j,k}$ of M (remember the different indexing in Eq. (A7) compared to matrix indices) is given by the number of entries in the jth row of T, which are less or equal than k. Conversely, given a GT pattern M of shape λ, the shape of the corresponding Young tableau T is determined by the first row of M and $M_{j,k} - M_{j,k-1}$ is the number of k's in the j'th row of T. Throughout this work, we assume that all illegal coefficients are set to 0. For instance, the Young tableaux in Eq. (A5) corresponds to the GT patterns

$$\begin{pmatrix} 5 & & 3 & & 2 & & 0 \\ & 5 & & 3 & & 2 & \\ & & 4 & & 2 & & \\ & & & 2 & & & \end{pmatrix}, \begin{pmatrix} 5 & & 3 & & 2 & & 0 \\ & 5 & & 3 & & 1 & \\ & & 5 & & 2 & & \\ & & & 5 & & & \end{pmatrix}, \tag{A11}$$

and the Weyl basis Eq. (A6) corresponds to the GT basis

$$\begin{pmatrix} 2 & & 1 & & 0 \\ & 2 & & 1 & \\ & & 2 & & \end{pmatrix}, \begin{pmatrix} 2 & & 1 & & 0 \\ & 2 & & 0 & \\ & & 2 & & \end{pmatrix}, \begin{pmatrix} 2 & & 1 & & 0 \\ & 2 & & 1 & \\ & & 1 & & \end{pmatrix}, \begin{pmatrix} 2 & & 1 & & 0 \\ & 2 & & 0 & \\ & & 1 & & \end{pmatrix},$$
$$\begin{pmatrix} 2 & & 1 & & 0 \\ & 1 & & 1 & \\ & & 1 & & \end{pmatrix}, \begin{pmatrix} 2 & & 1 & & 0 \\ & 1 & & 0 & \\ & & 1 & & \end{pmatrix}, \begin{pmatrix} 2 & & 1 & & 0 \\ & 2 & & 0 & \\ & & 0 & & \end{pmatrix}, \begin{pmatrix} 2 & & 1 & & 0 \\ & 1 & & 0 & \\ & & 0 & & \end{pmatrix}. \tag{A12}$$

For a given GT pattern M, the *weight* of $|M\rangle$ is the $(m-1)$-tuple $w_M := (w_1^{(M)}, \ldots, w_{m-1}^{(M)})$ introduced in Eq. (A2). Each entry $w_i^{(M)}$ can be determined by M as follows:

$$w_j^{(M)} = 2\sum_{i=1}^{j} M_{i,j} - \sum_{i=1}^{j-1} M_{i,j-1} - \sum_{i=1}^{j+1} M_{i,j+1}. \tag{A13}$$

We remark weights generalizes the notion of magnetic quantum number m for SU(2) in the quantum theory of angular momentum to arbitrary many modes. In the latter expression, we assume the convention that $\sum_{i=1}^{j-1} M_{i,j-1} = 0$ if $j = 1$.

All states $|M\rangle$ of the same weight w form a basis of the weight space of w. Note that these are typically not one dimensional, except for SU(2) [106–108]. For instance, the GT patterns

$$M = \begin{pmatrix} 3 & & 2 & & 0 \\ & 3 & & 0 & \\ & & 1 & & \end{pmatrix}, \quad \tilde{M} = \begin{pmatrix} 3 & & 2 & & 0 \\ & 2 & & 1 & \\ & & 1 & & \end{pmatrix} \tag{A14}$$

are such that $w^M = w^{\tilde{M}} = (-1, 0)$. Thus the dimension of the weight space of w (the inner multiplicity) corresponds to the number of GT states (or, equivalently, to the number of semistandard Young tableaux) with weight w. These amount to Kostka's numbers, and can be computed, e.g., with recursive algorithms [109].

It is worth recalling here a related definition of a *weight* for U(m) [or GL(m)] representations. Gelfand-Tsetlin patterns also label basis vectors of the corresponding irreps of such groups. However, the condition $M_{m,m} = 0$ is dropped. In this case, the weight of the GT pattern M is defined as $w^M_{\mathrm{U}(m)} := (w^M_{\mathrm{U}(m),1}, \ldots, w^M_{\mathrm{U}(m),m})$ with

$$w^M_{\mathrm{U}(m),j} := \sum_{i=1}^{j} M_{i,j} - \sum_{i=1}^{j-1} M_{i,j-1}, \tag{A15}$$

therefore

$$w_j^{(M)} = w^M_{\mathrm{U}(m),j} - w^M_{\mathrm{U}(m),j+1}. \tag{A16}$$

An equivalent definition that will be used in this work is the following: The *tableau weight* is the m-tuple $w^T = (w_1^T, \ldots, w_m^T)$ where w_i^T is the total number of i entries in T. If T is the semistandard Young tableau associated with M, we also have

$$w_j^T := \sum_{i=1}^{j} M_{i,j} - \sum_{i=1}^{j-1} M_{i,j-1}. \tag{A17}$$

The weights w_M and w^T are clearly related in a similar way:

$$w_j^{(M)} = w_j^T - w_{j+1}^T. \tag{A18}$$

We notice en passant that the tableau weight is always a sequence of non-negative integers, which sometimes

is more convenient for combinatorics. For instance, the tableaux T and $\tilde{T}$ associated with the GT patterns M and $\tilde{M}$ from the former examples are

$$T = \begin{array}{|c|c|c|}\hline 1&2&2\\\hline 3&3\\\cline{1-2}\end{array}, \quad \tilde{T} = \begin{array}{|c|c|c|}\hline 1&2&3\\\hline 2&3\\\cline{1-2}\end{array}$$

and we have $w^T = w^{\tilde{T}} = (1,2,2)$.

$$\tilde{M} = \begin{pmatrix} -M_{m,m} & & -M_{m-1,m} & & \cdots & & -M_{2,m} & & -M_{1,m} \\ & -M_{m-1,m-1} & & -M_{m-2,m-1} & \cdots & -M_{2,m-1} & & M_{1,m-1} & \\ & & \ddots & & \vdots & & \iddots & & \\ & & & -M_{2,2} & & -M_{1,2} & & & \\ & & & & -M_{1,1} & & & & \end{pmatrix}. \tag{A20}$$

By construction, $\bar{M}$ defines a basis state for the dual irrep $\lambda^* \cong \bar{\lambda}$. The conjugate operation is also such that each state $|M\rangle$ of λ is associated with a unique conjugate state $|\bar{M}\rangle$ of $\bar{\lambda}$. Specifically, the conjugation operation is such that [108]

$$|M\rangle = (-1)^{\varphi(M)}|\bar{M}\rangle, \tag{A21}$$

for a suitable phase function that can be determined as follows: For a GT pattern M, define the function

$$s_M(k) = \sum_{j=1}^{k}\sum_{i=1}^{j} M_{i,j}, \tag{A22}$$

which corresponds to the sum of the labels of M in the first k rows (counting from bottom to top). Then [108],

$$\varphi(M) = s_M(m-1) - s_{M_{\max}}(m-1), \tag{A23}$$

where $M_{\max}$ is defined in Eq. (A10). We remark that the latter holds up to a redefinition of every GT basis state by a global phase. In this work, we consider the Condon-Shortley convention that fixes the global phase in such a way that usual relations for SU(2) are retrieved.

d. Symmetric irreps in SU(m)

In this appendix, we summarize a few basic facts concerning symmetric irreps of SU(m), as they are of central importance throughout this work. By construction, the space of n particles over m modes is maximally symmetric under permutations over the modes. This implies that the action of $g \in \mathrm{SU}(m)$ on such a space is described by the irrep

$$\tau_n^m \equiv (n, \underbrace{0,\ldots,0}_{m-1}) = \underbrace{\square\cdots\square}_{n}, \tag{A24}$$

where the number of boxes has the interpretation of the number of particles in the system. Formally, the Young diagram on the right-hand side labels the maximally symmetric irrep in SU(m). Notably, the weights of the maximally symmetric irreps uniquely identify GT basis elements, as it can be easily checked via the associated tableaux weights.

In $\mathcal{H}_n^m$, a common orthonormal basis is the *Fock basis*, given by Fock states $\{|\mathbf{n}\rangle \mid \mathbf{n} \in \mathbb{N}^m, \sum_{i=1}^m n_i = n\}$. We remark that the GT basis, as well as the Weyl basis, labels the same set of orthonormal vectors as the Fock basis. In fact, for symmetric irreps, $\mathbf{n}$ is exactly the tableau weight of the corresponding Young tableau, i.e., n_i is the number of boxes filled with i for each $i \in [m]$, e.g.,

$$|3,2,1\rangle = \left|\begin{array}{|c|c|c|c|c|c|}\hline 1&1&1&2&2&3\\\hline\end{array}\right\rangle, \tag{A25}$$

from which follows the correspondence with the GT basis. In particular, for any Fock state $|\mathbf{n}\rangle = |n_1, \ldots, n_m\rangle$, the corresponding GT pattern—that will be denoted by N throughout this work—is given as follows:

$$N = \begin{pmatrix} n & & 0 & & \cdots & 0 & 0 \\ & \sum_{i=1}^{m-1} n_i & & 0 & \cdots\ 0 & & 0 \\ & & \ddots & & \vdots & \iddots & \\ & & & n_1 + n_2 & 0 & & \\ & & & & n_1 & & \end{pmatrix}. \tag{A26}$$

The complex conjugate representation (dual representation) on $\mathcal{H}_n^m \cong (\mathcal{H}_n^m)^*$ is identified by the Young diagram

$$\bar{\tau}_n^m = \begin{array}{l} m-1 \left\{ \begin{array}{|c|c|c|} \hline \quad & \cdots & \quad \\ \hline \vdots & \cdots & \vdots \\ \hline \quad & \cdots & \quad \\ \hline \end{array} \right. \\ \qquad\quad \underbrace{\qquad\qquad}_{n} \end{array}. \tag{A27}$$

Note that although $\bar{\tau}_n^m$ acts on $\mathcal{H}_n^m$, it is not symmetric (unless $m = 2$). We can construct the dual GT basis labeled by GT patterns $\bar{N}$ of the form [cf. Eqs. (A19) and (A26)]

$$\bar{N} = \begin{pmatrix} n & & n & & \cdots & & n & & 0 \\ & n & & n & \cdots & n & & n_m & \\ & & \ddots & & \vdots & & \iddots & & \\ & & & n & & \sum_{i=3}^{m} n_i & & & \\ & & & & \sum_{i=2}^{m} n_i & & & & \end{pmatrix}. \tag{A28}$$

By Eq. (A21), the dual GT basis again coincides with the Fock basis of $\mathcal{H}_n^m$, but modified with the phase function Eq. (A23).

Finally, unlike the general case of arbitrary irreps of SU(m), the weight spaces of symmetric irreps are clearly one dimensional: Each Fock state corresponds to one and only one Young tableau, as there are no degrees of freedom for box labeling. Weight spaces of dual symmetric irreps have the same property by duality.

e. Clebsch-Gordan coefficients

A crucial step for filtered RB is the decomposition of the reference representation into irreps. In this section, we recap the role of the Clebsch-Gordan series for SU(m) in the decomposition of any tensor-product representation, which will be employed in the remainder of this work. This topic has been investigated extensively over the years due to its relevance in particle physics, so we refer to standard references such as Refs. [74,110,111] for further details.

For two given irreps π_1, π_2 of SU(m), we consider the (completely reducible) tensor product representation $\pi_1 \otimes \pi_2 \colon \mathrm{SU}(m) \to \mathrm{U}(\mathcal{H}_{\pi_1} \otimes \mathcal{H}_{\pi_2})$. In the following, we will identify the carrier space $\mathcal{H}_\pi$ with π for any irrep of SU(m). By the compact version of Maschke's theorem [112, Theorem 5.2], we have

$$\pi_1 \otimes \pi_2 \simeq \bigoplus_{\lambda} \lambda^{\oplus m_\lambda}, \tag{A29}$$

where m_λ is the multiplicity of λ in $\pi_1 \otimes \pi_2$. For SU(m), such decomposition can be computed in terms of Young diagrams with *Littlewood-Richardson's rules* that we summarize in Appendix C.

In the context of second quantization, this decomposition can be interpreted as the generalization of the Clebsch-Gordan decomposition of sums of angular momenta in quantum mechanics [75,113–115]. In particular, there exists a unitary matrix C—here referred as the *Clebsch-Gordan matrix*—that realizes the isomorphism implicit in Eq. (A29):

$$C\,(\pi_1 \otimes \pi_2)\,C^\dagger = \bigoplus_{\lambda} \lambda \otimes \mathbb{1}_{m_\lambda}, \tag{A30}$$

where $\mathbb{1}_{m_\lambda}$ is the $m_\lambda \times m_\lambda$ identity matrix. We explicitly define C as the basis change matrix that takes the product GT basis on the left-hand side of Eq. (A30) to the union of GT bases of every λ on the right-hand side. More precisely, for GT patterns $M_1 \in \mathrm{GT}(\pi_1), M_2 \in \mathrm{GT}(\pi_2)$, we have

$$|M_1, M_2\rangle = \sum_{\lambda, r} \sum_{M \in \mathrm{GT}(\lambda)} C^{M,r}_{M_1,M_2} |M, r\rangle, \tag{A31}$$

where $r \in [m_\lambda]$ denotes the rth copy of λ in $\pi_1 \otimes \pi_2$. The matrix coefficients $C^{M,r}_{M_1,M_2}$ of C are called the *Clebsch-Gordan coefficients*. C is uniquely defined up to global phases, and by convention it is chosen to be real. Hence, we have the inverse transformation

$$|M, r\rangle = \sum_{M_1 \in \mathrm{GT}(\pi_1)} \sum_{M_2 \in \mathrm{GT}(\pi_2)} C^{M,r}_{M_1,M_2} |M_1, M_2\rangle. \tag{A32}$$

By unitarity of C, the following orthogonality relations hold true:

$$\sum_{\lambda, r} \sum_{M \in \mathrm{GT}(\lambda)} C^{M,r}_{M_1,M_2} C^{M,r}_{M_3,M_4} = \delta_{M_1,M_3} \delta_{M_2,M_4}, \tag{A33}$$

$$\sum_{M_1 \in \mathrm{GT}(\pi_1)} \sum_{M_2 \in \mathrm{GT}(\pi_2)} C^{M,r}_{M_1,M_2} C^{M',r'}_{M_1,M_2} = \delta_{M,M'} \delta_{r,r'}. \tag{A34}$$

As in the case of SU(2), selection rules for Clebsch-Gordan coefficients of SU(m) are available: For GT patterns $M_1 \in \mathrm{GT}(\pi_1), M_2 \in \mathrm{GT}(\pi_2), M \in \mathrm{GT}(\lambda)$, $C^{M,r}_{M_1,M_2} = 0$ if

$$w_M \neq w_{M_1} + w_{M_2}, \tag{A35}$$

where $w_{(\cdot)}$ is the weight defined in Eq. (A13).

2. Filtered randomized benchmarking

a. Filter functions

In Sec. II B, we introduced the filter function, Eq. (4), to isolate and analyze the exponential decays associated with each irrep of the reference representation ω_n^m. In this appendix, for the sake of completeness, we briefly motivate it in the bosonic case, before delving into the main technical results of this work. For a comprehensive discussion, we refer to Ref. [50].

In general, for an arbitrary compact group G represented by ω, an input state ρ and a POVM $\{|\mathbf{x}\rangle\langle\mathbf{x}|\}_{\mathbf{x}\in\Omega}$, one defines the filter function for an irrep $\lambda \subset \omega$ as

$$f_\lambda(\mathbf{x}, g) = \langle \mathbf{x}\,| P_\lambda \circ S^+ \circ \omega(g)^\dagger(\rho)\,|\mathbf{x}\rangle, \tag{A36}$$

where S^+ is the Moore-Penrose pseudoinverse of the *frame operator* S defined as

$$\begin{aligned} S &:= \int_\Omega d\mathbf{x} \int_G dg\ \mathrm{Tr}[\omega(g)^\dagger(|\mathbf{x}\rangle\langle\mathbf{x}|)(\cdot)]\,\omega(g)(|\mathbf{x}\rangle\langle\mathbf{x}|) \\ &= \int_G dg\,\omega(g)^\dagger \mathcal{M} \omega(g), \end{aligned} \tag{A37}$$

where $\mathcal{M} = \int_\Omega d\mathbf{x}\ \mathrm{Tr}[|\mathbf{x}\rangle\langle\mathbf{x}|(\cdot)]\,|\mathbf{x}\rangle\langle\mathbf{x}|$ is the (possibly infinite-dimensional) measurement channel associated with the POVM $\{|\mathbf{x}\rangle\langle\mathbf{x}|\}_{\mathbf{x}\in\Omega}$.

This choice of filter function is such that, in the ideal case of a noise-free, perfect implementation of the gates, the filtered RB signal is of the form $F_\lambda(l) = \mathrm{Tr}[\rho P_\lambda \circ S^+ \circ S(\rho)]$, where S^+S coincides with the projector onto the span of the POVM. In particular, in the case of an informationally complete POVM, $F_\lambda(l) = \mathrm{Tr}[\rho P_\lambda(\rho)]$, i.e., the filtered signal is the overlap of ρ with the filtering irrep.

Then, Eq. (4) follows from the following observation: As the reference representation $\omega = \omega_n^m := \tau_n^m(\cdot)\tau_n^{m\dagger}$ of $G = \mathrm{U}(m)$ preserves the number of particles, S acts nontrivially on the nth Fock sector only, i.e.,

$$S = \begin{pmatrix} \mathbf{0} & & & & & \\ & \ddots & & & & \\ & & \mathbf{0} & & & \\ & & & S^{(n)} & & \\ & & & & \mathbf{0} & \\ & & & & & \ddots \end{pmatrix}, \tag{A38}$$

where $S^{(n)}$ is obtained via the restriction of $\mathcal{M}$ to the subspace of n particles. Moreover, since ω_n^m decomposes as $\bigoplus_{k=0}^n \lambda_k$ (see Lemma 1), Schur's lemma implies [50]

$$S^{(n)} = \bigoplus_\lambda S^{(n)}_\lambda, \quad S^{(n)}_\lambda = s_\lambda \mathbb{1}_\lambda, \tag{A39}$$

where the direct sum is over all irreps of ω_n^m and, in general [50],

$$s_\lambda = d_\lambda^{-1}\,\mathrm{Tr}[P_\lambda \mathcal{M}] = d_\lambda^{-1} \int_\Omega d\mathbf{x}\ \mathrm{Tr}\left[|\mathbf{x}\rangle\langle\mathbf{x}| P_\lambda(|\mathbf{x}\rangle\langle\mathbf{x}|)\right]. \tag{A40}$$

Here, $d_\lambda \equiv \dim \mathcal{H}_\lambda$, with $\lambda \in \{\lambda_k\}_{k=0}^n$, and P_λ is the corresponding projector onto its carrier space. In the second step, we used the fact that the Bochner integral commutes with the trace since the latter is a continuous linear operator in the trace norm and the trace of $[|\mathbf{x}\rangle\langle\mathbf{x}|P_\lambda(|\mathbf{x}\rangle\langle\mathbf{x}|)]$ is finite.

b. Nonuniform sampling

The filtered RB framework is not restricted to Haar-random sampling and was, in fact, intentionally designed for nonuniform sampling, e.g., from generators of the considered group [50]. As this work builds on the filtered RB framework, it is straightforward to replace the Haar-random sampling in the passive RB protocol, Sec. II B, with the sampling from some other probability measure ν on U(m). For our results to uphold, it is sufficient that ν defines a random walk on U(m) that converges to the Haar measure μ_H, that is $\nu^{*l} \to \mu_H$ with $l \to \infty$. In fact, we only need that ν is suitably gapped with respect to the reference representation ω_n^m, this is that the *moment operator*

$$\mathsf{M}(\nu) := \int_{\mathrm{U}(m)} d\nu(g)\,\omega_n^m(g)^\dagger(\cdot)\omega_n^m(g), \tag{A41}$$

has a *spectral gap* $\Delta > 0$ such that

$$\|\mathsf{M}(\nu) - \mathsf{M}(\mu_H)\|_\infty \leq 1 - \Delta. \tag{A42}$$

This is for instance the case if ν has support on generators of $\mathrm{U}(m)$.

Using such a gapped probability measure ν instead of the Haar measure, typically has some advantages in practice. For instance, it might be easier to sample and to take some practical limitations into account (perhaps not all passive transformations are equally simple to implement). In particular, one can simply generate passive transformations using random beam splitters and single-mode rotations. Note that in such a case, the sequence length l changes its interpretation from the number of passive transformation to be applied to the number of *elementary* transformations. The filtered RB framework [50] then predicts that the sequence of elementary transformations has to be sufficiently long in order to "appear random enough" and this threshold l_0 scales with the inverse spectral gap Δ^{-1}. In practice, l_0 seems to be reasonably small such that we expect that already very short random sequences can be used for passive RB. In particular, this should outperform the quadratic depth needed to decompose Haar-random passive transformations in terms of elementary transformations.

3. Further notation

As the Clebsch-Gordan decomposition is naturally related with the direct sum decomposition of an Hilbert space of the form $\mathcal{H}_1 \otimes \mathcal{H}_2$, it will be convenient to introduce a vectorized notation for operators and superoperators on $\mathcal{H}_n^m$.

We consider the basis of linear operators for $\mathcal{B}(\mathcal{H}_n^m)$ given by $\Phi = \{|\mathbf{n}\rangle\langle\mathbf{m}|\}_{\mathbf{n},\mathbf{m}\in\mathbb{N}^m}$ with $\sum_{i=1}^m n_i = \sum_{i=1}^m m_i = n$. Any linear operator $A \in \mathcal{B}(\mathcal{H}_n^m)$ can be vectorized to an element $|A\rangle \in \mathcal{H}_n^m \otimes \mathcal{H}_n^m$ with respect to Φ as

$$|A\rangle = \sum_{\mathbf{n},\mathbf{m}} \langle \mathbf{n}\,|A\,|\mathbf{m}\rangle |\mathbf{n},\mathbf{m}\rangle, \quad |\mathbf{n},\mathbf{m}\rangle \equiv |\mathbf{n}\rangle \otimes |\mathbf{m}\rangle. \tag{A43}$$

Under vectorization, we have the induced mapping $\tau_n^m(\cdot)\tau_n^{m\dagger} \mapsto \tau_n^m \otimes \bar{\tau}_n^m$, where $\bar{\tau}_n^m$ denotes the complex conjugate representation of τ_n^m (in the Fock basis ϕ). Moreover, as long as it is clear from the context, we will not distinguish between superoperators and their corresponding quantities acting on $\mathcal{H}_1 \otimes \mathcal{H}_2$.

Then, the filter function defined in Eq. (4) becomes

$$f_\lambda(\mathbf{n}, g) = \frac{1}{s_\lambda} \langle \mathbf{n}_0, \mathbf{n}_0\,|P_\lambda(\tau_n^m \otimes \bar{\tau}_n^m)(g)^\dagger\,|\mathbf{n},\mathbf{n}\rangle, \tag{A44}$$

where $\rho = |\mathbf{n}_0\rangle\langle\mathbf{n}_0| \cong |\mathbf{n}_0,\mathbf{n}_0\rangle$ is the input state and $s_\lambda = (d_\lambda)^{-1} \sum_{\mathbf{n}\in\mathbb{N}^m} \langle \mathbf{n},\mathbf{n}\,|P_\lambda\,|\mathbf{n},\mathbf{n}\rangle$.

APPENDIX B: TECHNICAL DETAILS AND PROOFS

Here, we provide proofs for the theorems introduced in Sec. II: In Appendix B 2 we prove Theorem 1 and in Appendix B 3 we prove Theorem 2 based on notation and technical tools introduced in Appendix A 1. Throughout this appendix we assume that the number of modes is $m \geq 2$.

1. Clebsch-Gordan decomposition of the reference representation

In this appendix, we study the irrep decomposition of ω_n^m. From Sec. A 1, we have

$$\omega_n^m = \tau_n^m(\cdot)\tau_n^{m\dagger} \cong \tau_n^m \otimes \bar{\tau}_n^m, \tag{B1}$$

where again complex conjugate representation is taken in the Fock basis. We can restrict our focus to the irreps of $\mathrm{SU}(m)$ [or, equivalently, its corresponding Lie algebra $\mathfrak{su}(m)$] as τ_n^m can be extended to irreps of $\mathrm{U}(m)$ using nontrivial characters of the unit circle group [roughly speaking, resulting in a multiplication by a global phase, which vanishes in the conjugate action of $\mathcal{B}(\mathcal{H}_n^m)$]. The decomposition of ω_n^m into irreps can be computed using *Littlewood-Richardson's rules*, a general tool to classify the decomposition of tensor-product representations. We refer to Appendix C for a brief overview on how they can be employed in the context of $\mathrm{SU}(m)$.

Lemma 1. Let $\tau_n^m : \mathrm{SU}(m) \to \mathrm{U}(\mathcal{H}_n^m)$ be the irreducible representation of $\mathrm{SU}(m)$ on the space of n bosons distributed over m modes as in Eq. (A24). Define the Young diagram

$$\lambda_k \equiv \begin{array}{l} \overbrace{\square\cdots\square}^{k}\overbrace{\square\cdots\square}^{k} \\ m-1\left\{\begin{array}{l} \square\cdots\square\square\cdots\square \\ \vdots\quad\ddots\quad\vdots \\ \square\cdots\square \end{array}\right. \end{array}, \tag{B2}$$

where λ_0 and λ_1 denote the trivial irrep and the adjoint irrep of $\mathrm{SU}(m)$, respectively. Then, for any $n, m \in \mathbb{N} \setminus \{0\}$,

$$\omega_n^m = \bigoplus_{k=0}^{n} \lambda_k, \tag{B3}$$

where each λ_k, $k = 0, \ldots, n$, appears exactly one time.

Proof. We will prove the following equivalent fact by induction:

$$\omega_n^m = \lambda_n \oplus \omega_{n-1}^m, \quad \forall n \in \mathbb{N} \setminus \{0\}. \tag{B4}$$

First, notice that

$$\omega_1^m = \; m-1 \left\{ \begin{array}{c} \square\square \\ \vdots \\ \square \end{array} \right. \oplus \mathbf{1} \equiv \lambda_1 \oplus \omega_0^m \,, \tag{B5}$$

as $\omega_0^m = \mathbf{1}$ trivially.

The conjugate representation is associated with the tensor product of Young's diagrams

$$m-1 \left\{ \begin{array}{c} \overbrace{\square\cdots\square}^{n} \\ \vdots \quad \ddots \quad \vdots \\ \square\cdots\square \end{array} \right. \otimes \underbrace{\square\cdots\square}_{n} \tag{B6}$$

(swapping tensor factors does not influence the result). By Littlewood-Richardson's rules, we first have

$$m-1 \left\{ \begin{array}{c} \overbrace{\square\cdots\square}^{n} \\ \vdots \quad \ddots \quad \vdots \\ \square\cdots\square \end{array} \right. \otimes \overbrace{\boxed{a}\cdots\boxed{a}}^{n} = m-1 \left\{ \begin{array}{c} \overbrace{\square\cdots\square\boxed{a}}^{n} \\ \vdots \quad \ddots \quad \vdots \\ \square\cdots\square \end{array} \right. \otimes \overbrace{\boxed{a}\cdots\boxed{a}}^{n-1} \oplus m-1 \left\{ \begin{array}{c} \overbrace{\square\cdots\square}^{n-1} \\ \vdots \quad \ddots \quad \vdots \\ \square\cdots\square \end{array} \right. \otimes \overbrace{\boxed{a}\cdots\boxed{a}}^{n-1} . \tag{B7}$$

Notice that the second term in the right-hand side is by definition ω_{n-1}^m. Hence, we shall only prove that

$$m-1 \left\{ \begin{array}{c} \overbrace{\square\cdots\square\boxed{a}}^{n} \\ \vdots \quad \ddots \quad \vdots \\ \square\cdots\square \end{array} \right. \otimes \overbrace{\boxed{a}\cdots\boxed{a}}^{n-1} = \oplus_{k=0}^{n} \lambda_k \,. \tag{B8}$$

For this purpose, let us consider the factor

$$\tilde{\lambda}_r^{(s)} := m-1 \left\{ \begin{array}{c} \overbrace{\square\cdots\square}^{r}\overbrace{\boxed{a}\cdots\boxed{a}}^{s} \\ \vdots \quad \ddots \quad \vdots \\ \square\cdots\square \end{array} \right. . \tag{B9}$$

Clearly, $\tilde{\lambda}_r^{(r)} = \lambda_r$ and $\tilde{\lambda}_0^{(0)} = \mathbf{1}$. Notice that

$$\tilde{\lambda}_r^{(s)} \otimes \tau_l^m = \left(m-1 \left\{ \begin{array}{c} \overbrace{\square\cdots\square}^{r}\overbrace{\boxed{a}\cdots\boxed{a}}^{s+1} \\ \vdots \quad \ddots \quad \vdots \\ \square\cdots\square \end{array} \right. \oplus \left\{ \begin{array}{c} \overbrace{\square\cdots\square}^{r-1}\overbrace{\boxed{a}\cdots\boxed{a}}^{s} \\ \vdots \quad \ddots \quad \vdots \\ \square\cdots\square \end{array} \right. \right) \otimes \overbrace{\boxed{a}\cdots\boxed{a}}^{l-1} = \left(\tilde{\lambda}_r^{(s+1)} \oplus \tilde{\lambda}_{r-1}^{(s)} \right) \otimes \tau_{l-1}^m \,. \tag{B10}$$

With this notation, expanding the left-hand side of Eq. (B8) we get

$$\tilde{\lambda}_n^{(1)} \otimes \tau_{n-1}^m = \left(m-1 \left\{ \begin{array}{c} \overbrace{\square \cdots \square}^{n} \, a \, a \\ \vdots \quad \ddots \quad \vdots \\ \square \cdots \square \end{array} \right. \oplus \begin{array}{c} \overbrace{\square \cdots \square}^{n-1} \, a \\ \vdots \quad \ddots \quad \vdots \\ \square \cdots \square \end{array} \right) \otimes \overbrace{\boxed{a} \cdots \boxed{a}}^{n-2}$$

$$= \left(\tilde{\lambda}_n^{(2)} \oplus \tilde{\lambda}_{n-1}^{(1)}\right) \otimes \tau_{n-2}^m$$

$$= \left(\tilde{\lambda}_n^{(3)} \oplus \tilde{\lambda}_{n-1}^{(2)} \oplus \tilde{\lambda}_{n-1}^{(2)} \oplus \tilde{\lambda}_{n-2}^{(1)}\right) \otimes \tau_{n-3}^m$$

$$= \left(\tilde{\lambda}_n^{(3)} \oplus \tilde{\lambda}_{n-1}^{(2)} \oplus \tilde{\lambda}_{n-2}^{(1)}\right) \otimes \tau_{n-3}^m$$

$$\vdots$$

$$= \left(\tilde{\lambda}_n^{(i)} \oplus \tilde{\lambda}_{n-1}^{(i-1)} \oplus \cdots \oplus \tilde{\lambda}_{n-i+1}^{(1)}\right) \otimes \tau_{n-i}^m$$

$$\vdots$$

$$= \bigoplus_{i=0}^{n} \tilde{\lambda}_{n-i}^{(n-i)}$$

$$= \bigoplus_{k=0}^{n} \lambda_k \,. \tag{B11}$$

In the latter, we used the merging rule for Young's diagrams, see Appendix C. Finally, we have

$$\omega_n^m = \sum_{k=0}^{n} \lambda_k \oplus \omega_{n-1}^m = \sum_{k=0}^{n} \lambda_k \oplus \sum_{l=0}^{n-1} \lambda_l = \lambda_n \oplus \omega_{n-1}^m, \tag{B12}$$

by the merging rule again. ■

For instance, we have the following explicit decomposition for $n = m = 3$:

$$\omega_3^3 = \mathbf{1} \oplus \begin{array}{|c|c|}\hline \square & \square \\ \hline \square \\ \cline{1-1} \end{array} \oplus \begin{array}{|c|c|c|c|}\hline \square & \square & \square & \square \\ \hline \square & \square \\ \cline{1-2} \end{array} \oplus \begin{array}{|c|c|c|c|c|}\hline \square & \square & \square & \square & \square \\ \hline \square & \square & \square \\ \cline{1-3} \end{array}, \tag{B13}$$

since,

$$\begin{array}{|c|c|c|}\hline \square & \square & \square \\ \hline \square & \square & \square \\ \cline{1-3} \end{array} \otimes \begin{array}{|c|c|c|}\hline a & a & a \\ \cline{1-3} \end{array} = \left(\begin{array}{|c|c|c|c|}\hline \square & \square & \square & a \\ \hline \square & \square & \square \\ \cline{1-3} \end{array} \oplus \begin{array}{|c|c|}\hline \square & \square \\ \hline \square & \square \\ \cline{1-2} \end{array} \right) \otimes \begin{array}{|c|c|}\hline a & a \\ \cline{1-2} \end{array} \tag{B14}$$

$$= \left(\begin{array}{|c|c|c|c|c|}\hline \square & \square & \square & a & a \\ \hline \square & \square & \square \\ \cline{1-3} \end{array} \oplus \begin{array}{|c|c|c|}\hline \square & \square & a \\ \hline \square & \square \\ \cline{1-2} \end{array} \oplus \begin{array}{|c|}\hline \square \\ \hline \square \\ \cline{1-1} \end{array} \right) \otimes \begin{array}{|c|}\hline a \\ \cline{1-1} \end{array} \tag{B15}$$

$$= \begin{array}{|c|c|c|c|c|}\hline \square & \square & \square & a & a \\ \hline \square & \square & \square & a \\ \cline{1-4} \end{array} \oplus \begin{array}{|c|c|c|}\hline \square & \square & a & a \\ \hline \square & \square \\ \cline{1-2} \end{array} \oplus \begin{array}{|c|c|}\hline \square & a \\ \hline \square \\ \cline{1-1} \end{array} \oplus \mathbf{1} \,. \tag{B16}$$

The dimension of λ_k admits a nice closed-form expression in terms of the dimension of the number subspace,

$$\dim \mathcal{H}_k^m = \binom{k+m-1}{k}, \tag{B17}$$

as follows:

Proposition 2. For any $k \in \mathbb{N}$, set $d_{\lambda_k} \equiv \dim \lambda_k$. Then, the following holds:

$$d_{\lambda_k} = \left(1 - \frac{k^2}{(k+m-1)^2}\right) \left(\dim \mathcal{H}_k^m\right)^2$$

$$= \frac{2k+m-1}{m-1} \binom{k+m-2}{k}^2 . \tag{B18}$$

We prove this fact in Appendix D.

We remark that for the one-to-one correspondence of RB decays with irreps, it is important that the reference representation ω_n^m decomposes into *multiplicity-free* irreps [47,50]. Moreover, these irreps should be of *real type*. This is the case for the irreps $\lambda_k, k = 1, \ldots, n$, because each term in the decomposition is self-dual and multiplicity free [this can also be checked using, e.g., Ref. [104, Proposition 26.24], where all the complex, real, and quaternionic irreps of SU(m) are classified]. In general, both conditions are

not necessarily fulfilled, which can lead to more than one decay per irrep that may also be complex (i.e. oscillating).

2. Filter function for passive RB with PNR measurements

As the irrep decomposition of ω_n^m can be computed for any n and m (cf. Lemma 1), we can evaluate explicit expressions for the filter function. This will provide the proof of Theorem 1.

By construction, $\omega_n^m = \tau_n^m(\cdot)\tau_n^{m\dagger} \cong \tau_n^m \otimes \bar{\tau}_n^m$ acts on elements $|\mathbf{n}, \mathbf{n}\rangle$ (from here on referred as the uncoupled basis). However, as pointed out in Appendix A 1 b, the second entry shall be suitably interpreted as a basis element of $\bar{\tau}_n^m$, which requires the specification of the relative phases between states of τ_n^m and its dual. In particular, we have

$$|\mathbf{n}\rangle = |N\rangle = (-1)^{\varphi(N)}|\bar{N}\rangle, \tag{B19}$$

where $|N\rangle$ is the GT pattern defined in Eq. (A26), $|\bar{N}\rangle$ is the dual state, cf. Eq. (A19), and the relative phase is given in Eq. (A23). For the rest of this work, we fix the following notation: For each Fock state $|\mathbf{m}\rangle$, the corresponding GT pattern will be denoted with the corresponding Latin capital letter, namely the identification $|\mathbf{m}\rangle \equiv |M\rangle$ holds.

From previous considerations, it follows:

$$\begin{aligned}\rho \cong |\mathbf{n}_0, \mathbf{n}_0\rangle &= |N_0, N_0\rangle = (-1)^{\varphi(N_0)}|N_0, \bar{N}_0\rangle \\ &= (-1)^{\varphi(N_0)} \sum_{k=0}^{n} \sum_{M\in \mathrm{GT}(\lambda_k)} C^M_{N_0,\bar{N}_0}\, |M\rangle,\end{aligned} \tag{B20}$$

with $\{|M\rangle\}_{M\in\mathrm{GT}(\lambda_k)}$ being an orthonormal basis (referred as the coupled basis from here on) for the carrier space of λ_k. Notice that in Eq. (B20) we do not need to specify the multiplicity index of states and Clebsch-Gordan coefficients since λ_k is multiplicity free for each $k = 0, \ldots, n$.

Then, for a fixed irrep $\lambda \in \{\lambda_k\}_{k=0}^n$, we have $P_\lambda = \sum_{M\in\mathrm{GT}(\lambda)} |M\rangle\langle M|$ and the following relation holds true:

$$P_\lambda |N_0, \bar{N}_0\rangle = \sum_{M\in\mathrm{GT}(\lambda)} C^M_{N_0,\bar{N}_0} |M\rangle, \tag{B21}$$

We remark that—by the selection rules of Clebsch-Gordan coefficients Eq. (A35)—the sum is restricted to all the basis vectors such that the associated weight corresponds to the sum of the weights of the states $|N_0\rangle$ and $|\bar{N}_0\rangle$, cf. Eq. (A35). Specifically, by Eq. (A19), $C^M_{N_0,\bar{N}_0}$ is possibly nonzero provided that

$$\begin{aligned} w_j^{(M)} &= w_j^{(N_0)} + w_j^{(\bar{N}_0)} \\ &= 2\sum_{i=1}^{j} N_{i,j}^{(0)} - \left(\sum_{i=1}^{j-1} N_{i,j-1}^{(0)} + \sum_{i=1}^{j+1} N_{i,j+1}^{(0)}\right) \\ &\quad + 2\sum_{i=1}^{j} \bar{N}_{i,j}^{(0)} - \left(\sum_{i=1}^{j-1} \bar{N}_{i,j-1}^{(0)} + \sum_{i=1}^{j+1} \bar{N}_{i,j+1}^{(0)}\right) \\ &= 2\sum_{i=1}^{j} N_{1,m}^{(0)} - \left(\sum_{i=1}^{j-1} N_{1,m}^{(0)} + \sum_{i=1}^{j+1} N_{1,m}^{(0)}\right) \\ &= 0 \end{aligned} \tag{B22}$$

for each $j = 1, \ldots, m$, i.e. $w_{N_0} + w_{\bar{N}_0} = \mathbf{0}$.

Moreover, for the $\mathbf{0}$ weight spaces, the inner multiplicity $\gamma_{\lambda_k}(\mathbf{0})$ of $\mathbf{0}$ in λ_k can be easily computed, as we prove the following fact:

Lemma 2. Let λ_k be an irrep of SU(m) as in Eq. (B2) for any $k \in \mathbb{N}$. Then,

$$\gamma_{\lambda_k}(\mathbf{0}) = \binom{k+m-2}{k}. \tag{B23}$$

We prove this fact in Appendix E. This provides the number of (possibly) nonzero terms in Eq. (B21) and is relevant for the evaluation of the eigenvalues of the frame operator of passive RB with PNR measurements, for which we obtain the following simple expression:

Theorem 3. Let λ_k, $k = 0, \ldots, n$ be an irrep in ω_n^m. For a PNR measurement setting, the eigenvalues of the frame operator of the passive RB protocol are given by

$$s_{\lambda_k} = \frac{m-1}{2k+m-1}\gamma_{\lambda_k}(\mathbf{0})^{-1}, \tag{B24}$$

where $\gamma_{\lambda_k}(\mathbf{0})$ is as in Eq. (B23).

Proof. First, recall that a single mode (ideal) PNR detector measures the number of particles in such mode [116]. In the case of m modes, the (ideal) POVM is therefore given by $\{|\mathbf{n}\rangle\langle\mathbf{n}|\}_{\mathbf{n}\in\mathbb{N}^m}$ and the (vectorized) measurement channel can be written as

$$\mathcal{M} := \sum_{\mathbf{n}\in\mathbb{N}^m} |\mathbf{n}, \mathbf{n}\rangle\langle\mathbf{n}, \mathbf{n}| = \sum_{n=0}^{\infty} \sum_{n\in\mathrm{GT}(\tau_n^m)} |N, N\rangle\langle N, N|. \tag{B25}$$

Denoting by P_{λ_k} the projector onto $\lambda_k \in \hat{\omega}_n^m$, we have the following:

$$s_{\lambda_k} = \frac{1}{d_{\lambda_k}} \sum_{\mathbf{n}\in\mathbb{N}^m} \langle \mathbf{n}, \mathbf{n} | P_{\lambda_k} | \mathbf{n}, \mathbf{n} \rangle \tag{B26}$$

$$= \frac{1}{d_{\lambda_k}} \sum_{N\in \mathrm{GT}(\tau_n^m)} \langle N, N | P_{\lambda_k} | N, N \rangle \tag{B27}$$

$$= \frac{1}{d_{\lambda_k}} \sum_{N\in \mathrm{GT}(\tau_n^m)} (-1)^{2\varphi(N)} \langle N, \bar{N} | P_{\lambda_k} | N, \bar{N} \rangle \tag{B28}$$

$$= \frac{1}{d_{\lambda_k}} \sum_{N\in \mathrm{GT}(\tau_n^m)} \sum_{M\in \mathrm{GT}(\lambda_k)} |C^M_{N,\bar{N}}|^2 , \tag{B29}$$

where in the second step we used the fact that P_{λ_k} acts nontrivially on the n particle subspace, and in the fourth step we used the fact that the phases $\varphi(N)$ introduced in the labeling of GT dual patterns are integers by construction, see Eq. (A23). Finally, recall that the nontrivial Clebsch-Gordan coefficients are determined by the selection rule $w_M = w_N + w_{\bar{N}} = 0$. Moreover, symmetric irreps of SU(m)—and their dual—preserve the 1-to-1 correspondence between weights and basis vectors, see Appendix A 1 d. This implies

$$\sum_{N\in \mathrm{GT}(\tau_n^m)} |C^M_{N,\bar{N}}|^2 = \sum_{N\in \mathrm{GT}(\tau_n^m)} \sum_{\bar{N}'\in \mathrm{GT}(\bar{\tau}_n^m)} C^M_{N,\bar{N}'} C^M_{N,\bar{N}'} = 1 \tag{B30}$$

by orthogonality relations, cf. Eq. (A33). Therefore,

$$s_{\lambda_k} = \frac{\gamma_{\lambda_k}(\mathbf{0})}{d_{\lambda_k}} \tag{B31}$$

and the assertion follows from Eq. (B23) and Proposition 2. ■

Notice that s_{λ_k} scales exponentially in both k and m. In particular, in the case $k = n = m$, it is proportional to the mth Catalan number, and it scales as $\mathrm{O}(4^m/\sqrt{m})$ for large values of m.

Theorem 4 (Restatement of Theorem 1—PNR version). Let $\rho = |\mathbf{n}_0\rangle\langle\mathbf{n}_0| \cong |\mathbf{n}_0, \mathbf{n}_0\rangle = |N_0, N_0\rangle$ be a m modes state and let $\{|\mathbf{n}\rangle\langle\mathbf{n}|\}_{\mathbf{n}\in\mathbb{N}^m}$ be the Fock state POVM. Let N be the GT pattern associated with $\mathbf{n}$. Then, for a given irrep $\lambda_k \in$ in ω_n^m, and assuming $s_{\lambda_k} \neq 0$,

$$f_{\lambda_k}(\mathbf{n}, g) = \frac{1}{s_{\lambda_k}} \frac{(-1)^{\varphi(N_0)}}{\mathbf{n}!} \sum_{M\in \mathrm{GT}(\lambda_k)} C^M_{N_0,\bar{N}_0} \times \sum_{N'\in \mathrm{GT}(\tau_n^m)} \frac{(-1)^{\varphi(N')}}{\mathbf{n}'!} C^M_{N',\bar{N}'} \left|\mathrm{Per}(g_{\mathbf{n},\mathbf{n}'})\right|^2 , \tag{B32}$$

where s_{λ_k} is evaluated in Theorem 3, the sums are restricted to all basis states such that Eq. (B22) is satisfied and $\mathrm{Per}(g_{\mathbf{n},\mathbf{m}})$ denotes the permanent of the matrix obtained by g by taking m_j copies of the jth column of U and then by taking n_i copies of the ith row of the resulting matrix, and we used the multi-index notation $\mathbf{n}! := n_1! \dots n_m!$.

Proof. By Eq. (B20), and denoting by N_0 and N the GT patterns associated with $\mathbf{n}_0$ and $\mathbf{n}$, respectively, the filter function defined in Eq. (4) becomes

$$f_{\lambda_k}(N, g) = \frac{1}{s_{\lambda_k}} \langle N_0, N_0 | P_{\lambda_k} \tau_n^m \otimes \bar{\tau}_n^m(g)^\dagger | N, N \rangle \tag{B33}$$

$$= \frac{1}{s_{\lambda_k}} (-1)^{\varphi(N_0)} \sum_{M\in \mathrm{GT}(\lambda_k)} C^M_{N_0,\bar{N}_0} \langle M | (\tau \otimes \bar{\tau})(g)^\dagger | N, N \rangle \tag{B34}$$

$$= \frac{1}{s_{\lambda_k}} (-1)^{\varphi(N_0)} \sum_{M\in \mathrm{GT}(\lambda_k)} C^M_{N_0,\bar{N}_0} \times \sum_{N_1,N_2\in \mathrm{GT}(\tau_n^m)} C^M_{N_1,\bar{N}_2} \langle N_1, \bar{N}_2 | \tau_n^m \otimes \bar{\tau}_n^m(g)^\dagger | N, N \rangle \tag{B35}$$

$$= \frac{1}{s_{\lambda_k}} (-1)^{\varphi(N_0)} \sum_{M\in \mathrm{GT}(\lambda_k)} C^M_{N_0,\bar{N}_0} \sum_{N_1,N_2\in \mathrm{GT}(\tau_n^m)} (-1)^{\varphi(N_2)} \times C^M_{N_1,\bar{N}_2} \langle N_1, N_2 | \tau_n^m \otimes \bar{\tau}_n^m(g)^\dagger | N, N \rangle, \tag{B36}$$

where in Eq. (B33) we used Eq. (B21) and relabeled the second entries as dual basis vectors by introducing the corresponding relative phases [cf. Eq. (A23)]. In Eq. (B34), we used the Clebsch-Gordan decomposition $M = \sum_{N_1,N_2} C^M_{N_1,\bar{N}_2} |N_1, \bar{N}_2\rangle$, and in Eq. (B35) we relabeled $\bar{N}_2$ as a basis vector for τ_n^m. In particular, the latter implies that f_{λ_k} is manifestly related to the computation of permanents [76], as each inner product resembles the boson sampling problem when expressed in the Fock basis:

$$\langle N_1, N_2 | \tau_n^m \otimes \bar{\tau}_n^m(g)^\dagger | N, N \rangle$$

$$= \langle \mathbf{n}_1, \mathbf{n}_2 | \tau_n^m \otimes \bar{\tau}_n^m(g)^\dagger | \mathbf{n}, \mathbf{n} \rangle \tag{B37}$$

$$= \langle \mathbf{n}_1 | \tau_n^m(g)^\dagger | \mathbf{n} \rangle \langle \mathbf{n} | \tau_n^m(g) | \mathbf{n}_2 \rangle \tag{B38}$$

$$= \frac{1}{\mathbf{n}!\sqrt{\mathbf{n}_1!\mathbf{n}_2!}} \mathrm{Per}(g^\dagger_{\mathbf{n}_1,\mathbf{n}}) \mathrm{Per}(g_{\mathbf{n},\mathbf{n}_2}). \tag{B39}$$

Finally, since weights for symmetric irreps of SU(m) uniquely identify basis vectors, by selection rules of Clebsch-Gordan coefficients we have that $N_2 = N_1$ [see also Eq. (B30)], and the assertion follows by plugging in Theorem 3. ■

Clebsch-Gordan coefficients can be calculated in polynomial time [75] for approximately 20 modes before memory overhead limits the application of such algorithms [84]. We remark that—using exact formulae for CG coefficients for $\tau_n^m \otimes \bar{\tau}_n^m$ from Ref. [89]—one can compute the necessary Clebsch-Gordan coefficients for a higher number of modes m. Hence, the computational hardness of f_{λ_k} comes from the evaluation of the permanents appearing in Eq. (B32).

Alternatively, f_{λ_k} can be expressed as a linear combination of matrix coefficients of λ_k (in the corresponding GT basis). To show this fact, we introduce the following technical result that will be used extensively in the rest of this work:

Lemma 3. Let N, X be GT patterns, and let $\bar{N}, \bar{X}$ be their dual, respectively. Let τ_n^m be the n particles maximally symmetric irrep of SU(m) and consider $\lambda_k \in \omega_n^m \cong \tau_n^m \otimes \bar{\tau}_n^m$. Let P_{λ_k} be the projector onto λ_k. Then, the following holds:

$$\langle N, \bar{N} | P_{\lambda_k} (\tau_n^m \otimes \bar{\tau}_n^m)(g)^\dagger | X, \bar{X} \rangle = \sum_{M \in \mathrm{GT}(\lambda_k)} C^M_{N,\bar{N}} \sum_{M' \in \mathrm{GT}(\lambda_k)} C^{M'}_{X,\bar{X}} \langle M | \lambda_k(g)^\dagger | M' \rangle. \tag{B40}$$

Proof. By construction, P_{λ_k} selects the λ_kth component of $|N, \bar{N}\rangle$, which can be conveniently isolated by the Clebsch-Gordan decomposition of $\omega_n^m \cong \tau_n^m \otimes \bar{\tau}_n^m$. This implies

$$\langle N, \bar{N} | P_{\lambda_k} (\tau_n^m \otimes \bar{\tau}_n^m)(g)^\dagger | X, \bar{X} \rangle = \sum_{M \in \mathrm{GT}(\lambda_k)} C^M_{N,\bar{N}} \langle M | \tau_n^m \otimes \bar{\tau}_n^m(g)^\dagger | X, \bar{X} \rangle . \tag{B41}$$

To compute the inner product, recall that $\tau_n^m \otimes \bar{\tau}_n^m = \bigoplus_{l=0}^n \lambda_l$ [cf. Eq. (B3)]. In particular, observe that M is a basis element in λ_k, which implies the only nontrivial contributions from $\tau_n^m \otimes \bar{\tau}_n^m$ are associated with its λ_kth component. Likewise, the only relevant contributions to the inner product coming from $|X, \bar{X}\rangle$ are associated with its restriction to λ_k that can be expressed as

$$|X, \bar{X}\rangle\big|_{\lambda_k} = \sum_{M' \in \mathrm{GT}(\lambda_k)} C^{M'}_{X,\bar{X}} |M'\rangle. \tag{B42}$$

Hence,

$$\langle M | \tau_n^m \otimes \bar{\tau}_n^m(g)^\dagger | X, \bar{X} \rangle = \sum_{M' \in \mathrm{GT}(\lambda_k)} C^{M'}_{X,\bar{X}} \langle M | \lambda_k(g)^\dagger | M' \rangle, \tag{B43}$$

from which the assertion follows. ■

As mentioned before, a first consequence is the following explicit expression for the filter function.

Corollary 1. For a given irrep $\lambda_k \in \hat{\omega}_n^m$, and assuming $s_{\lambda_k} \neq 0$, the following holds true:

$$f_{\lambda_k}(\mathbf{n}, g) = \frac{1}{s_{\lambda_k}} (-1)^{\varphi(N_0)+\varphi(N)} \sum_{M \in \mathrm{GT}(\lambda_k)} C^M_{N_0,\bar{N}_0} \times \sum_{M' \in \mathrm{GT}(\lambda_k)} C^{M'}_{N,\bar{N}} \langle M | \lambda_k(g)^\dagger | M' \rangle, \tag{B44}$$

where the sums are restricted to all basis states such that Eq. (B22) is satisfied.

Proof. By Eq. (B20), and denoting by N_0 and N the GT patterns associated with $\mathbf{n}_0$ and $\mathbf{n}$, respectively, the filter function defined in Eq. (4) becomes

$$f_{\lambda_k}(N, g) = \frac{1}{s_{\lambda_k}} \langle N_0, N_0 | P_{\lambda_k} (\tau_n^m \otimes \bar{\tau}_n^m)(g)^\dagger | N, N \rangle \tag{B45}$$

$$= \frac{1}{s_{\lambda_k}} (-1)^{\varphi(N_0)+\varphi(N)} \langle N_0, \bar{N}_0 | P_{\lambda_k} (\tau_n^m \otimes \bar{\tau}_n^m)(g)^\dagger | N, \bar{N} \rangle \tag{B46}$$

$$= \frac{1}{s_{\lambda_k}} (-1)^{\varphi(N_0)+\varphi(N)} \sum_{M \in \mathrm{GT}(\lambda_k)} C^M_{N_0,\bar{N}_0} \times \sum_{M' \in \mathrm{GT}(\lambda_k)} C^{M'}_{N,\bar{N}} \langle M | \lambda_k(g)^\dagger | M' \rangle. \tag{B47}$$

In the last line, we used Lemma 3. ■

Notably, explicit expressions for the matrix elements of irreps of SU(m) are also available, see for instance [90, Chapter 3] for SU(2) and [91, Chapter 9] for SU(m). Moreover, numerical implementations of the bosonic realization of $\mathfrak{su}(m)$ are available [77] and matrix coefficients can be expressed as suitable permanents of $\lambda_k(g)$.

3. Moments of the filter function for PNR measurement settings

In this appendix, we provide explicit expressions for the first two moments of the filter function (4) with respect to the ideal probability distribution $p(\mathbf{n}|g) = \langle \mathbf{n}|\omega_n^m(g)(\rho)|\mathbf{n}\rangle$, $\mathbf{n} \in \mathbb{N}^m$. In particular, the ideal second moment will provide an upper bound to the sampling complexity of the protocol, cf. Sec. II C. Throughout this appendix dg denotes the Haar measure on SU(m).

The following technical result will be useful.

Lemma 4. Let N, X be GT patterns, and let $\bar{N}, \bar{X}$ be their dual, respectively. Let τ_n^m be the n particles maximally symmetric irrep of SU(m) and let λ_k be an irrep in ω_n^m. Then, the following holds:

$$\langle X, \bar{X}|(\tau_n^m \otimes \bar{\tau}_n^m)(g)|N, \bar{N}\rangle = \sum_{j=0}^{n} \sum_{M,M' \in \mathrm{GT}(\lambda_j)} C_{X,\bar{X}}^{M} C_{N,\bar{N}}^{M'} \langle M|\lambda_j(g)|M'\rangle . \tag{B48}$$

Proof. The expression follows immediately from the Clebsch-Gordan decomposition. More specifically, we have

$$|N, \bar{N}\rangle = \sum_{i=0}^{n} \sum_{M \in \mathrm{GT}(\lambda_i)} C_{N,\bar{N}}^{M} |M\rangle, \tag{B49}$$

$$|M, \bar{M}\rangle = \sum_{j=0}^{n} \sum_{M' \in \mathrm{GT}(\lambda_j)} C_{X,\bar{X}}^{M'} |M'\rangle, \tag{B50}$$

$$\tau_n^m \otimes \bar{\tau}_n^m = \bigoplus_{k=0}^{n} \lambda_k, \tag{B51}$$

cf. Eqs. (B20) and (B3). Hence, since M and M' are basis elements of λ_i and λ_j, respectively,

$$\langle M|\lambda_k(g)|M'\rangle \neq 0 \tag{B52}$$

only if $i = j = k$, from which the assertion follows. ■

We will also need the following standard result in the representation theory of compact groups, often referred as Schur's orthogonality relations, see Ref. [112, Theorem 5.8]: For a given irrep λ of SU(m) (or, in general, of any compact group G), if $M_1, M_2, M_1', M_2' \in \mathrm{GT}(\lambda)$, then the following relation holds true:

$$\int dg\, \langle M_1|\lambda(g)|M_1'\rangle \langle M_2|\lambda(g)^\dagger|M_2'\rangle = \frac{1}{d_\lambda} \delta_{M_1,M_2} \delta_{M_1',M_2'}, \tag{B53}$$

where dg denotes the Haar measure on G.

Before we prove the main results of this appendix, it is worthwhile to quickly consider the first moment $\mathbb{E}[f_{\lambda_k}]$, as the proof scheme is the same, but in the case of the second moment is hidden behind additional technical details concerning the representations involved.

Lemma 5. For a PNR measurement setting, $\rho = |\mathbf{n}_0\rangle\langle\mathbf{n}_0|$ as input state, and an irrep λ_k of $\omega^{(n)} = \tau_n^m(\cdot)\tau_n^{m\dagger}$, the following holds:

$$\mathbb{E}[f_{\lambda_k}] = \sum_{M \in \mathrm{GT}(\lambda_k)} \left| C_{N_0,\bar{N}_0}^{M} \right|^2, \tag{B54}$$

where N_0 is the GT pattern associated with $\mathbf{n}_0$, and $\bar{N}_0$ is its dual.

Proof. Since ρ is an n-particle state and ω_n^m is a passive transformation, the outcome of a PNR measurement must also be an n-particle Fock state. Hence, we have

$$\mathbb{E}[f_{\lambda_k}] := \frac{1}{s_{\lambda_k}} \sum_{\mathbf{n} \in \mathcal{H}_n^m} \int dg\, \langle \mathbf{n}_0, \mathbf{n}_0|P_{\lambda_k}(\tau_n^m \otimes \bar{\tau}_n^m)(g)^\dagger|\mathbf{n}, \mathbf{n}\rangle \times \langle \mathbf{n}, \mathbf{n}|(\tau_n^m \otimes \bar{\tau}_n^m)(g)|\mathbf{n}_0, \mathbf{n}_0\rangle \tag{B55}$$

$$= \frac{1}{s_{\lambda_k}} \sum_{N \in \mathrm{GT}(\tau_n^m)} \int dg\, \langle N_0, \bar{N}_0|P_{\lambda_k}(\tau_n^m \otimes \bar{\tau}_n^m)(g)^\dagger \times |N, \bar{N}\rangle\langle N, \bar{N}|(\tau_n^m \otimes \bar{\tau}_n^m)(g)|N_0, \bar{N}_0\rangle \tag{B56}$$

$$= \frac{1}{s_{\lambda_k}} \sum_{M \in \mathrm{GT}(\lambda_k)} C_{N_0,\bar{N}_0}^{M} \sum_{N \in \mathrm{GT}(\tau_n^m)} \int dg \times \langle M|\lambda_k(g)^\dagger|N, \bar{N}\rangle\langle N, \bar{N}|\bigoplus_{j=0}^{n} \lambda_j(g)|N_0, \bar{N}_0\rangle. \tag{B57}$$

The second line follows since the relative phases between $|M\rangle$ and $|\bar{M}\rangle$ highlighted in Eq. (A21) are integers and they appear an even number of times. In the third step, we projected $|N_0, \bar{N}_0\rangle$ onto its λ_kth component, see Eq. (B21). Accordingly, the only nontrivial contribution to the integral is determined by the λ_kth component of $\tau_n^m \otimes \bar{\tau}_n^m$. Similarly, by orthogonality relations, the integral is nonzero only if $\lambda_j = \lambda_k$. Hence, it is enough to consider the restricted Clebsch-Gordan decomposition to the λ_kth irrep, and the following holds:

$$\mathbb{E}[f_{\lambda_k}] = \frac{1}{s_{\lambda_k}} \sum_{M\in\mathrm{GT}(\lambda_k)} C^{M}_{N_0,\bar{N}_0} \sum_{N\in\mathrm{GT}(\tau_n^m)} \int dg\, \langle M\,|\lambda_k(g)^\dagger|\,N,\bar{N}\rangle\langle N,\bar{N}\,|\lambda_k(g)\,|N_0,\bar{N}_0\rangle \tag{B58}$$

$$= \frac{1}{s_{\lambda_k}} \sum_{M\in\mathrm{GT}(\lambda_k)} C^{M}_{N_0,\bar{N}_0} \sum_{N\in\mathrm{GT}(\tau_n^m)} \sum_{M_1,M_2,M_3\in\mathrm{GT}(\lambda_k)} C^{M_1}_{N,\bar{N}} C^{M_2}_{N,\bar{N}} C^{M_3}_{N_0,\bar{N}_0} \tag{B59}$$

$$\times \underbrace{\int dg\, \langle M\,|\lambda_k(g)^\dagger|\,M_1\rangle\langle M_2\,|\lambda_k(g)\,|M_3\rangle}_{=\frac{1}{d_{\lambda_k}}\delta_{M,M_3}\delta_{M_1,M_2}} \tag{B60}$$

$$= \frac{1}{d_{\lambda_k}}\frac{1}{s_{\lambda_k}} \sum_{M\in\mathrm{GT}(\lambda_k)} \left|C^{M}_{N_0,\bar{N}_0}\right|^2 \sum_{N\in\mathrm{GT}(\tau_n^m)} \sum_{M_1\in\mathrm{GT}(\lambda_k)} \left|C^{M_1}_{N,\bar{N}}\right|^2 \tag{B61}$$

$$= \sum_{M\in\mathrm{GT}(\lambda_k)} \left|C^{M}_{N_0,\bar{N}_0}\right|^2. \tag{B62}$$

In the second step, we expanded $|N,\bar{N}\rangle, |N_0,\bar{N}_0\rangle$ in the coupled basis, and restricted the decompositions to the λ_kth components. In the third step, we used Schur's orthogonality relations to compute the integral, and in the final step we used the definition of the frame operator, and in particular the result in Theorem 3. ■

In general, finding explicit expressions for the second moment $\mathbb{E}[f_\lambda{}^2]$ is more involved and the following technical result is necessary.

Lemma 6. Let λ_k be a Young diagram as in Eq. (B2) labeling an irrep of SU(m), $m \geq 3$. Then,

$$\lambda_k \otimes \lambda_k = \bigoplus_{l=0}^{k} \lambda_l^{(l+1)} \oplus \bigoplus_{l=k+1}^{2k} \lambda_l^{(2k-l+1)} \oplus L\,, \tag{B63}$$

where $\lambda_0 \equiv \mathbf{1}$, $\lambda_1 \equiv \mathrm{Ad}$, $\lambda_j^{(i)}$ denotes the ith copy of λ_j in $\lambda_l^{\otimes 2}$, and L is a suitable direct sum of irreps, which are not of the form λ_l for any $l \in \mathbb{N}$.

Specifically, all irreps λ_l in $\lambda_k^{\otimes 2}$ are computed by identifying all admissible ways of combining two copies of λ_k to a fixed shape using Littlewood-Richardson's rules. This result is proved in Appendix F.

Hence, we derive an explicit expression for $\mathbb{E}[f_{\lambda_k}{}^2]$ using Eq. (B53).

Theorem 5. For a PNR measurement setting, $\rho = |\mathbf{n}_0\rangle\langle\mathbf{n}_0|$ as input state, and an irrep λ_k of ω_n^m, the following holds:

$$\mathbb{E}[f_{\lambda_k}^2] = \frac{1}{s_{\lambda_k}^2}(-1)^{\varphi(N_0)} \sum_{N\in\mathrm{GT}(\tau_n^m)} (-1)^{\varphi(N)} g_k(N,N_0), \tag{B64}$$

where $g_k(N,N_0)$ is a function of Clebsch-Gordan coefficients of the representations $\tau_n^m \otimes \bar{\tau}_n^m$ and $\lambda_k^{\otimes 2}$ given by

$$g_k(N,N_0) = \sum_{l=0}^{\min(n,2k)} \frac{1}{d_{\lambda_l}} \sum_{r=1}^{m_l} \sum_{\substack{M,M'\in\mathrm{GT}(\lambda_k)\\ L,L'\in\mathrm{GT}(\lambda_k)\\ R,R'\in\mathrm{GT}(\lambda_l)}} C^{M}_{N_0,\bar{N}_0} C^{M'}_{N_0,\bar{N}_0} \times C^{R}_{N_0,\bar{N}_0} C^{L}_{N,\bar{N}} C^{L'}_{N,\bar{N}} C^{R'}_{N,\bar{N}} C^{R,r}_{M,M'} C^{R',r}_{L,L'}, \tag{B65}$$

where m_l is the multiplicity of λ_l in $\lambda_k^{\otimes 2}$ as in Lemma 6 and $d_{\lambda_l} \equiv \dim \lambda_l$.

Proof. For any irrep $\lambda_k \in \hat{\omega}_n^m$, and by relabeling the second entries as basis elements of the dual irrep $\bar{\tau}_n^m$, the

second moment can be expressed as follows:

$$\begin{aligned}\mathbb{E}[f_{\lambda_k}^2] :=& \frac{1}{s_{\lambda_k}^2}\sum_{\mathbf{n}\in\mathcal{H}_n^m}\int dg\,\langle \mathbf{n}_0,\mathbf{n}_0\,|P_{\lambda_k}(\tau_n^m\otimes\bar{\tau}_n^m)(g)^\dagger\,|\mathbf{n},\mathbf{n}\rangle^2\\ &\times\langle \mathbf{n},\mathbf{n}\,|\tau_n^m\otimes\tau_n^m(g)\,|\mathbf{n}_0,\mathbf{n}_0\rangle\\ =& \frac{1}{s_{\lambda_k}^2}\sum_{N\in\mathrm{GT}(\tau_n^m)}\int dg\,\langle N_0,N_0\,|P_{\lambda_k}(\tau_n^m\otimes\bar{\tau}_n^m)(g)^\dagger\\ &\times|N,N\rangle^2\langle N,N\,|\tau_n^m\otimes\tau_n^m(g)\,|N_0,N_0\rangle\\ =& \frac{1}{s_{\lambda_k}^2}\sum_{N\in\mathrm{GT}(\tau_n^m)}(-1)^{\varphi(N_0)+\varphi(N)}\\ &\times\int dg\,\langle N_0,\bar{N}_0\,|P_{\lambda_k}(\tau_n^m\otimes\bar{\tau}_n^m)(g)^\dagger\,|N,\bar{N}\rangle^2\\ &\times\langle N,\bar{N}\,|\tau_n^m\otimes\tau_n^m(g)\,|N_0,\bar{N}_0\rangle\\ =& \frac{1}{s_{\lambda_k}^2}(-1)^{\varphi(N_0)}\sum_{N\in\mathrm{GT}(\tau_n^m)}(-1)^{\varphi(N)}g_k(N,N_0),\end{aligned}\tag{B66}$$

where

$$\begin{aligned}g_k(N,N_0)\equiv&\int dg\,\langle N_0,\bar{N}_0\,|P_{\lambda_k}(\tau_n^m\otimes\bar{\tau}_n^m)(g)^\dagger\,|N,\bar{N}\rangle^2\\ &\times\langle N,\bar{N}\,|\tau_n^m\otimes\tau_n^m(g)\,|N_0,\bar{N}_0\rangle.\end{aligned}\tag{B67}$$

By Lemmas 4 and 3, we obtain

$$\begin{aligned}g_{k,l}(N,N_0)=&\sum_{M,M'\in\mathrm{GT}(\lambda_k)}C_{N_0,\bar{N}_0}^{M}C_{N_0,\bar{N}_0}^{M'}\sum_{L,L'\in\mathrm{GT}(\lambda_k)}\\ &\times C_{N,\bar{N}}^{L}C_{N,\bar{N}}^{L'}\sum_{j=0}^{n}\sum_{J,J'\in\mathrm{GT}(\lambda_j)}C_{N,\bar{N}}^{J}C_{N_0,\bar{N}_0}^{J'}\\ &\times\underbrace{\int dg\,\langle M,M'\,|\lambda_k(g)^{\dagger\otimes 2}\,|L,L'\rangle\langle J\,|\lambda_j(g)\,|J'\rangle}_{\equiv I}.\end{aligned}\tag{B68}$$

We compute the integral with Schur's orthogonality relations. Specifically, this requires the irrep decomposition of $\lambda_k^{\otimes 2}$: By Lemma 6, we have

$$\langle M,M'\,|\lambda_k(g)^{\dagger\otimes 2}\,|L,L'\rangle=\langle M,M'\,|\bigoplus_{l=0}^{2k}\lambda_l^{\oplus m_l}(g)^\dagger\,|L,L'\rangle,\tag{B69}$$

where $m_l\in\{0,1,\ldots,k\}$ is the multiplicity of λ_l in $\lambda_k^{\otimes 2}$ worked out in Lemma 6. Then, consider the following Clebsch-Gordan decompositions:

$$|M,M'\rangle=\sum_{i=0}^{2k}\sum_{r_i=1}^{m_i}\sum_{R\in\mathrm{GT}(\lambda_i)}C_{M,M'}^{R,r_i}|R,r_i\rangle,\tag{B70}$$

$$|L,L'\rangle=\sum_{h=0}^{2k}\sum_{r_h=1}^{m_h}\sum_{R'\in\mathrm{GT}(\lambda_h)}C_{L,L'}^{R',r_h}|R',r_h\rangle,\tag{B71}$$

where r_i, r_h denote the r_ith and r_hth copies of λ_i and λ_h in $\lambda_k^{\otimes 2}$, respectively. By orthogonality of irreps, it follows:

$$\begin{aligned}&\langle M,M'\,|\lambda_k(g)^{\dagger\otimes 2}\,|L,L'\rangle\\ &=\sum_{l=0}^{2k}\sum_{r=1}^{m_l}\sum_{R,R'\in\mathrm{GT}(\lambda_l)}C_{M,M'}^{R,r}C_{L,L'}^{R',r}\,\langle R,r\,|\lambda_l^{(r)}(g)^\dagger\,|R',r\rangle.\end{aligned}\tag{B72}$$

By Schur's orthogonality relations, this implies that the only nontrivial contributions in I are associated with irreps λ_l, which appears in the intersection of the sets of irreps of $\tau_n^m\otimes\bar{\tau}_n^m$ and $\lambda_k\otimes\lambda_k$, i.e., $j=l$ provided that λ_l appears in both decomposition. More specifically,

$$\begin{aligned}I=&\sum_{l=0}^{2k}\sum_{r=1}^{m_l}\sum_{R,R'\in\mathrm{GT}(\lambda_l)}C_{M,M'}^{R,r}C_{L,L'}^{R',r}\\ &\times\int dg\,\langle R,r\,|\lambda_l^{(r)}(g)^\dagger\,|R',r\rangle\langle J\,|\lambda_j(g)\,|J'\rangle\\ =&\sum_{l=0}^{2k}\delta_{l,j}\sum_{r=1}^{m_l}\sum_{R,R'\in\mathrm{GT}(\lambda_l)}C_{M,M'}^{R,r}C_{L,L'}^{R',r}\\ &\times\int dg\,\langle R,r\,|\lambda_l^{(r)}(g)^\dagger\,|R',r\rangle\langle J\,|\lambda_l(g)\,|J'\rangle\\ =&\sum_{l=0}^{2k}\frac{1}{d_{\lambda_l}}\delta_{l,j}\sum_{r=1}^{m_l}\sum_{R,R'\in\mathrm{GT}(\lambda_l)}C_{M,M'}^{R,r}C_{L,L'}^{R',r}\delta_{R,J'}\delta_{R',J}.\end{aligned}\tag{B73}$$

Therefore, we have

$$
\begin{aligned}
g_k(N,N_0) = &\sum_{M,M'\in \mathrm{GT}(\lambda_k)} C^{M}_{N_0,\tilde{N}_0} C^{M'}_{N_0,\tilde{N}_0} \sum_{L,L'\in \mathrm{GT}(\lambda_k)} C^{L}_{N,\tilde{N}} C^{L'}_{N,\tilde{N}} \sum_{j=0}^{n} \sum_{J,J'\in \mathrm{GT}(\lambda_j)} C^{J}_{N,\tilde{N}} C^{J'}_{N_0,\tilde{N}_0} \\
&\times \sum_{l=0}^{2k} \frac{1}{d_{\lambda_l}} \delta_{l,j} \sum_{r=1}^{m_l} \sum_{R,R'\in \mathrm{GT}(\lambda_l)} C^{R,r}_{M,M'} C^{R',r}_{L,L'} \delta_{R,J'} \delta_{R',J} \\
= &\sum_{l=0}^{\min(n,2k)} \frac{1}{d_{\lambda_l}} \sum_{r=1}^{m_l} \sum_{M,M'\in \mathrm{GT}(\lambda_k)} C^{M}_{N_0,\tilde{N}_0} C^{M'}_{N_0,\tilde{N}_0} \sum_{L,L'\in \mathrm{GT}(\lambda_k)} C^{L}_{N,\tilde{N}} C^{L'}_{N,\tilde{N}} \sum_{R,R'\in \mathrm{GT}(\lambda_l)} C^{R}_{N_0,\tilde{N}_0} C^{R'}_{N,\tilde{N}} C^{R,r}_{M,M'} C^{R',r}_{L,L'},
\end{aligned} \tag{B74}
$$

from which the assertion follows. ■

4. A worked out example

In the case of two-mode systems, Clebsch-Gordan coefficients reduce to the usual ones, and the analysis of the filter function and its moments drastically simplifies. In this appendix, we show explicit expressions for such a case, which will highlight some technicalities implicit in the general case of SU(m).

In the SU(2) case, it is convenient to switch from the bosonic realization of the SU(2) algebra to its spin realization, where Clebsch-Gordan coefficients are naturally introduced. This task is accomplished by the Jordan-Schwinger map [63]: For given annihilation operators a_1, a_2 acting on a two-mode system and satisfying the CCRs, the Jordan-Schwinger map is such that

$$
\begin{aligned}
&J_1 := \frac{1}{2}\left(a_2^\dagger a_1 + a_1^\dagger a_2\right), \quad J_2 := \frac{1}{2}\left(a_2^\dagger a_1 - a_1^\dagger a_2\right), \\
&J_3 := \frac{1}{2}\left(a_1^\dagger a_1 - a_2^\dagger a_2\right),
\end{aligned} \tag{B75}
$$

where $[J_i, J_j] = i\epsilon_{ijk} J_k$, ϵ is the Levi-Civita's pseudotensor, and

$$
\begin{aligned}
&J^2 = J_1^2 + J_2^2 + J_3^2 = \frac{n}{2}\left(\frac{n}{2}+1\right), \\
&n = n_1 + n_2,\ n_i = a_i^\dagger a_i.
\end{aligned} \tag{B76}
$$

This implies the normalized states $|n_1, n_2\rangle$ correspond to the eigenstates $|jm\rangle$ of J^2 and J_3, with the identification [114,115]

$$
n_1 = j + m, \quad n_2 = j - m, \tag{B77}
$$

hence, in this appendix, we consider an input state $\rho = |jm\rangle\langle jm|$ and the Fock state POVM becomes $\{|j'm'\rangle\langle j'm'|\}$, where $j' \in \frac{1}{2}\mathbb{N}$ and $m' = -j', \ldots, j'$. A spin state $|jm\rangle$ and its dual are identified by the GT patterns

$$
\begin{pmatrix} 2j & & 0 \\ & j+m & \end{pmatrix}, \quad \begin{pmatrix} 2j & & 0 \\ & j-m & \end{pmatrix}, \tag{B78}
$$

respectively, which implies the following relation:

$$
|jm\rangle = (-1)^{j-m} |j\ -m\rangle. \tag{B79}
$$

Moreover, given any irrep λ_J of SU(2), the following relations hold:

$$
P_J = \sum_{M=-J}^{J} |JM\rangle\langle JM|, \quad s_J = \frac{1}{2J+1}. \tag{B80}
$$

In particular, the expression for s_J follows from Eq. (B24), the fact that the inner multiplicities of SU(2) basis vectors are 1 (or, equivalently, each weight is uniquely associated with a unique weight vector).

In this case, with the identification $|x_1, x_2\rangle \mapsto |j\ l\rangle$, Eq. (B32) becomes

$$
f_J(l,g) = \frac{1}{2J+1} (-1)^{2j-m-l} C^{J0}_{jm,j-m} C^{J0}_{jl,j-l} \langle J0\,|\lambda_J(g)^\dagger|J0\rangle, \tag{B81}
$$

or, equivalently, it can be expressed as [cf. Eq. (B44)]

$$\begin{aligned} f_J(l,g) &= \frac{(-1)^{2j-m}}{2J+1} C^{J0}_{jm,j-m} \sum_{m'=-j}^{j} (-1)^{-m'} \\ &\quad \times C^{J0}_{jm',j-m'} \langle jm', j-m' | (\tau_n^2 \otimes \bar{\tau}_n^2)(g)^\dagger | x_1, x_2 \rangle \\ &= \frac{(-1)^{2j-m}}{2J+1} C^{J0}_{jm,j-m} \sum_{m'=-j}^{j} (-1)^{-m'} \\ &\quad \times C^{J0}_{jm',j-m'} |\langle x_1, x_2 | \tau_n^2(g) | n_1', n_2' \rangle|^2 \\ &= \frac{1}{2J+1} \frac{(-1)^{2j-m}}{x_1! x_2!} C^{J0}_{jm,j-m} \\ &\quad \times \sum_{m'=-j}^{j} \frac{(-1)^{-m'}}{n_1'! n_2'!} C^{J0}_{jm',j-m'} |\mathrm{Per}(g_{(n_1',n_2'),(x_1,x_2)})|^2, \end{aligned} \tag{B82}$$

where we set $|jm'\rangle = |n_1', n_2'\rangle$ by the inverse Jordan-Schwinger map.

The second moment expression also simplifies significantly. First, notice that, for a given representation $\lambda_J \otimes \lambda_J$, each λ_K, with $K \in \{0, \ldots, 2J\}$, is multiplicity free as all such irreps are clearly maximally symmetric. This implies the decomposition of $\lambda_J^{\otimes 2}$ is formally the same as the one of $\tau_n^2 \otimes \bar{\tau}_n^2$, i.e.,

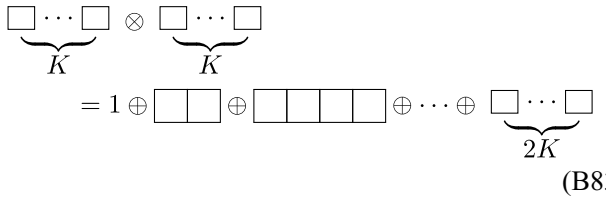

(B83)

and the second moment expression of Theorem 5 simplifies to

$$\begin{aligned} \mathbb{E}[f_J^2] &= \frac{1}{s_J^2} (-1)^{2j} |C^{J0}_{jm,j-m}|^2 \sum_{l=-j}^{j} (-1)^{m+l} |C^{J0}_{jl,j-l}|^2 \\ &\quad \times \sum_{K=0}^{2\min(J,j)} \frac{1}{2K+1} C^{K0}_{jl,j-l} C^{K0}_{jm,j-m} |C^{K0}_{J0,J0}|^2. \end{aligned} \tag{B84}$$

APPENDIX C: LITTLEWOOD-RICHARDSON'S RULES

In this appendix, we summarize Littlewood-Richardson's rules for the decomposition into irreps of the tensor product of two irreps of SU(m). For more details, see for instance Ref. [74, Sec. C.3]. In particular, let us consider the unitary irreps $\pi_{\lambda_1}, \pi_{\lambda_2}$ of SU(m) associated with Young's diagrams λ_1, λ_2. Then, the representation

$$\begin{aligned} \pi_{\lambda_1} \otimes \pi_{\lambda_2} : \mathrm{SU}(m) \ni g \mapsto \pi_{\lambda_1}(g) \otimes \pi_{\lambda_2}(g) \\ \in \mathrm{U}(\mathcal{H}_{\lambda_1} \otimes \mathcal{H}_{\lambda_2}) \end{aligned} \tag{C1}$$

is in general reducible [in particular, it is completely reducible, since SU(m) is compact].

For instance, in standard RB [50], one is interested in the irrep $U \otimes \bar{U}$, where $U : \mathrm{SU}(m) \to \mathrm{U}(m)$ is the defining representation and $\bar{U}$ its dual. Diagrammatically, they correspond to

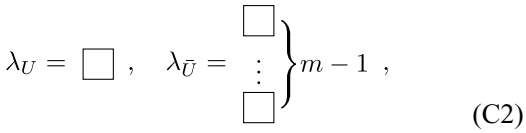

(C2)

It is well known that

$$U \otimes \bar{U} = 1 \oplus \mathrm{Ad}, \tag{C3}$$

where 1 denotes the trivial irrep and $\mathrm{Ad} : \mathrm{SU}(D) \ni g \mapsto \mathrm{Ad}_g \in \mathrm{Aut}(\mathfrak{su}(D))$ is the adjoint representation. Roughly speaking, the decomposition is achieved by combining the two Young diagrams in all possible ways, and summing up the results. In this case, there are only two possibilities that realize legal Young diagrams: λ_U can be attached on the right of the top row of $\lambda_{\bar{U}}$, or on the bottom of the column, i.e.,

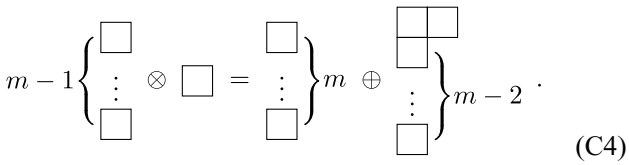

(C4)

The first diagram on the right-hand side is equivalent to the diagram with no boxes associated with the trivial irrep, while the second Young diagram identifies the adjoint representation acting on traceless matrices.

In general, *Littlewood-Richardson's rules* can be used to decompose the tensor product of two arbitrary irreps [74,117,118]. To spell out such rules, let us consider two Young diagrams λ_1, λ_2 associated with irreps of SU(m). The tensor-product representation $\lambda_1 \otimes \lambda_2$ can be evaluated algorithmically as follows [118, Sec. 13.5.3] (or also Ref. [74, Sec. C.3]):

(1) Assign distinct labels to boxes in each row of the Young diagram λ_2. For instance, the boxes in the first row will be labeled by "a," the boxes in the second row by "b" and so on.
(2) Attach boxes labeled by a to λ_1 in all possible ways such that no two a's appear in the same column, and the result is still a proper Young diagram.

(3) Repeat the steps above for all rows of λ_2.
(4) Elimination rule: For each box, assign numbers n_a = number of a's above and right to it, n_b = number of b's above and right to it, and so on. If, at any point, the relations $n_a \geq n_b \geq n_c \geq n_d \geq \ldots$ are not satisfied, discard this diagram.
(5) Merging rule. If two diagrams are the same, then they are counted as the same if the labels are the same. Otherwise, they refer to distinct irreps.
(6) Cancel columns with m boxes (since they correspond to constant shifts of the highest weight vector).
(7) Remove all the labels after the cancellation and the merging steps.

Example 1. Let us consider the following diagrams:

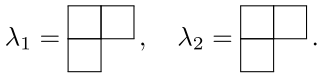

(C5)

Assigning labels to λ_2 as in rule 1, and using the second and third rules, we get

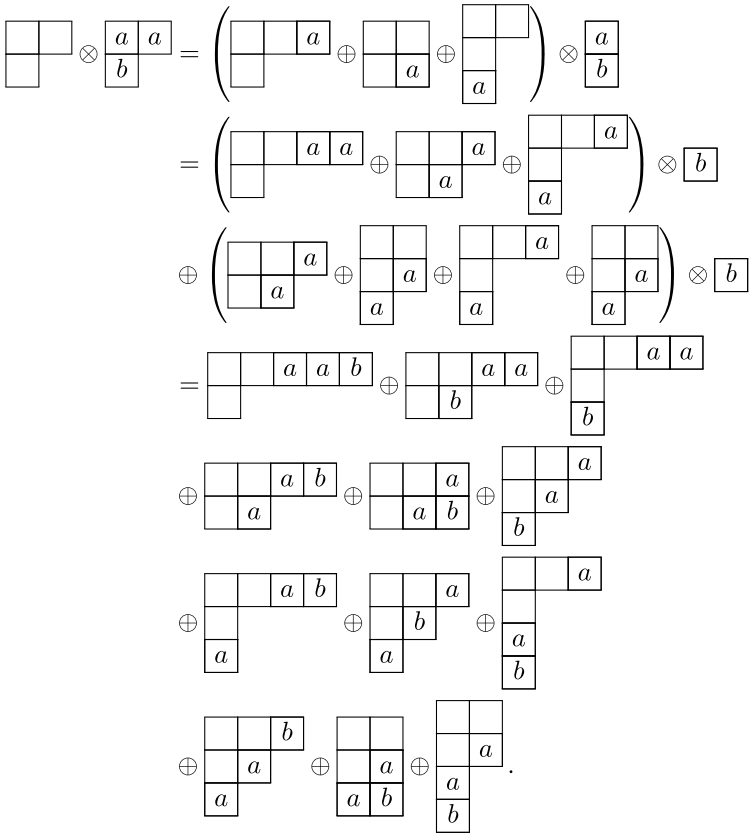

(C6)

In the second step we got few equivalent diagrams with labels in the same positions, hence they have been merged according to the merging rule. Moreover, we ignored the diagrams with two a's in the same column, in agreement with the symmetric constraint.
By the elimination rule, all the diagrams with a b box attached on the top right shall be eliminated, yielding the following decomposition:

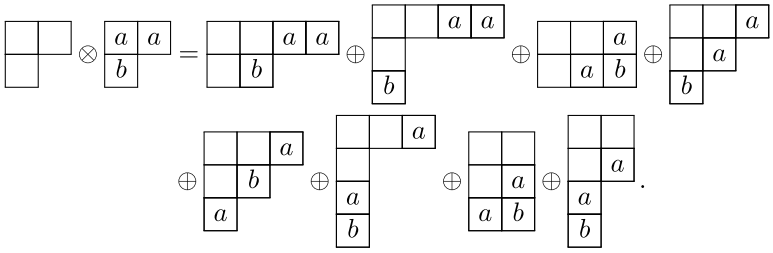

(C7)

Finally, suppose for instance that these diagrams are associated with SU(3) irreps. Then, all columns with three boxes can be omitted, while any diagram with more than three boxes in a column is not allowed. This yields the following decomposition:

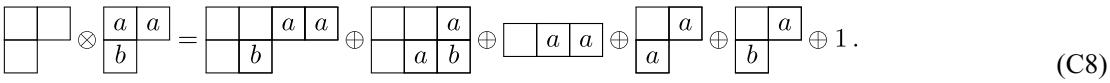

(C8)

In the latter, notice that the diagram  appears with multiplicity 2 in the decomposition, as different labels are assigned to the two copies.

In the high energy literature [118], this decomposition is also written in terms of the dimension of the irrep associated with each Young diagram as

$$\mathbf{8} \otimes \bar{\mathbf{8}} = \mathbf{27} \oplus \mathbf{10} \oplus \mathbf{10}' \oplus \mathbf{8} \oplus \mathbf{8} \oplus \mathbf{1}. \tag{C9}$$

Here, **10**, **10**′ indicates that the two irreps are inequivalent, while repeated dimensions denote the same irrep appears with a nontrivial multiplicity.

APPENDIX D: PROOF OF PROPOSITION 2

For convenience, we state again the proposition.

Proposition 3 (Restatement of Proposition 2). For any $k \in \mathbb{N}$, set $d_{\lambda_k} \equiv \dim \lambda_k$.

$$d_{\lambda_k} = \left(1 - \frac{k^2}{(k+m-1)^2}\right) \left(\dim \mathcal{H}_k^{(m)}\right)^2 . \tag{D1}$$

Proof. For any irrep $\lambda = (m_1, m_2, \ldots, m_m)$, the following fact holds [75]:

$$\dim \lambda = \prod_{1 \le j < j' \le m} \left(1 + \frac{m_j - m_{j'}}{j' - j}\right). \tag{D2}$$

Let us denote the irrep defined in Eq. (B2) as $\lambda_k = (2k, k, \ldots, k, 0)$. Hence, notice the following facts:

(1) For $j = 1$ and $j' = 2, \ldots, m-1$ we obtain the contribution $\prod_{j'=2}^{m-1} \left(1 + \frac{k}{j'-1}\right)$.
(2) For $j = 1$ and $j' = m$ we obtain the contribution $1 + \frac{2k}{m-1}$.
(3) For $2 \le j < j' \le m-1$ all the products are equal to 1.
(4) For $2 \le j \le m-1$ and $j' = m$ we obtain the contribution $\prod_{j=2}^{m-1} \left(1 + \frac{k}{m-j}\right)$.

Using the latter facts, we have

$$d_{\lambda_k} = \frac{2k+m-1}{m-1} \prod_{j=2}^{m-1} \frac{k+m-j}{m-j} \prod_{l=2}^{m-1} \frac{k+l-1}{l-1} \tag{D3}$$

$$= \frac{2k+m-1}{m-1} \frac{1}{((m-2)!)^2} \prod_{j=2}^{m-1} (k+m-j) \prod_{l=2}^{m-1} (k+l-1) \tag{D4}$$

$$= \frac{2k+m-1}{m-1} \frac{1}{((m-2)!)^2} \left(\frac{1}{k}(k)_{m-1}\right)^2 \tag{D5}$$

$$= \frac{1}{k^2} \frac{2k+m-1}{m-1} \left(\frac{(k)_{m-1}}{(m-2)!}\right)^2 \tag{D6}$$

$$= \frac{1}{k^2} \frac{2k+m-1}{m-1} (m-1)^2 \left(\frac{(k)_{m-1}}{(m-1)!}\right)^2 \tag{D7}$$

$$= \frac{(2k+m-1)(m-1)}{k^2} \left(\frac{(k+m-1)!}{k!(m-1)!} \frac{k}{k+m-1}\right)^2 \tag{D8}$$

$$= \frac{(2k+m-1)(m-1)}{k^2} \frac{k^2(m-1)}{(k+m-1)^2} \binom{k+m-1}{m-1}^2 \tag{D9}$$

$$= \frac{(2k+m-1)(m-1)}{(k+m-1)^2} \binom{k+m-1}{m-1}^2 \tag{D10}$$

$$= \left(1 - \frac{k^2}{(k+m-1)^2}\right) \left(\dim \mathcal{H}_k^{(m)}\right)^2 . \tag{D11}$$

In Eq. (D4) we factorized the denominators and observed that the factors range between 1 and $m-2$. In Eq. (D5) we introduced the Pochhammer raising factorial symbol, defined as $(a)_k := a(a+1)\ldots(a+k-1)$ for $a, k \in \mathbb{N}$. In Eq. (D8) we recognized that, by definition,

$$\frac{(k)_{m-1}}{(m-2)!} = \binom{k+m-2}{m-1} = \frac{(k+m-2)!}{(k-1)!(m-1)!} \cdot \frac{k}{k}. \tag{D12}$$

Finally, rearranging the terms and by symmetry of the binomial coefficient, the assertion follows. ■

APPENDIX E: PROOF OF LEMMA 2

In this appendix, for convenience, we will say that a box in a Young tableau is a k box if it is labeled by $k \in [m]$. Recall that for each $N \in \mathrm{GT}(\tau_n^m)$ we have

$$w_j^{(N)} + w_j^{(\bar{N})} = 0, \quad \forall j = 1, \dots m-1. \tag{E1}$$

Lemma 7 (Restatement of Lemma 2). Let λ_k be an irrep of SU(m) as in Eq. (B2) for any $k \in \mathbb{N}$. Then,

$$\gamma_{\lambda_k}(\mathbf{0}) = \binom{k+m-2}{k}. \tag{E2}$$

Proof. From the point of view of Young tableaux, we remark that a state with weight $\mathbf{0}$ implies that in the corresponding Young tableau T_M—where $M \in \mathrm{GT}(\lambda_k)$ satisfies the latter selection rules—all the entries appear the same number of times. Let $\mathcal{Y}(\lambda_k)$ be the set of semistandard Young tableaux of shape λ_k and consider the set

$$\begin{aligned}\mathcal{Y}^{(\mathbf{0})}(\lambda_k) := \{T \mid T \in \mathcal{Y}(\lambda_k) \text{ s.t. } w_i^T \\ = w_{i+1}^T \ \forall i \in [m-1]\}.\end{aligned} \tag{E3}$$

It follows that $\gamma_{\lambda_k}(\mathbf{0}) = \left|\mathcal{Y}^{(\mathbf{0})}(\lambda_k)\right|$ is the inner multiplicity of $\mathbf{0}$ in λ_k. Clearly, $\gamma(w) = 1$ for each weight w in SU(2), and Eq. (B2) holds trivially.

In a similar fashion, counting Young tableaux T_{λ_k} for SU(3) is straightforward: any Young tableau $T \in \mathcal{Y}^{(\mathbf{0})}(\lambda_k)$ contains the labels $\{1,2,3\}$ exactly k times, with the 1's forced to be placed in the first k boxes of the first row, otherwise T would not be a legal tableau. Then, if we consider a starting Young tableau of the form

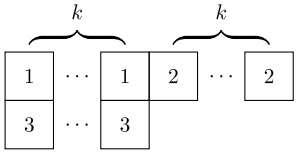

(E4)

all remaining $T \in \mathcal{Y}^{(\mathbf{0})}(\lambda_l)$ can be obtained by permuting the last 2 box in the first row with the first 3 box in the second row. The total number of allowed swaps is k, which implies $\gamma_{\lambda_k}(\mathbf{0}) = k+1$.

Consider now $m > 3$. As in the previous case, the 1 boxes are fixed to be placed at the beginning of the first row. Suppose the m boxes are all placed in the $m-1$th row, i.e., we consider

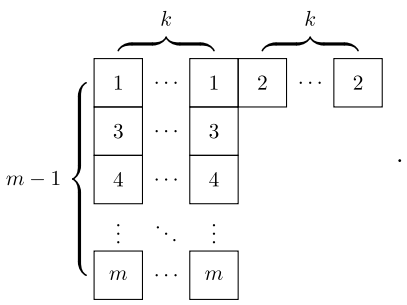

(E5)

As long as the last row is fixed to contain m boxes only, the total number of such Young tableaux is $\binom{k+m-3}{k}$. Then, we only have to count the remaining allowed configurations of k boxes. For this purpose, observe that the remaining allowed positions for m boxes are only in the first row, and there are k such configurations. Hence, it is enough to count all possible configurations for each placement of m boxes in the first row, which is given by

$$\binom{k-l+m-2}{k-l}, \tag{E6}$$

where l is the number of free boxes in the first row of the tableau. Therefore, the total number of such configurations is

$$\begin{aligned}\sum_{l=1}^{k}\binom{(k-l)+m-2}{k-l} &= \sum_{j=0}^{k-1}\binom{j+m-2}{j} \\ &= \sum_{j=0}^{k-1}\binom{j+m-2}{m-2} \\ &= \binom{k+m-3}{k-1},\end{aligned} \tag{E7}$$

where we used Fermat's identity [119, Eq. (1.48)]

$$\sum_{j=0}^{n}\binom{j+a}{j} = \binom{a+n+1}{n}. \tag{E8}$$

Therefore, by Pascal's identity, we have

$$\gamma_{\lambda_k}(\mathbf{0}) = \binom{k+m-3}{k} + \binom{k+m-3}{k-1} = \binom{k+m-2}{k} \tag{E9}$$

and the proof is complete. ■

APPENDIX F: PROOF OF LEMMA 6

Lemma 8 (Restatement of Lemma 6). Let λ_k be a Young diagram as in Eq. (B2) labeling an irrep of SU(m), $m \geq 3$.

Then,

$$\lambda_k \otimes \lambda_k = \bigoplus_{l=0}^{k} \lambda_l^{(l+1)} \oplus \bigoplus_{l=k+1}^{2k} \lambda_l^{(2k-l+1)} \oplus L, \tag{F1}$$

where $\lambda_0 \equiv \mathbf{1}$, $\lambda_1 \equiv \mathrm{Ad}$, $\lambda_j^{(i)}$ denotes the ith copy of λ_j in $\lambda_l^{\otimes 2}$, and L is a suitable direct sum of irreps, which are not of the form λ_l for any $l \in \mathbb{N}$.

Proof. Consider for any $k \in \mathbb{N}$ the tensor product

$\lambda_k \otimes \lambda_k =$ 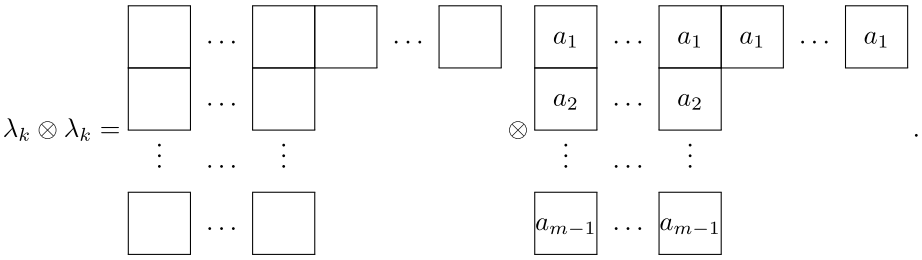

(F2)

By Littlewood-Richardson's rules, the number of Young diagrams λ_l that can be constructed from $\lambda_k^{\otimes 2}$ is determined by all possible allowed configurations we can attach the a_1 boxes to the first λ_k, since the way the remaining a_i boxes, $i = 2, \ldots, m-1$, are attached must follow accordingly. First, notice that only the a_1 boxes can be attached to the first row of the first copy of λ_k due to the elimination rule. Hence, we have two different "generating" Young diagrams conditioned by whether $l \le k$ or $k+1 \le l \le 2k$.

Suppose $l \le k$ at first. The a_1 boxes are attached to the first copy of λ_k as follows: The first l boxes are attached to the first row, the next k boxes are attached to the second row and the remaining $k-l$ boxes are attached to the mth row. Then, all the a_i boxes, for any $i = 2, 3, \ldots, m-2$ are attached to the $i+1$th row. Finally, the a_{m-1} boxes are attached to the mth row. The resulting Young diagram is given by

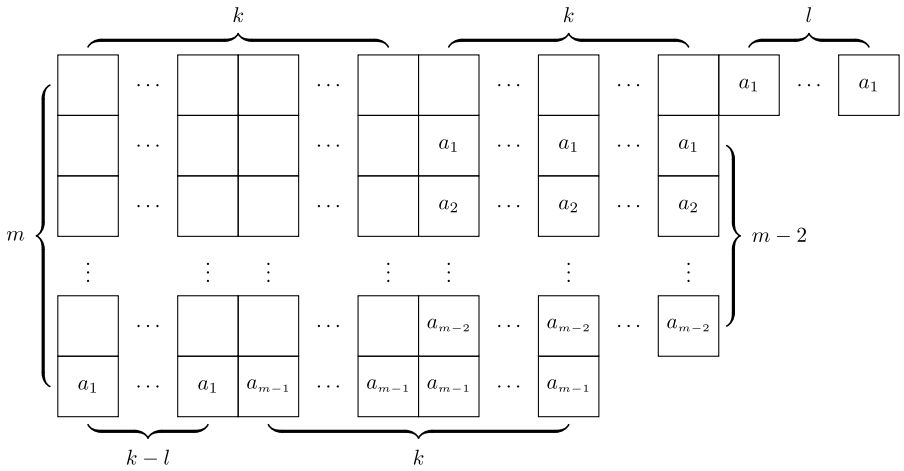

(F3)

Suppose now $l \ge k+1$. The a_1 boxes are attached to the first copy of λ_k as follows: The first l boxes are attached to the first row, while the remaining ones are attached to the second row of λ_k. Then, for the a_i boxes, for any $i = 2, 3, \ldots, m-2$, the first $2k-l$ are attached to the ith row of λ_k, while the remaining ones are attached to the $i+1$th row of λ_k. The first a_{m-1} boxes are attached to the $m-1$th row of T_k and the remaining ones will form the mth row of the diagram. The resulting Young diagram is

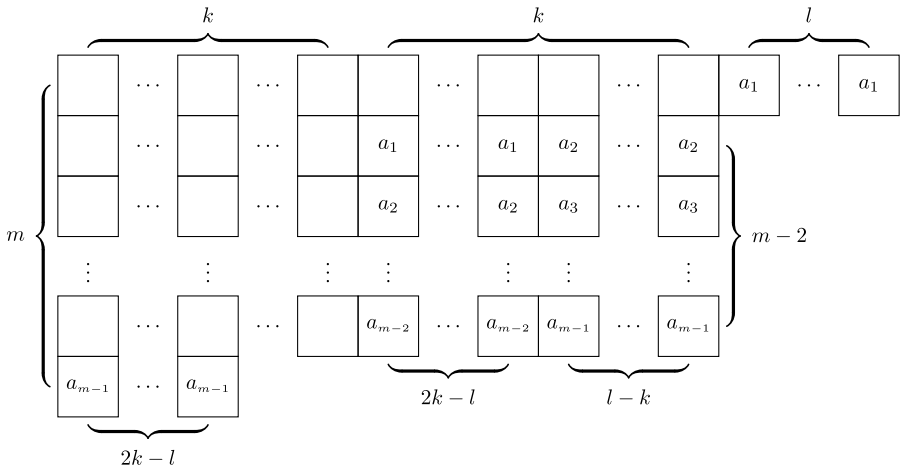

(F4)

For notation purpose, let us refer to the latter two Young diagrams as the generating Young diagrams.

At this point, we can generate all the remaining copies of λ_l in the following way:

(1) For any $i = 1, \ldots, m-2$, replace the last a_i box in the $i+1$th row with an a_{i+1} box.
(2) Replace the first a_{m-1} box in the mth row of the diagram with a_1.

It follows that the multiplicity of λ_l in the decomposition of $\lambda_k^{\otimes 2}$ is determined by the number of a_1 boxes in the second row of the generating Young diagram. ■

APPENDIX G: PASSIVE RB WITH HETERODYNE MEASUREMENT

In this appendix, we prove Theorems 1 and 2 for passive RB with (balanced) heterodyne measurements. As before, the filter function (A36) plays a central role and here assumes the following form:

$$f_{\lambda_k}(\alpha, g) = \frac{1}{s_{\lambda_k}} \langle \mathbf{n}_0, \mathbf{n}_0 | P_{\lambda_k} \tau_n^m \otimes \bar{\tau}_n^m(g)^\dagger | \alpha, \alpha \rangle, \tag{G1}$$

where $\rho = |\mathbf{n}_0\rangle\langle\mathbf{n}_0|$ is the input state, λ_k is an irrep in $\tau_n^m \otimes \bar{\tau}_n^m$ and $\alpha \in \mathbb{C}^m$ denotes an m-modes coherent state.

Throughout this appendix, we use the usual multi-index notation [120, Sec. 9.1]: For elements $\mathbf{n}_1, \mathbf{n}_2 \in \mathcal{H}_n^m$, $\mathbf{n}_1 + \mathbf{n}_2$ denotes the componentwise sum. The multi-index factorial of $\mathbf{n} \in \mathcal{H}_n^m$ is defined as $\mathbf{n}! := n_1! \ldots n_m!$. Also, for a given $\alpha \in \mathbb{C}^m$, we consider the power $\alpha^{\mathbf{n}} := \alpha_1^{n_1} \ldots \alpha_m^{n_m}$, and we set $|\alpha|^p := \alpha_1^p + \cdots + \alpha_m^p$ for $p \geq 1$. We also use the shorthand notation

$$\int d^2\alpha \equiv \int d^2\alpha_1 \ldots \int d^2\alpha_m, \tag{G2}$$

where $d^2\alpha_i$ is the complex measure on $\mathbb{C}$. With this notation, the multimode coherent state $|\alpha\rangle$ can be expanded as

$$|\alpha\rangle = e^{-|\alpha|^2/2} \sum_{\mathbf{n} \in \mathcal{F}_m} \frac{\alpha^{\mathbf{n}}}{\sqrt{\mathbf{n}!}} |\mathbf{n}\rangle. \tag{G3}$$

Consider now the following quantity for any $K \in 2\mathbb{N}$:

$$I(\{\mathbf{n}_i\}_{i=1}^K) = \frac{1}{\sqrt{\mathbf{n}_1! \mathbf{n}_2! \ldots \mathbf{n}_K!}} \times \int d^2\alpha \, e^{-K/2|\alpha|^2} \bar{\alpha}^{\mathbf{n}_1 + \ldots \mathbf{n}_{K/2}} \alpha^{\mathbf{n}_{K/2+1} + \ldots \mathbf{n}_K}. \tag{G4}$$

The latter can be evaluated writing down the integral in polar coordinates and integrating by parts. Specifically, for the single-mode integral, and for any $\eta > 0$, we have

$$\begin{aligned} &\int d^2\alpha \, e^{-\eta|\alpha|^2} \alpha^{a+b} \bar{\alpha}^{c+d} \\ &\quad = \int_0^\infty dr \, e^{-\eta r^2} r^{a+b+c+d+1} \int_0^{2\pi} d\theta \, e^{i\theta(a+b-c-d)} \\ &\quad = \pi \left(\frac{a+b+c+d}{2} \right)! \eta^{-\frac{a+b+c+d}{2}} \delta_{a+b,c+d}. \end{aligned} \tag{G5}$$

Notice that the expression in parenthesis is a proper factorial due to the δ. This implies

$$\begin{aligned} &I(\{\mathbf{n}_i\}_{i=1}^K) \\ &\quad = \frac{\pi^m}{(K/2)^n} \frac{(\mathbf{n}_1 + \cdots + \mathbf{n}_{K/2})!}{\sqrt{\mathbf{n}_1! \ldots \mathbf{n}_K!}} \delta_{\mathbf{n}_1 + \cdots + \mathbf{n}_{K/2}, \mathbf{n}_{K/2+1} + \cdots + \mathbf{n}_K}, \end{aligned} \tag{G6}$$

where

$$\delta_{\mathbf{n}_1+\cdots+\mathbf{n}_{K/2},\mathbf{n}_{K/2+1}+\cdots+\mathbf{n}_K} = \begin{cases} 1, & \text{if } \sum_{i=1}^{K/2}\mathbf{n}_i = \sum_{i=K/2+1}^{K}\mathbf{n}_i, \\ 0, & \text{otherwise} \end{cases} \tag{G7}$$

and we used the fact that $|\mathbf{n}_i| = n$ for each $i = 1, \ldots K$.

Lastly, we recall the identification between Fock states and GT patterns: we will write $|\mathbf{n}_i\rangle = |N_i\rangle$, meaning that $N_i = N_i(\mathbf{n}_i)$.

The coherent state POVM $\{|\alpha\rangle\langle\alpha|\}_{\alpha\in\mathbb{C}^m}$ is informationally complete [121], which implies $s_{\lambda_k} \neq 0$ for any $\lambda_k \in \hat{\omega}_n^m$ [50]. Specifically, we work out explicit formulae for the eigenvalues s_{λ_k}:

Theorem 3. Let λ_k an irrep of $\tau_n^m \otimes \bar{\tau}_n^m$ as in Eq. (B2). For a balanced heterodyne measurement setting, the eigenvalues of the frame operator of the filtered RB protocol are given by

$$s_{\lambda_k} = \frac{\pi^m 2^{-n}}{d_{\lambda_k}} \sum_{\mathbf{n}_1,\mathbf{n}_2} (-1)^{\varphi(N_1)+\varphi(N_2)} \binom{\mathbf{n}_1+\mathbf{n}_2}{\mathbf{n}_1} \times \sum_{M\in \mathrm{GT}(\lambda_k)} C^M_{N_1,\bar{N}_1} C^M_{N_2,\bar{N}_2}, \tag{G8}$$

where $N_1, N_2 \in \mathrm{GT}(\tau_n^m)$ are the GT patterns associated with $\mathbf{n}_1, \mathbf{n}_2$, respectively, and

$$\binom{\mathbf{n}_1+\mathbf{n}_2}{\mathbf{n}_2} \equiv \binom{n_{1,1}+n_{2,1}}{n_{2,1}} \cdots \binom{n_{1,m}+n_{2,m}}{n_{2,m}}, \tag{G9}$$

where $\mathbf{n}_i = (n_{i,1}, \ldots, n_{i,m})$.

Proof. For the balanced heterodyne measurement setting the corresponding (ideal) POVM is $\{|\alpha\rangle\langle\alpha| \equiv E_\alpha\}_{\alpha\in\mathbb{C}^m}$, where $|\alpha\rangle = \bigotimes_{i=1}^m |\alpha_i\rangle$ is an m modes coherent state. The associated measurement channel is given by

$$\mathcal{M}(\cdot) := \int_{\mathbb{C}^m} d^2\alpha \, \mathrm{Tr}[|\alpha\rangle\langle\alpha|(\cdot)] \, |\alpha\rangle\langle\alpha|. \tag{G10}$$

To evaluate Eq. (A39), we use the multimode expansion defined in Eq. (G3). Moreover, since P_{λ_k} is defined onto a subspace of $\mathcal{H}_n^m$, such expansions of the copies of α are truncated. Hence, by Eq. (G4), we have

$$s_{\lambda_k} = \frac{1}{d_{\lambda_k}} \int d^2\alpha \, \langle\alpha| P_{\lambda_k}(|\alpha\rangle\langle\alpha|) |\alpha\rangle \tag{G11}$$

$$= \frac{1}{d_{\lambda_k}} \sum_{\substack{\mathbf{n}_1,\mathbf{n}_2\in\mathcal{H}_n^m \\ \mathbf{m}_1,\mathbf{m}_2\in\mathcal{H}_n^m}} I(\mathbf{n}_1,\mathbf{n}_2,\mathbf{m}_1,\mathbf{m}_2) \times \langle\mathbf{n}_1| P_{\lambda_k}(|\mathbf{n}_2\rangle\langle\mathbf{m}_2|) |\mathbf{m}_1\rangle \tag{G12}$$

$$= \frac{1}{d_{\lambda_k}} \sum_{\substack{\mathbf{n}_1,\mathbf{n}_2\in\mathcal{H}_n^m \\ \mathbf{m}_1,\mathbf{m}_2\in\mathcal{H}_n^m}} I(\mathbf{n}_1,\mathbf{n}_2,\mathbf{m}_1,\mathbf{m}_2) \langle\mathbf{n}_1,\mathbf{m}_1| P_{\lambda_k} |\mathbf{n}_2,\mathbf{m}_2\rangle \tag{G13}$$

$$= \frac{1}{d_{\lambda_k}} \sum_{\substack{\mathbf{n}_1,\mathbf{n}_2\in\mathcal{H}_n^m \\ \mathbf{m}_1,\mathbf{m}_2\in\mathcal{H}_n^m}} I(\mathbf{n}_1,\mathbf{n}_2,\mathbf{m}_1,\mathbf{m}_2) \langle N_1,M_1| P_{\lambda_k} |N_2,M_2\rangle \tag{G14}$$

$$= \frac{1}{d_{\lambda_k}} \sum_{\substack{\mathbf{n}_1,\mathbf{n}_2\in\mathcal{H}_n^m \\ \mathbf{m}_1,\mathbf{m}_2\in\mathcal{H}_n^m}} (-1)^{\varphi(M_1)+\varphi(M_2)} \times I(\mathbf{n}_1,\mathbf{n}_2,\mathbf{m}_1,\mathbf{m}_2) \langle N_1,\bar{M}_1| P_{\lambda_k} |N_2,\bar{M}_2\rangle \tag{G15}$$

$$= \frac{1}{d_{\lambda_k}} \sum_{\substack{\mathbf{n}_1,\mathbf{n}_2\in\mathcal{H}_n^m \\ \mathbf{m}_1,\mathbf{m}_2\in\mathcal{H}_n^m}} (-1)^{\varphi(M_1)+\varphi(M_2)} I(\mathbf{n}_1,\mathbf{n}_2,\mathbf{m}_1,\mathbf{m}_2) \times \sum_{M\in\mathrm{GT}(\lambda_k)} C^M_{N_1,\bar{M}_1} C^M_{N_2,\bar{M}_2}, \tag{G16}$$

where the phase $\varphi(M)$ is defined in Eq. (A23) and in the last step we used the definition of P_{λ_k}, cf. Eq. (B21):

$$\langle N_1,\bar{M}_1| P_{\lambda_k} |N_2,\bar{M}_2\rangle = \sum_{M\in\mathrm{GT}(\lambda_k)} \langle N_1,\bar{M}_1|M\rangle\langle M|N_2,M_2\rangle = \sum_{M\in\mathrm{GT}(\lambda_k)} C^M_{N_1,\bar{M}_1} C^M_{N_2,\bar{M}_2}. \tag{G17}$$

Since $N_1, N_2 \in \mathrm{GT}(\tau_n^m)$ and $M_1, M_2 \in \mathrm{GT}(\bar{\tau}_n^m)$, selection rules for Clebsch-Gordan coefficients imply $M_1 = N_1$ and $M_2 = N_2$. Hence,

$$s_{\lambda_k} = \frac{1}{d_{\lambda_k}} \sum_{\mathbf{n}_1,\mathbf{n}_2\in\mathcal{H}_n^m} (-1)^{\varphi(N_1)+\varphi(N_2)} I(\mathbf{n}_1,\mathbf{n}_2) \times \sum_{M\in\mathrm{GT}(\lambda_k)} C^M_{N_1,\bar{N}_1} C^M_{N_2,\bar{N}_2}. \tag{G18}$$

By Eq. (G6), we have

$$I(\mathbf{n}_1,\mathbf{n}_2) = \frac{\pi^m}{2^n} \binom{\mathbf{n}_1+\mathbf{n}_2}{\mathbf{n}_1}, \tag{G19}$$

with

$$\binom{\mathbf{n}_1+\mathbf{n}_2}{\mathbf{n}_2} \equiv \binom{n_{1,1}+n_{2,1}}{n_{2,1}} \cdots \binom{n_{1,m}+n_{2,m}}{n_{2,m}}, \quad \text{(G20)}$$

from which Eq. (G8) follows. ■

A result similar to Eq. (B32) is available for heterodyne detectors:

Theorem 4 (Restatement of Theorem 1— heterodyne version). Let $\rho = |\mathbf{n}_0\rangle\langle\mathbf{n}_0|$ be a m modes state and let $\{|\alpha\rangle\langle\alpha|\}_{\alpha\in\mathbb{C}^m}$ be the coherent state POVM. Let λ_k an irrep of $\tau_n^m \otimes \bar{\tau}_n^m$ as in Eq. (B2). Then, the filter function (4) is given by

$$f_{\lambda_k}(\alpha, g) = \frac{(-1)^{\varphi(N_0)}}{s_{\lambda_k}} \sum_{M\in \mathrm{GT}(\lambda_k)} C^M_{N_0,\bar{N}_0} \times \sum_{N'\in \mathrm{GT}(\tau_n^m)} (-1)^{\varphi(N')} C^M_{N',\bar{N}'} |\langle\alpha\,|\,\tau_n^m(g)\,|\mathbf{n}'\rangle|^2, \quad \text{(G21)}$$

where $|\mathbf{n}'\rangle = |N'\rangle$.

Proof. The proof is analogous to the PNR case. By a slight generalization of Lemma 3 to include coherent state measurements, we have

$$\begin{aligned} f_{\lambda_k}(\alpha, g) &= \frac{1}{s_{\lambda_k}} \langle \mathbf{n}_0, \mathbf{n}_0\,|P_{\lambda_k} \tau_n^m \otimes \bar{\tau}_n^m(g)^\dagger\,|\alpha,\alpha\rangle && \text{(G22)}\\ &= \frac{1}{s_{\lambda_k}} (-1)^{\varphi(N_0)} \langle N_0, \bar{N}_0\,|P_{\lambda_k} \tau_n^m \otimes \bar{\tau}_n^m(g)^\dagger\,|\alpha,\alpha\rangle && \text{(G23)}\\ &= \frac{1}{s_{\lambda_k}} (-1)^{\varphi(N_0)} \sum_{M\in \mathrm{GT}(\lambda_k)} C^M_{N_0,\bar{N}_0} \times \langle M\,|\tau_n^m \otimes \bar{\tau}_n^m(g)^\dagger\,|\alpha,\alpha\rangle && \text{(G24)}\\ &= \frac{1}{s_{\lambda_k}} (-1)^{\varphi(N_0)} \sum_{M\in \mathrm{GT}(\lambda_k)} C^M_{N_0,\bar{N}_0} \sum_{N_1,N_2\in \mathrm{GT}(\tau_n^m)} \times C^M_{N_1,\bar{N}_2} \langle N_1, \bar{N}_2\,|\,\tau_n^m \otimes \bar{\tau}_n^m(g)^\dagger\,|\alpha,\alpha\rangle && \text{(G25)}\\ &= \frac{1}{s_{\lambda_k}} (-1)^{\varphi(N_0)} \sum_{M\in \mathrm{GT}(\lambda_k)} C^M_{N_0,\bar{N}_0} \sum_{N_1,N_2\in \mathrm{GT}(\tau_n^m)} \times (-1)^{\varphi(N_2)} C^M_{N_1,\bar{N}_2} \langle N_1, N_2\,|\,\tau_n^m \otimes \bar{\tau}_n^m(g)^\dagger\,|\alpha,\alpha\rangle && \text{(G26)}\\ &= \frac{1}{s_{\lambda_k}} (-1)^{\varphi(N_0)} \sum_{M\in \mathrm{GT}(\lambda_k)} C^M_{N_0,\bar{N}_0} \sum_{N_1\in \mathrm{GT}(\tau_n^m)} \times (-1)^{\varphi(N_1)} C^M_{N_1,\bar{N}_1} \langle N_1, N_1\,|\,\tau_n^m \otimes \bar{\tau}_n^m(g)^\dagger\,|\alpha,\alpha\rangle. && \text{(G27)} \end{aligned}$$

In Eq. (G23), we used the identification with GT patterns and introduced the phases described in Eq. (A23). In Eq. (G24), we projected $|N_0, \bar{N}_0\rangle$ onto λ_k, cf. Equation (B21). In Eq. (G25), we applied the Clebsch-Gordan decomposition $|M\rangle = \sum_{N_1,N_2\in \mathrm{GT}(\tau_n^m)} C^M_{N_1,\bar{N}_2} |N_1, N_2\rangle$. In Eq. (G26), we used again Eq. (A23), and in Eq. (G27) we used selection rules for Clebsch-Gordan coefficients, since $N_1, N_2 \in \mathrm{GT}(\tau_n^m)$. By the identification $|\mathbf{n}_1\rangle = |N_1\rangle$, we have

$$\langle N_1, N_1\,|\,\tau_n^m \otimes \bar{\tau}_n^m(g)^\dagger\,|\alpha,\alpha\rangle = |\langle \mathbf{n}_1\,|\,\tau_n^m(g)\,|\alpha\rangle|^2, \quad \text{(G28)}$$

and the assertion is proved. ■

We remark that an expression analogous to Eq. (B44) as a weighted sum of matrix coefficients of λ_k can be worked out by considering the expansion of $|\alpha\rangle$ in the Fock basis.

1. Moments for the heterodyne measurement setting

In this appendix, we provide explicit expressions for first two moments of probability of the filter function (4) in the case of heterodyne measurements, for which the ideal probability distribution is $p(\alpha|g) = \langle\alpha\,|\omega_n^m(g)(\rho)\,|\alpha\rangle$, $\alpha \in \mathbb{C}^m$. In particular, the ideal second moment will provide an upper bound to the sampling complexity of the protocol, cf. Sec. II C. As in Appendix B 3, the proofs rely on the application of Schur's orthogonality relations (B53).

Lemma 3. For a heterodyne measurement setting, $\rho = |\mathbf{n}_0\rangle\langle\mathbf{n}_0|$ as input state, and an irrep λ_k of $\tau_n^m \otimes \bar{\tau}_n^m$, the following holds:

$$\mathbb{E}[f_{\lambda_k}] = \frac{1}{d_{\lambda_k} s_{\lambda_k}} \sum_{M\in \mathrm{GT}(\lambda_k)} \left|C^M_{N_0,\bar{N}_0}\right|^2 \times \sum_{\substack{\mathbf{n}_1,\mathbf{n}_2\in\mathcal{H}_n^m \\ \mathbf{m}_1,\mathbf{m}_2\in\mathcal{H}_n^m}} (-1)^{\varphi(M_1)+\varphi(M_2)} I(\mathbf{n}_1,\mathbf{n}_2,\mathbf{m}_1,\mathbf{m}_2) \times \sum_{S\in \mathrm{GT}(\lambda_k)} C^S_{N_1,\bar{M}_1} C^S_{N_2,\bar{M}_2}, \quad \text{(G29)}$$

where $|\mathbf{n}_0\rangle = |N_0\rangle$, $|\mathbf{n}_1\rangle \equiv |N_1\rangle$, $|\mathbf{n}_2\rangle \equiv |N_2\rangle$, $|\mathbf{m}_1\rangle \equiv |M_1\rangle$, $|\mathbf{m}_1\rangle \equiv |M_1\rangle$, I is as in Eq. (G4) and φ is defined in Eq. (A23).

Proof. As in the proof of Theorem 3, considering the multimode expansion of α, only the n-particle component provides nontrivial contribution to the first moment, since ω_n^m acts nontrivially on $\mathcal{H}_n^m$ only. Recalling Eq. (G4), it follows

$$\mathbb{E}[f_{\lambda_k}] = \frac{1}{s_{\lambda_k}} \int d^2\alpha \int dg \, \langle \mathbf{n}_0 | P_{\lambda_k} \circ \omega_n^m(g)^\dagger(|\alpha\rangle\langle\alpha|) | \mathbf{n}_0 \rangle \langle \alpha | \omega_n^m(g)(|\mathbf{n}_0\rangle\langle\mathbf{n}_0|) | \alpha \rangle \tag{G30}$$

$$= \frac{1}{s_{\lambda_k}} \sum_{\substack{\mathbf{n}_1,\mathbf{n}_2 \in \mathcal{H}_n^m \\ \mathbf{m}_1,\mathbf{m}_2 \in \mathcal{H}_n^m}} I(\mathbf{n}_1,\mathbf{n}_2,\mathbf{m}_1,\mathbf{m}_2) \int d^2\alpha \int dg \, \langle \mathbf{n}_0 | P_{\lambda_k} \circ \omega_n^m(g)^\dagger(|\mathbf{n}_1\rangle\langle\mathbf{m}_1|) | \mathbf{n}_0 \rangle \langle \mathbf{n}_2 | \omega_n^m(g)(|\mathbf{n}_0\rangle\langle\mathbf{n}_0|) | \mathbf{m}_2 \rangle. \tag{G31}$$

In particular,

$$H \equiv \int d^2\alpha \int dg \, \langle \mathbf{n}_0 | P_{\lambda_k} \circ \omega_n^m(g)^\dagger(|\mathbf{n}_1\rangle\langle\mathbf{m}_1|) | \mathbf{n}_0 \rangle \langle \mathbf{n}_2 | \omega_n^m(g)(|\mathbf{n}_0\rangle\langle\mathbf{n}_0|) | \mathbf{m}_2 \rangle \tag{G32}$$

$$= \int dg \, \langle \mathbf{n}_0, \mathbf{n}_0 | P_{\lambda_k} \tau_n^m \otimes \bar{\tau}_n^m(g)^\dagger | \mathbf{n}_1, \mathbf{m}_1 \rangle \langle \mathbf{n}_2, \mathbf{m}_2 | \tau_n^m \otimes \bar{\tau}_n^m(g) | \mathbf{n}_0, \mathbf{n}_0 \rangle \tag{G33}$$

$$= \int dg \, \langle N_0, N_0 | P_{\lambda_k} \tau_n^m \otimes \bar{\tau}_n^m(g)^\dagger | N_1, M_1 \rangle \langle N_2, M_2 | \tau_n^m \otimes \bar{\tau}_n^m(g) | N_0, N_0 \rangle \tag{G34}$$

$$= (-1)^{\varphi(M_1)+\varphi(M_2)} \int dg \langle N_0, \bar{N}_0 | P_{\lambda_k} \tau_n^m \otimes \bar{\tau}_n^m(g)^\dagger | N_1, \bar{M}_1 \rangle \langle N_2, \bar{M}_2 | \tau_n^m \otimes \bar{\tau}_n^m(g) | N_0, \bar{N}_0 \rangle \tag{G35}$$

$$= (-1)^{\varphi(M_1)+\varphi(M_2)} \sum_{M \in \mathrm{GT}(\lambda_k)} C^M_{N_0,\bar{N}_0} \int dg \, \langle M | \lambda_k(g)^\dagger | N_1, \bar{M}_1 \rangle \langle N_2, \bar{M}_2 | \bigoplus_{j=0}^{n} \lambda_j(g) | N_0, \bar{N}_0 \rangle. \tag{G36}$$

In the last step, we projected $|N_0, \bar{N}_0\rangle$ onto λ_k and we used the irrep decomposition of $\tau_n^m \otimes \bar{\tau}_n^m$, see Lemma 1. The latter can be computed by slight modifications of Lemmas 3 and 4. In particular, by orthogonality relations, the integral is nonzero only if $j = k$ and for basis vectors of λ_k. In other words, it is enough to restrict the Clebsch-Gordan decompositions to the λ_kth components:

$$|N_1, \bar{M}_1\rangle\big|_{\lambda_k} = \sum_{S_1 \in \mathrm{GT}(\lambda_k)} C^{S_1}_{N_1,\bar{M}_1} |S_1\rangle, \tag{G37}$$

$$|N_2, \bar{M}_2\rangle\big|_{\lambda_k} = \sum_{S_2 \in \mathrm{GT}(\lambda_k)} C^{S_2}_{N_2,\bar{M}_2} |S_2\rangle, \tag{G38}$$

$$|N_0, \bar{N}_0\rangle\big|_{\lambda_k} = \sum_{S_3 \in \mathrm{GT}(\lambda_k)} C^{S_3}_{N_0,\bar{N}_0} |S_3\rangle. \tag{G39}$$

Therefore, Schur's orthogonality relations (B53), we have

$$H = \frac{1}{d_{\lambda_k}} (-1)^{\varphi(M_1)+\varphi(M_2)} \sum_{M \in \mathrm{GT}(\lambda_k)} \left| C^M_{N_0,\bar{N}_0} \right|^2 \times \sum_{S \in \mathrm{GT}(\lambda_k)} C^S_{N_1,\bar{M}_1} C^S_{N_2,\bar{M}_2} \tag{G40}$$

from which the assertion follows. ■

Lastly, we have the following explicit expression for the second moment:

Theorem 5. Consider a passive RB experiment with balanced heterodyne measurement setting, initial Fock state $\rho = |\mathbf{n}_0\rangle\langle\mathbf{n}_0|$, and λ is an irrep of $\omega_n^m = \tau_n^m(\cdot)\tau_n^{m\dagger}$. Then, the following holds:

$$\mathbb{E}[f_{\lambda_k}^2] = \frac{1}{s_{\lambda_k}^2} (-1)^{\varphi(N_0)} \sum_{\substack{\mathbf{n}_1,\mathbf{n}_2,\mathbf{n}_3, \\ \mathbf{m}_1,\mathbf{m}_2,\mathbf{m}_3}} \times (-1)^{\sum_{i=1}^3 \varphi(M_i)} I((\mathbf{n}_i)_{i=1}^3 (\mathbf{m}_i)_{i=1}^3) g_k(\mathbf{N}, \mathbf{M}, N_0), \tag{G41}$$

where $\mathbf{N} \equiv (N_1, N_2, N_3), \mathbf{M} \equiv (M_1, M_2, M_3)$, $N_i \equiv N(\mathbf{n}_i)$, $M_i \equiv M(\mathbf{m}_i)$ are GT patterns associated with $\mathbf{n}_i, \mathbf{m}_i$, respectively, $I((\mathbf{n}_i)_{i=1}^3, (\mathbf{m}_i)_{i=1}^3) \equiv I(\mathbf{n}_1, \mathbf{n}_2, \mathbf{n}_3, \mathbf{m}_1, \mathbf{m}_2, \mathbf{m}_3)$ is as in Eq. (G6) and

$$g_k(\mathbf{N}, \mathbf{M}, N_0) = \sum_{l=0}^{\min\{n,2k\}} \frac{1}{d_{\lambda_k}} \sum_{r=1}^{m_l} \times \sum_{\substack{M,M' \in \mathrm{GT}(\lambda_k) \\ L,L' \in \mathrm{GT}(\lambda_k) \\ R,R' \in \mathrm{GT}(\lambda_l)}} C^M_{N_0,\bar{N}_0} C^{M'}_{N_0,\bar{N}_0} C^{R,r}_{M,M'} C^R_{N_0,\bar{N}_0} C^{R'}_{N_3,\bar{M}_3} C^L_{N_1,\bar{M}_1} \times C^{L'}_{N_2,\bar{M}_2} C^{R',r}_{L,L'}. \tag{G42}$$

Proof. By Eqs. (G3) and (G4), we have, for any λ_k,

$$\mathbb{E}[f_{\lambda_k}^2] = \frac{1}{s_{\lambda_k}^2} \int d^2\alpha \int dg \, \langle \mathbf{n}_0 | P_{\lambda_k} \circ \omega_n^m(g)^\dagger (|\alpha\rangle\langle\alpha|) | \mathbf{n}_0 \rangle^2 \langle \alpha | \omega_n^m(g)(|\mathbf{n}_0\rangle\langle\mathbf{n}_0|) | \alpha \rangle \tag{G43}$$

$$= \frac{1}{s_{\lambda_k}^2} \sum_{\substack{\mathbf{n}_1,\mathbf{n}_2,\mathbf{n}_3 \in \mathcal{H}_n^m \\ \mathbf{m}_1,\mathbf{m}_2,\mathbf{m}_3 \in \mathcal{H}_n^m}} I((\mathbf{n}_i)_{i=1}^3, (\mathbf{m}_i)_{i=1}^3) \int dg \, \langle \mathbf{n}_0 | P_{\lambda_k} \circ \omega_n^m(g)^\dagger (|\mathbf{n}_1\rangle\langle\mathbf{m}_1|) | \mathbf{n}_0 \rangle \tag{G44}$$

$$\times \langle \mathbf{n}_0 | P_{\lambda_k} \circ \omega_n^m(g)^\dagger (|\mathbf{n}_2\rangle\langle\mathbf{m}_2|) | \mathbf{n}_0 \rangle \langle \mathbf{n}_3 | \omega_n^m(g)(|\mathbf{n}_0\rangle\langle\mathbf{n}_0|) | \mathbf{m}_3 \rangle \tag{G45}$$

$$\equiv \frac{1}{s_{\lambda_k}^2} \sum_{\substack{\mathbf{n}_1,\mathbf{n}_2,\mathbf{n}_3, \\ \mathbf{m}_1,\mathbf{m}_2,\mathbf{m}_3}} I((\mathbf{n}_i)_{i=1}^3, (\mathbf{m}_i)_{i=1}^3) \, G_k((\mathbf{n}_i)_{i=1}^3, (\mathbf{m}_i)_{i=1}^3, \mathbf{n}_0), \tag{G46}$$

where

$$G_k((\mathbf{n}_i)_{i=1}^3, (\mathbf{m}_i)_{i=1}^3, \mathbf{n}_0) \equiv \int dg \, \langle \mathbf{n}_0 | P_{\lambda_k} \circ \omega_n^m(g)^\dagger (|\mathbf{n}_1\rangle\langle\mathbf{m}_1|) | \mathbf{n}_0 \rangle \times \langle \mathbf{n}_0 | P_{\lambda_k} \circ \omega_n^m(g)^\dagger (|\mathbf{n}_2\rangle\langle\mathbf{m}_2|) | \mathbf{n}_0 \rangle \times \langle \mathbf{n}_3 | \omega_n^m(g)(|\mathbf{n}_0\rangle\langle\mathbf{n}_0|) | \mathbf{m}_3 \rangle. \tag{G47}$$

Introducing GT patterns, we have

$$G_k((\mathbf{n}_i)_{i=1}^3, (\mathbf{m}_i)_{i=1}^3, \mathbf{n}_0) \equiv G_k(\mathbf{N}, \mathbf{M}, N_0), \quad \mathbf{N} = (N_1, N_2, N_3), \quad \mathbf{M} = (M_1, M_2, M_3). \tag{G48}$$

Then, by Eq. (A23), the latter assumes the following form:

$$G_k(\mathbf{N}, \mathbf{M}, N_0) = \int dg \, \langle N_0, N_0 | P_{\lambda_k} \tau_n^m \otimes \bar{\tau}_n^m(g)^\dagger | N_1, M_1 \rangle \langle N_0, N_0 | P_{\lambda_k} \tau_n^m \otimes \bar{\tau}_n^m(g)^\dagger | N_2, M_2 \rangle \tag{G49}$$

$$\times \langle N_3, M_3 | \tau_n^m \otimes \bar{\tau}_n^m(g) | N_0, N_0 \rangle \tag{G50}$$

$$= (-1)^{\varphi(N_0) + \sum_{i=1}^3 \varphi(M_i)} \sum_{M, M' \in \mathrm{GT}(\lambda_k)} C_{N_0, \bar{N}_0}^{M} \, C_{N_0, \bar{N}_0}^{M'} \tag{G51}$$

$$\times \int dg \, \langle M, M' | \lambda_k(g)^{\otimes 2\dagger} | N_1, \bar{M}_1, N_2, \bar{M}_2 \rangle \langle N_3, \bar{M}_3 | \bigoplus_{j=0}^{n} \lambda_j(g) | N_0, \bar{N}_0 \rangle \tag{G52}$$

$$\equiv (-1)^{\varphi(N_0) + \sum_{i=1}^3 \varphi(M_i)} g_k(\mathbf{N}, \mathbf{M}, N_0) \, . \tag{G53}$$

We compute the integral

$$g_k(\mathbf{N}, \mathbf{M}, N_0) \equiv \int dg \, \langle M, M' | \lambda_k(g)^{\otimes 2\dagger} | N_1, \bar{M}_1, N_2, \bar{M}_2 \rangle \times \langle N_3, \bar{M}_3 | \bigoplus_{j=0}^{n} \lambda_j(g) | N_0, \bar{N}_0 \rangle \tag{G54}$$

as in the proof of Theorem 5: Consider the irrep decomposition of $\lambda_k^{\otimes 2}$ as in Lemma 6. Then, by orthogonality of the matrix coefficients, the nontrivial contributions to the integral come from irreps that appear–with their multiplicities—in both ω_n^m and $\lambda_k^{\otimes 2}$. This implies

$$g_k(\mathbf{N}, \mathbf{M}, N_0) = \sum_{l=0}^{\min\{n, 2k\}} \sum_{r=1}^{m_l} \int dg \times \langle M, M' | \lambda_l^{(r)}(g)^\dagger | N_1, \bar{M}_1, N_2, \bar{M}_2 \rangle \times \langle N_3, \bar{M}_3 | \lambda_l(g) | N_0, \bar{N}_0 \rangle. \tag{G55}$$

Therefore, by the Clebsch-Gordan decompositions

$$|M, M'\rangle = \sum_{R \in \mathrm{GT}(\lambda_l)} C_{M,M'}^{R,r} |R, r\rangle, \tag{G56}$$

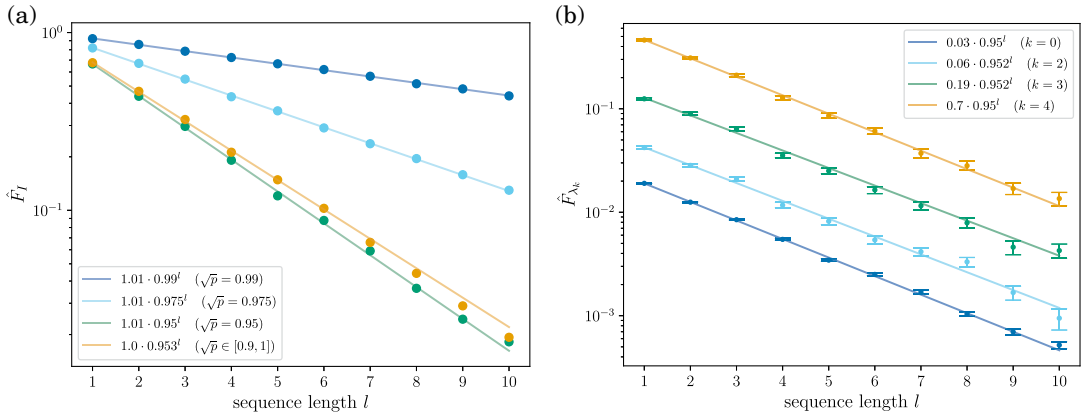

FIG. 4. Signal forms of passive RB with $n = m =$ and input state $|\mathbf{1}_4\rangle$ using $\mathbb{T} = 10\,000$ samples. (a) Postselection on particle loss events under different values of transmittivity. (b) Passive RB signal in the presence of particles loss with transmittivity $\sqrt{p} = 0.95$.

$$|N_3, \bar{M}_3\rangle = \sum_{J \in \mathrm{GT}(\lambda_l)} C^{J}_{N_3,\bar{M}_3} |J\rangle, \tag{G57}$$

$$|N_0, \bar{N}_0\rangle = \sum_{J' \in \mathrm{GT}(\lambda_l)} C^{J'}_{N_0,\bar{N}_0} |J'\rangle, \tag{G58}$$

$$|N_1, \bar{M}_1, N_2, \bar{M}_2\rangle = \sum_{L,L' \in \mathrm{GT}(\lambda_k)} C^{L}_{N_1,\bar{M}_1} C^{L'}_{N_2,\bar{M}_2} |L, L'\rangle, \tag{G59}$$

$$|L, L'\rangle = \sum_{R' \in \mathrm{GT}(\lambda_l)} C^{R'r}_{L,L'} |R', r\rangle, \tag{G60}$$

it follows

$$\int dg \, \langle R, r | \lambda^{(r)}_l(g)^\dagger | R', r\rangle \langle J | \lambda_l(g) | J'\rangle = \frac{1}{d_{\lambda_l}} \delta_{R,J'} \delta_{R',J} \tag{G61}$$

by Schur's orthogonality relations (B53). Hence,

$$\begin{aligned} g_k(\mathbf{N}, \mathbf{M}, N_0) = & \sum_{l=0}^{\min\{n,2k\}} \frac{1}{d_{\lambda_k}} \sum_{r=1}^{m_l} \sum_{\substack{M,M' \in \mathrm{GT}(\lambda_k) \\ L,L' \in \mathrm{GT}(\lambda_k) \\ R,R' \in \mathrm{GT}(\lambda_l)}} \\ & \times C^{M}_{N_0,\bar{N}_0} C^{M'}_{N_0,\bar{N}_0} C^{R,r}_{M,M'} C^{R}_{N_0,\bar{N}_0} C^{R'}_{N_3,\bar{M}_3} \\ & \times C^{L}_{N_1,\bar{M}_1} C^{L'}_{N_2,\bar{M}_2} C^{R',r}_{L,L'}, \end{aligned} \tag{G62}$$

and the assertion follows from a suitable sorting of all the terms. ■

APPENDIX H: ADDITIONAL DETAILS ON NUMERICAL EXPERIMENTS

Here we provide additional details and plots for the numerical experiment discussed in Fig. 4 and the numerical implementation of the filter function (B32). Computation of the filter function was performed on a MacBook Pro 2020 with Intel Quad-Core i5 (1,4 GHz), 8 GB LPDDR3 (2133 MHz).

The specifics of the simulation are the following: We consider the collision-free input state $|\mathbf{n}_0\rangle = |\mathbf{1}_4\rangle \equiv |1111\rangle \in \mathcal{H}^4_n$ and filter onto the λ_k irrep for $k = 0, \ldots, 4$. Random unitaries $g^{(i)}_j \in \mathrm{SU}(4), i \in [\mathbb{T}], j \in [l]$ are drawn from the Haar-probability measure according to the procedure described in Refs. [122,123], the sequence lengths considered consisting of $l = 1, \ldots, 10$ Haar random unitaries. We assume each gate comes with a probability $1 - p$ of losing a particle on each mode. In particular, we consider experiments with gate independent noise, where $\sqrt{p} = 0.95, 0.975, 0.99$ and simulate a gate dependent noise experiment where the transmittivity $\sqrt{p_j}$ of the jth unitary in the sequence is drawn uniformly at random from the interval $[0.9, 1]$. Concretely, denoting with $\mathcal{L}(g)$ the single-mode lossy channel, this means that the noisy gate is modeled as $\omega^m_n(g) \circ \mathcal{L}(g)^{\otimes m}$ for each gate g in the sequence. Lastly, random Fock states are drawn performing a boson-sampling simulation using the Python module Piquasso [102,124]. Additionally, we collected noiseless samples for evaluation of $\mathbb{E}[f^2_{\lambda_k}]_{\mathrm{ideal}}$ by simply letting $p = 1$. We collect $\mathbb{T} = 10\,000$ sampled pairs $((g^{(i)}_j)^l_{j=1}, \mathbf{n}^{(i)})$ and store them for postprocessing. We remark that the unitaries $g^{(i)}_1, \ldots, g^{(i)}_l$ are used to collect exactly one state from the boson sampler, as throughout this work we consider the so-called *single-shot estimator* (2) [50].

By postselecting on the outcome of the boson-sampling experiment, we capture the estimation of particle loss rates

as described in Sec. II B 4. The results, which employ the indicator filter function (6) are shown in Fig. 4(a) (the estimator is again the empirical average of the filter function). Since we run simulations under particle loss only, the estimated decay rates are similar to the ones shown in Fig. 4.

Next, we evaluate the filter function (B32) for each sampled pair. Specifically, we compute Clebsch-Gordan coefficients using the SUNRepresentations Julia library [125], which implements Alex *et al.*'s algorithm for the computation of SU(m) Clebsch-Gordan coefficients [75]. The algorithm can be sketched as follows: For each irrep λ_k in $\tau_n^m \otimes \bar{\tau}_n^m$ (or—in the case of the second moment—for each irrep in $\lambda_k^{\otimes 2}$) one shall first find the Clebsch-Gordan coefficients of the highest weight state of λ_k (and possibly resolve the ambiguity on the multiplicities by a suitable Gaussian elimination, in the case of $\lambda_k^{\otimes 2}$). Lower weight states are obtained by repeated application of ladder operators. This implies the calculation of all remaining Clebsch-Gordan coefficients by solving linear systems of equations. We remark the computation of Clebsch-Gordan coefficients can be sped up by exploiting the symmetries of the weight spaces under the action of the Weyl group [84] or using analytic expressions for the coefficients $C^M_{N,\bar{N}}$, with $N \in \mathrm{GT}(\tau_n^m), M \in \mathrm{GT}(\lambda_k)$ [89].

Lastly, we analyze the signal form for the irreps $\lambda_0, \ldots, \lambda_4$ (we do not include λ_1 as there is no overlap with the chosen input state). The results are shown in Fig. 4(b).

[1] M. Kliesch and I. Roth, Theory of quantum system certification, PRX Quantum **2**, 010201 (2021).

[2] J. Eisert, D. Hangleiter, N. Walk, I. Roth, D. Markham, R. Parekh, U. Chabaud, and E. Kashefi, Quantum certification and benchmarking, Nat. Rev. Phys. **2**, 382 (2020).

[3] Y.-D. Wu, G. Chiribella, and N. Liu, Efficient learning of continuous-variable quantum states, Phys. Rev. Res. **6**, 033280 (2024).

[4] F. A. Mele, A. A. Mele, L. Bittel, J. Eisert, V. Giovannetti, L. Lami, L. Leone, and S. F. E. Oliviero, Learning quantum states of continuous variable systems, arXiv:2405.01431 [quant-ph].

[5] A. I. Lvovsky and M. G. Raymer, Continuous-variable optical quantum-state tomography, Rev. Mod. Phys. **81**, 299 (2009).

[6] C. C. López, A. Bendersky, J. P. Paz, and D. G. Cory, Progress toward scalable tomography of quantum maps using twirling-based methods and information hierarchies, Phys. Rev. A **81**, 062113 (2010).

[7] C. T. Schmiegelow, A. Bendersky, M. A. Larotonda, and J. P. Paz, Selective and efficient quantum process tomography without ancilla, Phys. Rev. Lett. **107**, 100502 (2011).

[8] A. Bendersky and J. P. Paz, Selective and efficient quantum state tomography and its application to quantum process tomography, Phys. Rev. A **87**, 012122 (2013).

[9] R. Namiki, Schmidt-number benchmarks for continuous-variable quantum devices, Phys. Rev. A **93**, 052336 (2016).

[10] J. B. Altepeter, D. Branning, E. Jeffrey, T. C. Wei, P. G. Kwiat, R. T. Thew, J. L. O'Brien, M. A. Nielsen, and A. G. White, Ancilla-assisted quantum process tomography, Phys. Rev. Lett. **90**, 193601 (2003).

[11] G. Bai and G. Chiribella, Test one to test many: A unified approach to quantum benchmarks, Phys. Rev. Lett. **120**, 150502 (2018).

[12] E. Knill, R. Laflamme, and G. J. Milburn, A scheme for efficient quantum computation with linear optics, Nature **409**, 46 (2001).

[13] M. Koashi, T. Yamamoto, and N. Imoto, Probabilistic manipulation of entangled photons, Phys. Rev. A **63**, 030301(R) (2001).

[14] P. Kok, W. J. Munro, K. Nemoto, T. C. Ralph, J. P. Dowling, and G. J. Milburn, Linear optical quantum computing with photonic qubits, Rev. Mod. Phys. **79**, 135 (2007).

[15] T. Rudolph, Why I am optimistic about the silicon-photonic route to quantum computing, APL Photonics **2**, 030901 (2017).

[16] S.-H. Tan and P. P. Rohde, The resurgence of the linear optics quantum interferometer—recent advances & applications, Rev. Phys. **4**, 100030 (2019).

[17] K. Alexander *et al.*, A manufacturable platform for photonic quantum computing, arxiv:2404.17570 [physics, physics:quant-ph].

[18] A. Politi, M. J. Cryan, J. G. Rarity, S. Yu, and J. L. O'Brien, Silica-on-silicon waveguide quantum circuits, Science **320**, 646 (2008).

[19] J. P. Sprengers, A. Gaggero, D. Sahin, S. Jahanmirinejad, G. Frucci, F. Mattioli, R. Leoni, J. Beetz, M. Lermer, M. Kamp, S. Höfling, R. Sanjines, and A. Fiore, Waveguide superconducting single-photon detectors for integrated quantum photonic circuits, Appl. Phys. Lett. **99**, 181110 (2011).

[20] J. W. Silverstone, D. Bonneau, K. Ohira, N. Suzuki, H. Yoshida, N. Iizuka, M. Ezaki, C. M. Natarajan, M. G. Tanner, R. H. Hadfield, V. Zwiller, G. D. Marshall, J. G. Rarity, J. L. O'Brien, and M. G. Thompson, On-chip quantum interference between silicon photon-pair sources, Nat. Photonics **8**, 104 (2014).

[21] T. Meany, M. Gräfe, R. Heilmann, A. Perez-Leija, S. Gross, M. J. Steel, M. J. Withford, and A. Szameit, Laser written circuits for quantum photonics, Laser Photonics Rev. **9**, 363 (2015).

[22] J. E. Bourassa, R. N. Alexander, M. Vasmer, A. Patil, I. Tzitrin, T. Matsuura, D. Su, B. Q. Baragiola, S. Guha, G. Dauphinais, K. K. Sabapathy, N. C. Menicucci, and I. Dhand, Blueprint for a scalable photonic fault-tolerant quantum computer, Quantum **5**, 392 (2021).

[23] S. Aaronson and A. Arkhipov, in *Proceedings of the Forty-Third Annual ACM Symposium on Theory of Computing*, STOC '11 (Association for Computing Machinery, New York, NY, USA, 2011), pp. 333–342.

[24] C. S. Hamilton, R. Kruse, L. Sansoni, S. Barkhofen, C. Silberhorn, and I. Jex, Gaussian boson sampling, Phys. Rev. Lett. **119**, 170501 (2017).

[25] L. Chakhmakhchyan and N. J. Cerf, Boson sampling with Gaussian measurements, Phys. Rev. A **96**, 032326 (2017).

[26] H.-S. Zhong *et al.*, Quantum computational advantage using photons, Science **370**, 1460 (2020).

[27] H.-S. Zhong *et al.*, Phase-programmable Gaussian boson sampling using stimulated squeezed light, Phys. Rev. Lett. **127**, 180502 (2021).

[28] L. S. Madsen, F. Laudenbach, M. F. Askarani, F. Rortais, T. Vincent, J. F. F. Bulmer, F. M. Miatto, L. Neuhaus, L. G. Helt, M. J. Collins, A. E. Lita, T. Gerrits, S. W. Nam, V. D. Vaidya, M. Menotti, I. Dhand, Z. Vernon, N. Quesada, and J. Lavoie, Quantum computational advantage with a programmable photonic processor, Nature **606**, 75 (2022).

[29] K. Sharma and M. M. Wilde, Characterizing the performance of continuous-variable Gaussian quantum gates, Phys. Rev. Res. **2**, 013126 (2020).

[30] R. Blume-Kohout and P. S. Turner, The curious nonexistence of Gaussian 2-designs, Commun. Math. Phys. **326**, 755 (2014).

[31] Q. Zhuang, T. Schuster, B. Yoshida, and N. Y. Yao, Scrambling and complexity in phase space, Phys. Rev. A **99**, 062334 (2019).

[32] J. T. Iosue, K. Sharma, M. J. Gullans, and V. V. Albert, Continuous-variable quantum state designs: Theory and applications, Phys. Rev. X **14**, 011013 (2024).

[33] R. M. S. Farias and L. Aolita, Certification of continuous-variable gates using average channel-fidelity witnesses, Quantum Sci. Technol. **6**, 035014 (2021).

[34] J. Emerson, R. Alicki, and K. Życzkowski, Scalable noise estimation with random unitary operators, J. Opt. B **7**, S347 (2005).

[35] B. Lévi, C. C. López, J. Emerson, and D. G. Cory, Efficient error characterization in quantum information processing, Phys. Rev. A **75**, 022314 (2007).

[36] C. Dankert, R. Cleve, J. Emerson, and E. Livine, Exact and approximate unitary 2-designs and their application to fidelity estimation, Phys. Rev. A **80**, 012304 (2009).

[37] J. Emerson, M. Silva, O. Moussa, C. Ryan, M. Laforest, J. Baugh, D. G. Cory, and R. Laflamme, Symmetrized characterization of noisy quantum processes, Science **317**, 1893 (2007).

[38] E. Knill, D. Leibfried, R. Reichle, J. Britton, R. B. Blakestad, J. D. Jost, C. Langer, R. Ozeri, S. Seidelin, and D. J. Wineland, Randomized benchmarking of quantum gates, Phys. Rev. A **77**, 012307 (2008).

[39] E. Magesan, J. M. Gambetta, and J. Emerson, Scalable and robust randomized benchmarking of quantum processes, Phys. Rev. Lett. **106**, 180504 (2011).

[40] E. Magesan, J. M. Gambetta, and J. Emerson, Characterizing quantum gates via randomized benchmarking, Phys. Rev. A **85**, 042311 (2012).

[41] T. Proctor, K. Rudinger, K. Young, M. Sarovar, and R. Blume-Kohout, What randomized benchmarking actually measures, Phys. Rev. Lett. **119**, 130502 (2017).

[42] J. J. Wallman, Randomized benchmarking with gate-dependent noise, Quantum **2**, 47 (2018).

[43] S. T. Merkel, E. J. Pritchett, and B. H. Fong, Randomized benchmarking as convolution: Fourier analysis of gate dependent errors, Quantum **5**, 581 (2021).

[44] R. Harper, I. Hincks, C. Ferrie, S. T. Flammia, and J. J. Wallman, Statistical analysis of randomized benchmarking, Phys. Rev. A **99**, 052350 (2019).

[45] D. S. França and A.-L. Hashagen, Approximate randomized benchmarking for finite groups, J. Phys. A: Math. Theor. **51**, 395302 (2018).

[46] J. Helsen, X. Xue, L. M. K. Vandersypen, and S. Wehner, A new class of efficient randomized benchmarking protocols, npj Quantum Inf. **5**, 1 (2019).

[47] J. Helsen, I. Roth, E. Onorati, A. H. Werner, and J. Eisert, General framework for randomized benchmarking, PRX Quantum **3**, 020357 (2022).

[48] J. Helsen, M. Ioannou, J. Kitzinger, E. Onorati, A. H. Werner, J. Eisert, and I. Roth, Shadow estimation of gate-set properties from random sequences, Nat. Commun. **14**, 5039 (2023).

[49] L. Kong, A framework for randomized benchmarking over compact groups, arxiv:2111.10357 [quant-ph].

[50] M. Heinrich, M. Kliesch, and I. Roth, Randomized benchmarking with random quantum circuits, arxiv:2212.06181 [quant-ph] presented at QIP 2023 as a talk.

[51] C. H. Valahu, T. Navickas, M. J. Biercuk, and T. R. Tan, Benchmarking bosonic modes for quantum information with randomized displacements, PRX Quantum **5**, 040337 (2024).

[52] Y. Liu, M. Otten, R. Bassirianjahromi, L. Jiang, and B. Fefferman, Benchmarking near-term quantum computers via random circuit sampling, arXiv:2105.05232 [quant-ph].

[53] S. Boixo, S. V. Isakov, V. N. Smelyanskiy, R. Babbush, N. Ding, Z. Jiang, M. J. Bremner, J. M. Martinis, and H. Neven, Characterizing quantum supremacy in near-term devices, Nat. Phys. **14**, 595 (2018).

[54] F. Arute *et al.*, Quantum supremacy using a programmable superconducting processor, Nature **574**, 505 (2019).

[55] X. Liu, C. Guo, Y. Liu, Y. Yang, J. Song, J. Gao, Z. Wang, W. Wu, D. Peng, P. Zhao, F. Li, H.-L. Huang, H. Fu, and D. Chen, Redefining the quantum supremacy baseline with a new generation sunway supercomputer, arXiv:2111.01066 [quant-ph].

[56] D. Hangleiter and J. Eisert, Computational advantage of quantum random sampling, Rev. Mod. Phys. **95**, 035001 (2023).

[57] G. Adesso, S. Ragy, and A. R. Lee, Continuous variable quantum information: Gaussian states and beyond, Open Syst. Inf. Dyn. **21**, 1440001 (2014).

[58] Arvind, B. Dutta, N. Mukunda, and R. Simon, The real symplectic groups in quantum mechanics and optics, Pramana - J. Phys. **45**, 471 (1995).

[59] M. Reck, A. Zeilinger, H. J. Bernstein, and P. Bertani, Experimental realization of any discrete unitary operator, Phys. Rev. Lett. **73**, 58 (1994).

[60] J. Carolan, C. Harrold, C. Sparrow, E. Martín-López, N. J. Russell, J. W. Silverstone, P. J. Shadbolt, N. Matsuda, M. Oguma, M. Itoh, G. D. Marshall, M. G. Thompson, J. C. F. Matthews, T. Hashimoto, J. L. O'Brien, and A. Laing, Universal linear optics, Science **349**, 711 (2015).

[61] W. R. Clements, P. C. Humphreys, B. J. Metcalf, W. S. Kolthammer, and I. A. Walmsley, Optimal design for universal multiport interferometers, Optica **3**, 1460 (2016).

[62] H. de Guise, O. Di Matteo, and L. L. Sánchez-Soto, Simple factorization of unitary transformations, Phys. Rev. A **97**, 022328 (2018).

[63] P. Aniello, C. Lupo, and M. Napolitano, Exploring representation theory of unitary groups via linear optical passive devices, Open Syst. Inf. Dyn. **13**, 415 (2006).

[64] https://github.com/MirkoArienzo/passiveRB.

[65] C. Stark, Self-consistent tomography of the state-measurement Gram matrix, Phys. Rev. A **89**, 052109 (2014).

[66] S. T. Merkel, J. M. Gambetta, J. A. Smolin, S. Poletto, A. D. Córcoles, B. R. Johnson, C. A. Ryan, and M. Steffen, Self-consistent quantum process tomography, Phys. Rev. A **87**, 062119 (2013).

[67] E. Nielsen, J. K. Gamble, K. Rudinger, T. Scholten, K. Young, and R. Blume-Kohout, Gate set tomography, Quantum **5**, 557 (2021).

[68] R. Brieger, I. Roth, and M. Kliesch, Compressive gate set tomography, PRX Quantum **4**, 010325 (2023).

[69] Here, $\lambda_0 = \mathbf{1}$ is the trivial irrep and $\lambda_1 = \mathrm{Ad}$ is the adjoint irrep of $\mathrm{U}(m)$.

[70] Note that this coincides with a suitably rescaled filter function (4) for the trivial irrep λ_0.

[71] M. Cooper, L. J. Wright, C. Söller, and B. J. Smith, Experimental generation of multi-photon Fock states, Opt. Express **21**, 5309 (2013).

[72] A. I. Lvovsky, P. Grangier, A. Ourjoumtsev, V. Parigi, M. Sasaki, and R. Tualle-Brouri, Production and applications of non-Gaussian quantum states of light, arxiv:2006.16985 [physics, physics:quant-ph].

[73] M. Walschaers, Non-Gaussian quantum states and where to find them, PRX Quantum **2**, 030204 (2021).

[74] S. Sternberg, *Group Theory and Physics* (Cambridge University Press, Cambridge, 1994).

[75] A. Alex, M. Kalus, A. Huckleberry, and J. von Delft, A numerical algorithm for the explicit calculation of SU(N) and SL($n, \mathbb{C}$) Clebsch–Gordan coefficients, J. Math. Phys. **52**, 023507 (2011).

[76] S. Scheel, Permanents in linear optical networks, arxiv:quant-ph/0406127.

[77] I. Dhand, B. C. Sanders, and H. de Guise, Algorithms for SU(n) boson realizations and D-functions, J. Math. Phys. **56**, 111705 (2015).

[78] U. Chabaud, T. Douce, D. Markham, P. van Loock, E. Kashefi, and G. Ferrini, Continuous-variable sampling from photon-added or photon-subtracted squeezed states, Phys. Rev. A **96**, 062307 (2017).

[79] J. Marshall and N. Anand, Simulation of quantum optics by coherent state decomposition, Opt. Quantum **1**, 78 (2023).

[80] J. E. Bourassa, N. Quesada, I. Tzitrin, A. Száva, T. Isacsson, J. Izaac, K. K. Sabapathy, G. Dauphinais, and I. Dhand, Fast simulation of bosonic qubits via Gaussian functions in phase space, PRX Quantum **2**, 040315 (2021).

[81] S. Rahimi-Keshari, T. C. Ralph, and C. M. Caves, Sufficient conditions for efficient classical simulation of quantum optics, Phys. Rev. X **6**, 021039 (2016).

[82] N. Heurtel, S. Mansfield, J. Senellart, and B. Valiron, Strong simulation of linear optical processes, Comput. Phys. Commun. **291**, 108848 (2023).

[83] W. Roga and M. Takeoka, Classical simulation of boson sampling with sparse output, Sci. Rep. **10**, 14739 (2020).

[84] L. Everding, Bachelor's thesis, Calculation of Clebsch-Gordan coefficients via Weyl group symmetry, LMU Munich, 2011.

[85] H. J. Ryser, *Combinatorial Mathematics* (American Mathematical Soc., Washington, D.C., 1963), Vol. 14.

[86] A. Nijenhuis and H. S. Wilf, *Combinatorial Algorithms: for Computers and Calculators* (Academic Press, Inc., New York, 1978), 2nd ed.

[87] This is necessary as specially engineered noise can drastically change the behavior of the RB signal, for instance, by relabeling the measurement outcomes. Similar assumptions can be found throughout the RB literature [44,126].

[88] We expect Eq. (17) can be evaluated for a moderate number of modes exploiting the symmetries of the weight diagrams under the action of the Weyl group [84].

[89] N. J. Vilenkin and A. U. Klimyk, *Representation of Lie Groups and Special Functions: Volume 3: Classical and Quantum Groups and Special Functions* (Springer Science & Business Media, Dordrecht, 1992).

[90] N. Vilenkin and A. Klimyk, *Representation of Lie Groups and Special Functions, Vol. 1: Simplest Lie Groups, Special Functions and Integral Transforms*, Mathematics and its Applications (Springer, 1993).

[91] N. Vilenkin and A. Klimyk, *Representation of Lie Groups and Special Functions, Vol. 2: Class I Representations, Special Functions, and Integral Transforms*, Mathematics and its Applications (Springer, 1993).

[92] Note that ω restricted to $\mathcal{B}(\mathcal{H}_n^m)$ is equal to ω_n^m and—as mentioned in Sec. II B 3—each λ_k appears in all ω_n^m for $n \geq k$.

[93] V. V. Albert, Bosonic coding: Introduction and use cases, in *Proceedings of the International School of Physics "Enrico Fermi"* (Como, 2025), Vol. 209, pp. 79–107.

[94] M. Bentivegna, N. Spagnolo, C. Vitelli, F. Flamini, N. Viggianiello, L. Latmiral, P. Mataloni, D. J. Brod, E. F. Galvão, A. Crespi, R. Ramponi, R. Osellame, and F. Sciarrino, Experimental scattershot boson sampling, Sci. Adv. **1**, e1400255 (2015).

[95] Y. Benoist and J.-F. Quint, *Random Walks on Reductive Groups* (Springer, Berlin, 2016).

[96] E. Breuillard, Random walks on Lie groups, (2004).

[97] B. Bekka, P. de la Harpe, and A. Valette, *Kazhdan's Property (T)*, New Mathematical Monographs (Cambridge University Press, 2008).

[98] R. Howe, Perspectives on invariant theory: Schur duality, multiplicity-free actions and beyond, Israel Math. Conf. Proc. **8**, 1 (1995).

[99] R. Howe, The oscillator semigroup, Proc. Symp. Pure Math., Amer. Math. Soc. **48**, 61 (1988).

[100] G. Folland, *Harmonic Analysis in Phase Space*, Annals of Mathematics Studies No. 122 (Princeton University Press, 1989).

[101] J. Wilkens, M. Ioannou, E. Derbyshire, J. Eisert, D. Hangleiter, I. Roth, and J. Haferkamp, Benchmarking bosonic and fermionic dynamics, arXiv:2408.11105 [quant-ph].

[102] Z. Kolarovszki, T. Rybotycki, P. Rakyta, Ágoston Kaposi, B. Poór, S. Jóczik, D. T. R. Nagy, H. Varga, K. H.

El-Safty, G. Morse, M. Oszmaniec, T. Kozsik, Z. Zimborás, Piquasso: A photonic quantum computer simulation software platform, arXiv:2403.04006 [quant-ph].

[103] B. C. Hall, *Lie Groups, Lie Algebras, and Representations: An Elementary Introduction*, Graduate Texts in Mathematics, Vol. 222 (Springer International Publishing, Cham, 2015).

[104] W. Fulton and J. Harris, *Representation Theory*, Graduate Texts in Mathematics, Vol. 129 (Springer, New York, NY, 2004).

[105] R. Goodman and N. R. Wallach, *Symmetry, Representations, and Invariants*, Graduate Texts in Mathematics, Vol. 255 (Springer, New York, NY, 2009).

[106] L. C. Biedenharn, On the representations of the semisimple Lie groups. I. The explicit construction of invariants for the unimodular unitary group in N dimensions, J. Math. Phys. **4**, 436 (2004).

[107] G. E. Baird and L. C. Biedenharn, On the representations of the semisimple Lie groups. II, J. Math. Phys. **4**, 1449 (2004).

[108] G. E. Baird and L. C. Biedenharn, On the representations of the semisimple Lie groups. III. The explicit conjugation operation for SU_n, J. Math. Phys. **5**, 1723 (1964).

[109] R. M. Delaney and B. Gruber, Inner and restriction multiplicity for classical groups, J. Math. Phys. **10**, 252 (1969).

[110] J. F. Cornwell, *Group Theory in Physics* (Academic Press, New York, 1984), Vol. 1.

[111] J. F. Cornwell, *Group Theory in Physics* (Academic Press, New York, 1984), Vol. 2.

[112] G. B. Folland, *A Course in Abstract Harmonic Analysis* (Chapman and Hall/CRC, New York, 2015), 2nd ed.

[113] A. Alex, Non-Abelian symmetries in the numerical renormalization group, Ph.D. thesis, Ludwig-Maximilians-Universität Münich, 2009.

[114] M. Mathur, I. Raychowdhury, and R. Anishetty, SU(N) irreducible Schwinger bosons, J. Math. Phys. **51**, 093504 (2010).

[115] M. Mathur, I. Raychowdhury, and T. P. Sreeraj, Invariants, projection operators and $SU(N) \times SU(N)$ irreducible Schwinger bosons, J. Math. Phys. **52**, 113505 (2011).

[116] J. Provazník, L. Lachman, R. Filip, and P. Marek, Benchmarking photon number resolving detectors, Opt. Express **28**, 14839 (2020).

[117] W. Fulton, *Young Tableaux: With Applications to Representation Theory and Geometry*, London Mathematical Society Student Texts (Cambridge University Press, Cambridge, 1996).

[118] P. Di Francesco, P. Mathieu, and D. Sénéchal, *Conformal Field Theory*, Graduate Texts in Contemporary Physics (Springer, New York, NY, 1997).

[119] H. W. Gould, *Combinatorial Identities: A Standardized set of Tables Listing 500 Binomial Coefficients Summations* (Morgantown, W. Va., 1972).

[120] M. Reed and B. Simon, *Functional Analysis*, Methods of Modern Mathematical Physics, Vol. 1 (Academic Press, New York, San Fransisco, London, 1972).

[121] G. M. D'Ariano, P. Perinotti, and M. F. Sacchi, Informationally complete measurements and groups representation, J. Opt. B: Quantum Semiclass. Opt. **6**, S487 (2004).

[122] F. Mezzadri, How to generate random matrices from the classical compact groups, NOTICES of the AMS **54**, 592 (2007).

[123] M. Ozols, How to generate a random unitary matrix (03, 2009).

[124] Á. Kaposi, Z. Kolarovszki, T. Kozsik, Z. Zimborás, and P. Rakyta, Polynomial speedup in Torontonian calculation by a scalable recursive algorithm, arxiv:2109.04528 [quant-ph].

[125] L. Devos, https://github.com/QuantumKitHub/SUNRepresentations.jl.

[126] S. T. Flammia and J. J. Wallman, Efficient estimation of Pauli channels, ACM Trans. Quantum Comput. **1**, 1 (2020).